Department of Biotechnology and Chemical Technology

Molecular interactions of hydrophobin proteins with their surroundings

Mathias S. Grunér

Aalto University

DOCTORAL DISSERTATIONS

Aalto University publication series
DOCTORAL DISSERTATIONS 206/2015
VTT SCIENCE 114

Molecular interactions of hydrophobin proteins with their surroundings

Mathias S. Grunér

A doctoral dissertation completed for the degree of Doctor of Science (Technology) to be defended, with the permission of the Aalto University School of Chemical Technology, at a public examination held at the lecture hall KE2 at the Aalto University School of Chemical Technology (Espoo, Finland) on the 10th of December 2015, at 12 o'clock noon.

Aalto University
School of Chemical Technology
Department of Biotechnology and Chemical Technology
Biomolecular materials

Supervising professors
Professor Markus B. Linder
Aalto University, Finland

Thesis advisors
Professor Markus B. Linder
Aalto University, Finland

Preliminary examiners
Professor Ewa Rogalska
University of Lorraine, France

Professor Paola Giardina
Universitario Monte S. Angelo, Italy

Opponents
Professor Guy Derdelinckx
KU Leuven, Belgium

Aalto University publication series
DOCTORAL DISSERTATIONS 206/2015

VTT SCIENCE 114

ISBN 978-952-60-6556-4 (printed)
ISBN 978-952-60-6557-1 (pdf)
ISSN-L 1799-4934
ISSN 1799-4934 (printed)
ISSN 1799-4942 (pdf)
http://urn.fi/URN:ISBN:978-952-60-6557-1

ISBN 978-951-38-8367-6 (printed)
ISBN 978-951-38-8366-9 (pdf)
ISSN-L 2242-119X
ISSN 2242-119X (printed)
ISSN 2242-1203 (pdf)
http://urn.fi/URN:ISBN:978-951-38-8366-9

Unigrafia Oy
Helsinki 2015

Finland

441 697
Printed matter

Author
Mathias S. Grunér

Name of the doctoral dissertation
Molecular interactions of hydrophobin proteins with their surroundings

Publisher School of Chemical Technology

Unit Department of Biotechnology and Chemical Technology

Series Aalto University publication series DOCTORAL DISSERTATIONS 206/2015

Field of research Biotechnology

Manuscript submitted 5 June 2015 **Date of the defence** 10 December 2015

Permission to publish granted (date) 6 November 2015 **Language** English

☐ **Monograph** ☒ **Article dissertation (summary + original articles)**

Abstract

This thesis describes the properties of a group of proteins named hydro-phobins, which fulfil a variety of functions in the growth and function of filamentous fungi. Hydrophobins can be utilized as coatings/protective agents, in adhesion, in surface modifications and overall functions that require surfactant-like properties. This work is concentrated on the hydrophobins HFBI,
HFBII and HFBIII expressed by Trichoderma reesei. The aims of this study were to examine in what manner hydrophobins function when interacting with their surroundings and how their surroundings affect their function.
Hydrophobins were shown strongly to adhere to surfaces of varying polarity and structure by self-assembly, governed by their amphiphilic nature, and to adsorb with different orientation on hydrophilic and hydrophobic surfaces. The proteins were shown to selectively recruit other proteins and molecules to a self-assembled amphiphilic film of hydrophobin. HFBI variants bound to a surface were shown to recruit T. reesei enzymes specifically depending on localized protein surface charge on the hydrophilic part of the protein, and HFBII adsorbed on nanoparticles was shown to bind layers of human plasma proteins in different manner when adsorbed on nanoparticles of varying polarity. Surface films formed by hydrophobins were shown to be highly elastic, and charged residues on the side of the proteins were shown to have a role in stabilizing the protein films formed. The surroundings in which the proteins exist were shown to also affect their function. Surfaces of varying polarity in the protein surroundings affected how they self-assemble, and hydrophobin multimer exchange in solution was shown to be governed by hydrophobic interactions and the multimer exchange behaviour was shown to be affected by other proteins and molecules. HFBII and HFBI were shown to interact in solution, altering multimer kinetics and thermodynamics considerably.
Solution association methods, surface characterization analysis methods and size measurement techniques such as stopped-flow spectroscopy, quartz crystal microbalance with dissipation and differential centrifugal sedimentation were used.
The results presented here show that hydrophobins function by selectively interacting with their surroundings assembled at various interfaces specifically recruiting other proteins and molecules and that the surroundings in which the proteins exist also affects their function in terms of multimer exchange behaviour and surface adhesion properties. The knowledge learned here regarding hydrophobins, show that these proteins can be specialized to function as highly selective self-assembling building blocks in applications such as biosensors and biocompatible coatings, and gives new insight in the growth and function of filamentous fungi.

Keywords Hydrophobin, self-assembly, HFBI, HFBII, adhesion

ISBN (printed) 978-952-60-6556-4 **ISBN (pdf)** 978-952-60-6557-1

ISSN-L 1799-4934 **ISSN (printed)** 1799-4934 **ISSN (pdf)** 1799-4942

Location of publisher Helsinki **Location of printing** Helsinki **Year** 2015

Pages 110 **urn** http://urn.fi/URN:ISBN:978-952-60-6557-1

Författare
Mathias S. Grunér

Doktorsavhandlingens titel
Molecular interactions of hydrophobin proteins with their surroundings

Utgivare Högskolan för kemiteknik

Enhet Institutionen för bio- och kemiteknik

Seriens namn Aalto University publication series DOCTORAL DISSERTATIONS 206/2015

Forskningsområde Bioteknik

Inlämningsdatum för manuskript 05.06.2015 **Datum för disputation** 10.12.2015

Beviljande av publiceringstillstånd (datum) 06.11.2015 **Språk** Engelska

☐ **Monografi** ☒ **Sammanläggningsavhandling (sammandrag plus separata artiklar)**

Sammandrag

Denna avhandling beskriver egenskaperna av en grupp proteiner kallade hydrofobiner, vilka utför en rad viktiga funktioner i fråga om tillväxt och funktion av filamentösa svampar. Hydrofobiner kan användas som skyddade lager och beläggningar, i adhesion, ytmodifiering och allmänt där ytaktivitet är av vikt. Detta arbete fokuserar på hydrofobinerna HFBI, HFBII och HFBIII uttryckta av Trichoderma reesei. Målen med arbetet var att undersöka hydrofobiners funktion att interagera med sin omgivning och hur omgivningen i sin tur påverkar hydrofobinernas funktion.

Hydrofobiner påvisades att starkt fästa till ytor av varierande polaritet och struktur genom självorganisering drivna av sin amfifila natur, och att adsorbera med skild orientering på hydrofila respektive hydrofoba ytor. Resultaten visade även att proteinerna selektivt kan rekrytera andra proteiner till en självorganiserad film av hydrophobin. Muterade varianter av HFBI bundna till en yta påvisades att rekrytera enzymer av T. reesei beroende på lokala laddningar på den hydrofila delen av proteinets yta, och HFBII adsorberat på nanopartiklar band till sig humana plasmaproteiner i lager med olika sammansättning och typ beroende polaritet av nanopartikel. Hydrofobinfilmer formade på ytor konstaterades även vara mycket elastiska, och laddade sidokedjor på sidan proteinet verkar stabiliserande på hydrofobinfilmen. Omgivningen i vilken hydrofobinerna verkar konstaterades att påverka deras funktion. Ytor av varierande polaritet i proteinernas omgivning påverkar hur de självorganiserar. Utbyte av hydrofobinmultimerer i lösning påvisades vara styrt av hydrofoba interaktioner och multimerutbytet påverkas av andra proteiner och molekyler. HFBI och HFBII konstaterades interagera i lösning vilket i hög grad påverkade kinetiken och termodynamiken av multimerutbytetet.

Lösningsassocieringsmetoder, ytkarakteriseringsanalysmetoder och storleksanalystekniker som stopped-flow spektroskopi, QCM-D (Quartz crystal microbalance with dissipation) och DCS (differential centrifugal sedimentation) användes.

Resultaten av detta arbete visar att hydrofobiner verkar genom att selektivt interagera med sin omgivning, ordnade vid olika gränsytor, där de specifikt rekryterar olika proteiner och molekyler, samt att omgivingen där proteinerna uppträder även påverkar hydrofobinernas funktion i termer av multimerutbyte i lösning och ytadhesionsegenskaper. Kunskapen som förvärvats i detta arbete rörande hydrofobiner visar att dessa proteiner kan specialiseras för att fungera som ytterst selektiva självorganiserande byggklossar för applikationer som t.ex. biosensorer och biokompatibla beläggningar, samt ger ny insikt i tillväxt och funktion av filamentösa svampar.

Nyckelord Hydrophobin, self-assembly, HFBI, HFBII, adhesion

ISBN (tryckt) 978-952-60-6556-4	**ISBN (pdf)** 978-952-60-6557-1	
ISSN-L 1799-4934	**ISSN (tryckt)** 1799-4934	**ISSN (pdf)** 1799-4942
Utgivningsort Helsingfors	**Tryckort** Helsingfors	**År** 2015
Sidantal 110	**urn** http://urn.fi/URN:ISBN:978-952-60-6557-1	

Acknowledgements

Starting in autumn 2010 I got the chance to perform my master thesis in the guidance of Professor Markus Linder at the VTT Nanobiomaterials group. I was at an early stage inspired by the creative possibilities of the field and by the opportunity to work with such talented people. My work of the fascinating hydrophobin proteins continued as thesis work in the same group from September 2011 until November 2012.

There are numerous people whom I wish to acknowledge for their valuable contributions and for making this thesis possible.

I express my deepest gratitude to my thesis supervisor Professor Markus Linder for his support, encouragement, patience and for always finding time for discussions, meetings and questions. I want to thank Dr. Géza Szilvay for educating and supporting me, and for introducing me to the world of science in the best way possible. I also want to thank Dr. Michael Lienemann for his kind support and for useful discussions, especially during the later stages of my research.

I thank the technology managers Dr. Raija Lantto and Dr. Niklas von Weymarn for the great working facilities. I acknowledge the School of Chemical Technology, Aalto University for the possibility to perform my doctoral degree. The National graduate school in informational and structural biology and the director Professor Mark Johnson are thanked for financial support.

Dr. Riitta Partanen is thanked for being an excellent and inspiring team leader. Dr. Arja Paananen is thanked for her advice, interesting scientific discussions and guidance in experiments. Riitta Suihkonen is appreciated for practical advice in the laboratory and for all discussions, especially in Finnish.

At University College Dublin, Professor Kenneth Dawson is thanked for accepting me as a guest researcher in his group and Dr. Marco Monopoli for his continuous support, guidance and inspiration.

I also would like to thank my colleagues, Jani-Markus, Jaana, Suvi, Päivi, Evi, Timo, Bartosz and Roberto and all other members of the Nanobiomaterials group for practical support and for creating a warm work atmosphere, as well as my other colleagues at VTT Biotechnology, Greta, Wesley, Georg, Ronny and Harry for inspiring discussions.

I would like to especially thank my family for their interest, participation and fantastic support, for always encouraging me to move forward and to trust my intuition and for always finding time to listen to my thoughts and reflections.

Mariehamn 12.11.2015

Mathias S. Grunér

Contents

List of Abbreviations and Symbols

AFM	Atomic force microscopy
DCS	Differential centrifugal sedimentation
DLS	Dynamic light scattering
Ea	Activation energy
FRET	Förster resonance energy transfer
HC	Hard corona
IS	*In situ* corona
LB	Langmuir-Blodgett
NP	Nanoparticle
QCM-D	Quartz crystal microbalance with dissipation
SAM	Self-assembled monolayer
SEC	Size exclusion chromatography
SDS-PAGE	Polyacrylamide gel electrophoresis using sodium dodecyl sulfate
SF	Stopped-Flow spectroscopy
$t_{1/2}$	Half-life
WCA	Water contact angle

List of Publications

This doctoral dissertation consists of a summary and of the following publications which are referred to in the text by their numerals

I. Grunér, Mathias S; Kauscher, Ulrike; Linder, Markus B; Monopoli, Marco P. An environmental route of exposure affects the formation of nanoparticle coronas in blood plasma. Accepted for publication in the journal Journal of Proteomics, Elsevier B.V. in the year 2015

II. Lienemann, Michael; Grunér, Mathias S; Paananen, Arja; Siika-Aho, Matti; Linder, Markus B; 2015. Charge-Based Engineering of Hydrophobin HFBI: Effect on Interfacial Assembly and Interactions. ACS Publications. Biomacromolecules, volume 16, issue 4, pages 1283-1292. ISSN 1526-4602.DOI: 10.1021/acs.biomac.5b00073

III. Grunér, Mathias S; Szilvay, Géza R; Berglin, Mattias; Lienemann, Michael; Laaksonen, Päivi; and Linder, Markus B. 2012. Self-assembly of Class II Hydrophobins on Polar Surfaces. American Chemical Society. Langmuir, volume 28, issue 9, pages 4293–4300. ISSN 0743-7463. DOI:10.1021/la300501u

IV. Grunér, Mathias S; Paananen, Arja; Szilvay, Géza R; Linder, Markus B. Dynamics and interactions of hydrophobin HFBII assembly in solution by stopped-flow spectroscopy. Submitted manuscript in the year 2015.

Author's Contribution

I. The author carried out all the experiments, planned the work, interpreted the results and wrote the publication in collaboration with the co-authors.

II. The author carried out QCM-D measurements including BCA assays and SAM surface preparation, performed Langmuir-through film preparation and surface pressure experiments, studies on plateau forming time, as well as part of the SEC studies and assisted in AFM measurements. The author planned the work and interpreted the results in collaborations with the co-authors and contributed to the writing of segments related to QCM-D and plateau forming time in the publication.

III. The author carried out all experiments except AFM measurements, planned the work, interpreted the results and wrote the publication in collaboration with the co-authors.

IV. The author carried out all the experiments, planned the work, interpreted the results and wrote the publication in collaboration with the co-authors.

1. Introduction

This work describes the properties of a group of proteins termed hydrophobins, which fulfil a variety of functions in the growth and function of filamentous fungi. The common button mushroom *Agaricus bisporus*, a common part of our normal diet, is an example of such a fungus expressing the protein. Hydrophobins function as coatings/protective agents, in adhesion, surface modification and overall functions that require surfactant-like properties (Wösten 2001; Linder et al. 2005). This thesis is concentrated on the hydrophobins HFBI, HFBII and HFBIII expressed by *Trichoderma reesei*.

Hydrophobins are small, about 10 kDa sized proteins that are surface active, meaning that they adsorb at the air-water interface lowering the surface tension of water. Comparing the properties and sequences of hydrophobins a classification of the proteins was made (Wessels 1994), where two classes where distinguished. The classes, class I and class II hydrophobins, were based on the occurrence of hydrophilic and hydrophobic amino acid residues in the protein sequence i.e. their hydrophaty plots (Kyte & Doolittle 1982). Class I hydrophobins form assemblies that appear to be more resistant towards solvents and detergents compared to class II hydrophobins and are highly insoluble in aqueous solution. Members of class II hydrophobins form assemblies that are much easier to dissolve. Furthermore, class I hydrophobins tend to form a mosaic of rod-like structures, called rodlets, on surfaces whereas class II hydrophobins do not. So far, class II hydrophobins have been found only in fungal taxonomic group of Ascomycetes, whereas class I hydrophobins have been found in both Ascomycetes and Basidiomycetes (Linder et al. 2005; Whiteford & Spanu 2002).

1.1 Biological functions of hydrophobins

Hydrophobins are involved in the adaptation of the fungi to the environment by altering interfacial interactions. Fungi have evolved to use hydrophobins for multiple tasks and most fungal genomes contain multiple copies of hydrophobins that may have different expression profiles. Fungal hyphae growing in aqueous medium secrete hydrophobins into the surrounding medium which adsorb at the air-water interface, lowering the water surface tension thereby enabling the hyphae to penetrate the air-water barrier and grow into the air (Wösten et al. 1999).

Hyphae growing into the air are also expressing hydrophobin genes and as the hydrophobins are not diffusing into a medium, they self-assemble between the hydrophilic cell wall and the air (Wösten et al. 1993; Wösten et al. 1994). As a result, aerial hyphae (Wösten et al. 1993; Wösten et al. 1994; Askolin et al. 2005), fruiting bodies (Wessels et al. 1991; Lugones et al. 1996; De Groot et al. 1997) and spores (Bell-Pedersen et al. 1992; Stringer et al. 1991) become hydrophobic. The hydrophobicity of aerial hyphae and fruiting bodies have been suggested as preventing the structures to fall back into the moist substrate (Wösten et al. 1993; Wösten et al. 1994), as well as to serve as a protection against bacterial and fungal infections (Wösten 2001). As much as 60 % of the total mRNA of the outer peel tissues of the caps of the common button mushroom *A. bisporus* is produced by the gene encoding the hydrophobin ABHI (HYPHA) (De Groot et al. 1997). Hydrophobins have also been shown to line gas channels of fruiting bodies thereby preventing the channels from filling with water (Lugones et al. 1999; van Wetter et al. 2000).

1.2 Hydrophobin role in nature

Fungi are important in the carbon cycle in their environment, in ecology, as well as being industrially and economically important. Fungi are used as biocontrol agents, for food- and enzyme production and e.g. for breaking down cellulose for biofuels and have a crucial role in nature in the breakdown and turnover of plant material. Fungi can also function as pathogens and cause damage on buildings and crops.

The amounts of hydrophobins secreted into the soil during breakdown and turnover of plant material by fungi are so high that geological effects such as changes in soil hydrophobicity are anticipated (Rillig 2005; Rillig et al. 2007). The soil might itself turn hydrophobic and water repellent as hydrophobins are resistant to degradation and have been shown to turn hydrophilic surfaces hydrophobic (Linder et al. 2005).

Hydrophobins have been shown to enable the attachment of hyphae to solid substrates including hydrophobic surfaces (Wösten et al. 1994; Talbot et al. 1996; Lugones et al. 2004). The hydrophobicity of spores has been suggested as facilitating the spreading in the environment by wind and insects as well as to prevent desiccation (Stringer et al. 1991; Bell-Pedersen et al. 1992; Temple et al. 1997). Hydrophobic fungal conidiospores with a hydrophobin coating can easily adhere to hydrophobic biotic or abiotic surfaces. Adsorption of pathogenic fungi to the surface of a host organism has also been shown to be involving hydrophobins (St Leger et al. 1992; Talbot et al. 1996; Kazmierczak et al. 2005). The hydrophobin gene mpg1 has been shown to be involved in the adhesion of the rice pathogen *Magnaporthe grisea* to its host (Talbot et al. 1996; Talbot et al. 1993) and expression of hydrophobins has also been shown for the tomato pathogen *Cladosporium fulvum* (Spanu 1997) suggesting that hydrophobins are widely important in the infection process of pathogenic fungi (Zampieri et al. 2010).

Hydrophobins also have roles in interactions between fungi and plants (Viterbo & Chet 2006), and have been shown to be important in the symbiotic interactions between fungi and plants, mycorrhizas (Tagu et al. 2001; Tagu et al. 1996; Mankel et al. 2002), as well as symbiotic interactions between fungi and algae or cyanobacteria, i.e. lichens (Scherrer et al. 2000).

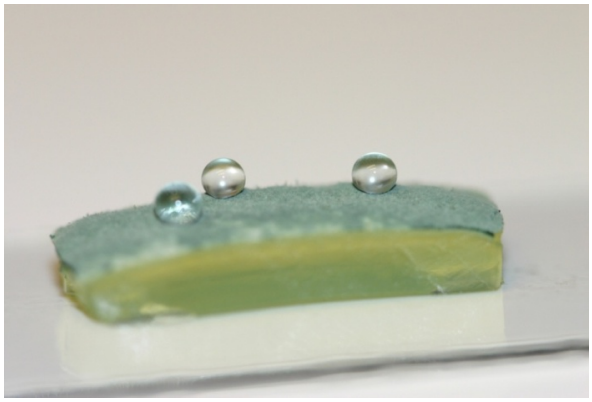

Figure 1. The surface of a mycelial mat of *T. reesei* growing on agar is highly hydrophobic as shown by water drop contact angles of about 140° (I)

1.2.1 Hydrophobin role in Immune recognition of spores

Hydrophobins have been shown to prevent immune recognition of airborne fungal spores, conidiospores (Aimanianda et al. 2009), and hiding the spores from clearance by neutrophils and macrophages in early stages of infection (Aimanianda et al. 2009; Paris et al. 2003; Shibuya et al. 1999; Bruns et al. 2010).

1.3 Structure of hydrophobins

The sequences of the two classes of hydrophobins share a unifying feature, where there are typically eight cysteine residues in a specific pattern. The second and third Cys-residues follow each other in immediate proximity, forming a pair, and a similar pair is formed by Cys-residues six and seven. The rest of the eight residues do not form pairs, resulting in a pattern of separated, pair, separated, separated, pair, separated (Linder et al. 2005; Wösten 2001).

1.3.1 Class II hydrophobins

The crystallographic structures of the class II hydrophobins HFBI and HFBII reveal important information on how hydrophobins function. The structure consists of a small antiparallel β-barrel formed by two β-hairpins connected by a stretch of α-helix (Figure 2). Proteins are often stabilized by hydrophobic interactions, but in these proteins the core is stabilized by an extended network of disulphide bonds. In hydrophobins, about 80 % of the hydrophobic side-chains are exposed on one side of the protein, forming a “hydrophobic

patch", a planar surface area formed by hydrophobic aliphatic amino acids, and formed to a large extent by two loop regions in the central β-barrel structure. In HFBII, the patch constitutes 12 % of the total surface area, which is otherwise mainly hydrophilic. The structure can thus be regarded as a protein amphiphile – a protein with distinct hydrophilic and hydrophobic regions. The hydrophobic patch can be seen comparing HFBI and HFBII to other class II hydrophobins, indicating an important functional role and suggesting a similar amphiphilic protein surface of all class II hydrophobins.

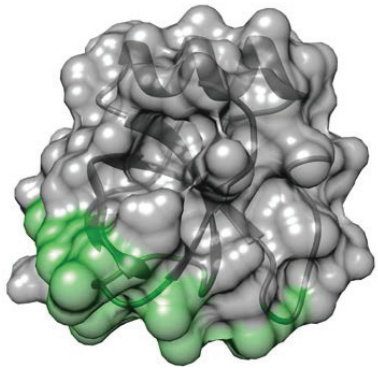

Figure 2. X-ray crystal structure of HFBII (PDB ID 2PL6) (Kallio et al. 2007) Cartoon of the surface representation of HFBII with the hydrophobic patch shown in green. The protein backbone visible showing a β-barrel formed by two β-hairpins and a connecting α-helix.

1.3.2 Class I hydrophobins

The structure of class I hydrophobins have been shown to be similar to structures of class II hydrophobins. The class I hydrophobins EAS from *Neurospora crassa* and SC3 of *Schizophyllum commune* shows a similar fold to HFBII (Kwan et al. 2006; Fan et al. 2006). Comparing EAS with HFBII it can be seen that the disulphide bridging pattern is the same as in HFBII. Differences can be seen comparing the hydrophobic patches of the proteins where much larger loops are formed between the strands of the beta barrel structure of EAS compared to HFBII.

1.4 HFB solution behaviour

The amphiphilic structure of hydrophobins is important for their function in aqueous solutions. Water molecules interact poorly with hydrophobic molecules, called the hydrophobic effect, and as a result hydrophobic molecules such as hydrophobins with their hydrophobic patch are clustered together, shielding the patches from water. In solution hydrophobins have been shown to form different dimers and oligomers. The class I hydrophobin SC3 has been shown to exist as monomers, dimers and tetramers in solution (Wang et al. 2004), whereas EAS has been suggested to occur only as monomers (Mackay et al. 2001). Class II hydrophobins HFBI and HFBII have been shown to form dimers and tetramers in solution (Torkkeli et al. 2002; Kisko et al. 2008),

clustered together through their hydrophobic patches (Hakanpää et al. 2004; Hakanpää 2006). Furthermore, oligomerization of HFBI has been shown to be dependent on hydrophobin concentration, as a change from monomers to tetramers was seen when the HFBI concentration increased. The HFBI multimers were shown to continuously disassemble and reassemble in solution. The affinity of solution multimerization of HFBI multimers was showed to be lower than the air-water interface affinity, and as a result hydrophobin was shown to adsorb at interfaces even in the presence of multimers (Szilvay et al. 2006; Szilvay, Kisko, et al. 2007). A continuous dynamic state between interface assembled hydrophobin and hydrophobin in solution has also been suggested by (Krivosheeva et al. 2013).

1.5 Interfacial self-assembly

The multimers formed in solution disassociate at interfaces and the hydrophobins rearrange and form surface membranes (Fan et al. 2006; Kallio et al. 2007; Wang et al. 2004; Szilvay, Paananen, et al. 2007). At the air-water interface hydrophobins assemble into films that can display a very ordered structure (Linder 2009; Szilvay, Paananen, et al. 2007). Class I hydrophobins form rod-like structures, called rodlets, about 5 -10 nm in width and several hundred nm in length, and can typically be seen when a solution of hydrophobin is dried down on a solid surface (Wösten et al. 1993). Class II hydrophobins have not been observed to form rodlets. Instead, e.g. HFBI, HFBII and HFBII have been shown to form interfacial films with a self-assembled hexagonally ordered structure (Figure 3) (Paananen et al. 2003; Kisko et al. 2005; Kisko et al. 2007). It has been shown that also multimers disassemble at the interfaces to form monolayers (Szilvay, Paananen, et al. 2007). The surface adsorbed films of class II hydrophobins are more easily dissolved than class I films.

Values of surface tension of hydrophobin films have been reported as high as 45 – 27 mNm^{-1} (Askolin et al. 2006; Lumsdon et al. 2005) and surface elasticity between 0.5 – 1.0 Nm^{-1} which is orders of magnitude higher than measured for any other surface active protein (Cox et al. 2007, II). The high surface elasticity of hydrophobins is connected to their tendency to form very stable foams (Bailey et al. 2002; Sarlin et al. 2005). Foams and bubbles of HFBII have been shown to be stable for months and even years (Cox et al. 2009).

Hydrophobins have been shown to efficiently adhere to surfaces. Adhesion onto hydrophobic surfaces has been studied extensively (Lugones et al. 1996; Wang et al. 2010; Askolin et al. 2006; de Vries et al. 1999; De Stefano et al. 2008). E.g. SC3 has been shown to be able to bind to Teflon and form a very insoluble layer (de Vocht et al. 2002). The assembly of class II hydrophobins onto polar hydrophilic surfaces under aqueous solution is studied in Publication III. Previously, coating on hydrophilic surfaces has been performed by drying down a hydrophobin film typically on filter paper were the film was first formed at the air-water interface (Wösten & de Vocht 2000). Class I hydrophobin HGFI has been shown to slightly increase the hydrophobicity of a hydrophilic mica surface (Hou et al. 2009).When binding to solid surfaces,

hydrophobins can form films that are very tightly bound, with class I generally adhering more strongly than class II hydrophobins (Askolin et al. 2006). Interestingly, Class I and class II hydrophobins have also been shown to form mixed membranes despite their differences in adhesion strength.

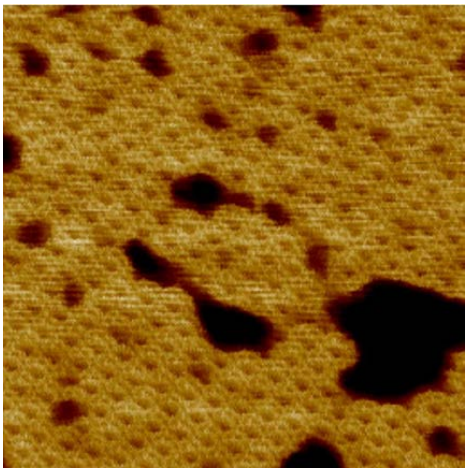

Figure 3. HFBI self-assembled at the air-water interface into a hexagonally ordered monolayer. Imaged with tapping mode in air on mica, image size 100 nm x 100 nm (Image courtesy of Arja Paananen)

1.5.1 Recruitment of molecules to surfaces

Hydrophobins of both classes are able to adsorb proteins and molecules when bound to a surface without losing activity. Glucose oxidase (GOx) of *Aspergillus niger,* bovine serum albumin (BSA), chicken egg avidin and monoclonal IgG has been shown to adsorb onto a solid hydrophobic surface coated with Class I hydrophobin HGFI or class II hydrophobin HFBI (Wang et al. 2010; Qin et al. 2007). The adsorption of these proteins was suggested as being dependant on electrostatic interactions, and the hydrophobins were shown to transform a non-polar surface into a polar one and to adsorb proteins specifically without denaturation of the adsorbed proteins (Wang et al. 2010; Qin et al. 2007). Hydrophobins adsorbed on surfaces have been used to immobilize enzymes (Zampieri et al. 2010; Palomo et al. 2003). E.g. a film of adsorbed hydrophobin RolA was shown to specifically recruit the enzyme CutL1 to the surface (Takahashi et al. 2005). The immobilization of enzymes has also been suggested as possible uses in biosensors (Corvis et al. 2006; Zhao et al. 2009; Hou et al. 2009; Bilewicz et al. 2001), e.g. the class I hydrophobin SC3 has been used to immobilise GOx and horseradish peroxidase (HRP) onto glassy carbon electrodes (Corvis et al. 2005).

1.6 Application potential of hydrophobins

Application potential for hydrophobins has been suggested for both technical and medical applications. Biocompatible surfaces are needed for various bio-

medical applications such as implants and artificial tissues, and hydrophobin coatings have been suggested to increase the biocompatibility by preventing immunogenic reactions, as hydrophobin coating in spores has been shown to prevent immune recognition of airborne fungal spores (Aimanianda et al. 2009; Zampieri et al. 2010). Hydrophobin coated polystyrene has showed promising results in terms of biocompatibility (Misra et al. 2006). Also cell growth on Teflon (Janssen et al. 2002; Scholtmeijer et al. 2002) and poly(dimethylsiloxane) (PDMS) (Hou et al. 2008) using hydrophobins has been shown.

In order to selectively create films, engineered hydrophobins can function as adsorption mediating modules conjugated with DNA-binding macromolecules, (Kostiainen et al. 2006), chelating groups (Corvis et al. 2006) as well as fused with enzymes (Linder et al. 2002) or protein binding targets (Szilvay, Paananen, et al. 2007). An engineered version of class I hydrophobin DewA has been used to deposit a thin film of titanium dioxide on top of a self-assembled layer of the hydrophobin. Silicone surfaces and graphene have been functionalized with gold nanoparticles using HFBI derivatives (Laaksonen et al. 2009; Laaksonen et al. 2010). Films based hydrophobins could be included in biosensors, diagnostic kits, photonic devices and microelectronics (Linder 2009). Hydrophobins have e.g. been shown to form a KOH protective coating on a silicon surface, demonstrating the use of hydrophobins during etching for silicon micromachining techniques (De Stefano et al. 2007).

Hydrophobins can also be used to stabilize hydrophobic liquids in water such as emulsions for cream or ointments for pharmaceutical or cosmetic use. The ability to easily form stable foams (Bailey et al. 2002; Cox et al. 2009) can be used to produce foams for food products and to detect foaming agents where excessive foaming is unwanted, e.g. beer (Sarlin et al. 2005).

Hydrophobins have also been suggested as a method to make drugs accessible for oral (Haas Jimoh Akanbi et al. 2010), topical (Vejnovic et al. 2010) or intravenous (Fang et al. 2014) delivery. Furthermore, coating on drug-loaded nanoparticles for possible drug delivery has been studied (Valo et al. 2010; Sarparanta et al. 2012)

Aims of the study

Related to the remarkable properties of hydrophobins, a largely unanswered question is in what manner hydrophobins function when interacting with their surroundings and how their surroundings affect their function. Following this, the aim of this study is to examine the following issues:

1. How do hydrophobins function when interacting with their surroundings?

2. How do proteins, molecules and interfaces surrounding hydrophobins interact with hydrophobins and thereby affect their function?

These issues are in this work examined by studying how hydrophobins function when assembling on different types of surfaces including nanoparticles, how they function when interacting with their surroundings to recruit other proteins and molecules, and how their structure is affecting their self-assembly and recruiting behaviour. The effect of different surfaces on hydrophobin self-assembling function, and how hydrophobins behave in terms of solution dynamics and how surrounding proteins and molecules affect this behaviour is also examined.

2. Materials and Methods

A summary of the materials and methods used in this study is presented in this section. More detailed information is given in the publications I – IV.

2.1 Hydrophobins

The class II hydrophobins HFBI, HFBII and HFBII were purified from either mycelium or culture supernatant of *T. reesei* using two-phase extraction and reversed phase chromatography (Paananen et al. 2003; Linder et al. 2001). FRET variants are described in (IV), variants of charged residues in (II).

2.2 Surface characterization methods

2.2.1 Quartz crystal microbalance with dissipation

In quartz crystal microbalance with dissipation (QCM-D), resonance frequency and dissipation is measured simultaneously and the mass of a bound protein layer can be calculated using the Sauerbrey relation, $\Delta m = -C\Delta f/n$, where Δm is adsorbed mass, Δf is frequency change, C = 17.7 ng Hz cm−2, and using the third overtone (n = 3) (D4-QCM system, Q-Sense, Sweden). By combining the frequency measurements with dissipation measurements, the rigidity of the formed layer can be determined depending on decay of oscillations of the layer thereby describing the viscoelastic properties of the layer. Hydrophobins were dissolved in buffer at 0.1 mg/mL and protein solution (300 µL) was pumped through the measuring chamber with a flow rate of 100 µL/min. The sensors were left to stabilize until a stable signal was achieved and then washed with running buffer (II, III).

2.2.2 Water contact angle

Water contact angle (WCA) is a measure of surface hydrophobicity. A drop of typically 6 µL Milli-Q water was applied on a surface and the average contact angle of the drop on the surface is calculated from a series of 15 pictures with a 5 s interval, as an average of three measurements (CAM 200, KSV NIMA, Finland). Here, WCA values were measured before and after hydrophobin adsorption (III).

2.2.3 Atomic force microscopy

Atomic force microscopy (AFM) was used for imaging of LB-films formed on mica using a NanoScopeV Multimode 8 AFM (E scanner, Bruker, Germany). A scanning probe image processor (SPIP, Image Metrology, Denmark) was used for image analysis. Topography images were acquired using tapping mode in air using scan rates in the range of 0.7 - 1 Hz where amplitude changes in oscillations of a cantilever driven by a small piezoelectric element is detected in order to gain information of surface topography and phase contrast (Geisse 2009). Topography and phase contrast images were captured simultaneously. (II)

2.2.4 Langmuir film preparations

Langmuir Blodgett (LB) through was used to compress surface layers of hydrophobin at the air-water interface in a controller manner in order to measure surface pressure and produce monolayers on mica for AFM measurements.

Surface pressure of a hydrophobin monolayer was analysed in a humidified atmosphere using a Langmuir through and pre-soaked 20.6 mm perimeter Wilhelmy paper plates (KSV Minimacro Trough, KSV NIMA, Finland). The hydrophobin sample was dissolved at a concentration of 0.85 – 1.0 μM by short magnetic stirring prior to probing. Surface pressure was measured at equilibrium (typically reached after 20 min – 1 h) The Wilhelmy plate was submerged prior to protein addition.

LB films: A monolayer of hydrophobin was assembled by injecting 20 μg of dissolved protein into 55 mL of 5 mM Na-acetate buffer pH 5.5 at 21° C. After the surface pressure had been stabilized (typically 45 minutes) the compression of the protein monolayer formed at the interface was started and compressed at a barrier speed of 2 mm/min until 35 mN/m surface pressure was reached. A monolayer of hydrophobin was then transferred to a flat mice substrate for AFM imaging (II).

2.3 Solution association analysis methods

2.3.1 Förster resonance energy transfer

Förster resonance energy transfer (FRET) is here used to measure the efficiency of energy transfer E, determined by measuring the enhanced fluorescence of an acceptor fluorophore in a fluorescence spectrophotometer (Cary Eclipse, Varian, USA). A donor fluorophore initially in its excited state transfers energy to an acceptor fluorophore when in close proximity. Here engineered variants of HFBII, HFBII-CysC were used which has an additional Cys residue at the C-terminus, conjugated with either cyanine dye 3 (donor) or cyanine dye 5 (acceptor) forming a FRET pair for measurements (Clegg 1992). Samples used here were excited at 516 nm (donor excitation) and the emission spectra from

both donor and accepter was recorded in order to determine hydrophobin multimerization states at different concentrations (IV).

2.3.2 Stopped-Flow spectroscopy

Stopped-Flow spectroscopy (SF) is used to study the kinetics of fast reactions in solution. Donor and acceptor are placed in two different syringes and liquid from both syringes are simultaneously injected into a small cuvette after which the flow is stopped and the resulting fluorescence is measured (Clegg 1992) (Chirascan SF.3 spectrometer, Applied Photophysics, UK). Here, the FRET pair of cy3 and cy5 labelled HFBII-CysC were used. A change in fluorescence could be seen as described regarding FRET, as a change in hydrophobin monomer association or disassociation occurring in the sample. Each syringe was loaded with 100 µg/ml hydrophobin, 10 µg/ml labelled and 90 µg/ml wild-type hydrophobin. The addition of wild-type was made in order to achieve appropriate fluorescence signal. The drive volume was set to 140 µL and FRET signal was measured at acceptor emission of 665 nm.

Activation energy, (Ea) was determined by measuring the exchange rate at three different temperatures, 21.5°, 17.5° and 12.5° Celsius in order to examine the temperature dependency of hydrophobin multimerization. The Arrhenius equation, k=Ae^(-Ea/RT)gives activation energy Ea and frequency factor A by plotting ln(k) vs. 1/T, where k is the reaction rate constant and T temperature (K). The reaction rate constant was here attained by using Pro-data viewer (Applied Photophysics, UK) using a Marquardt-Levenberg algorithm. The algorithm iterate until convergence to a chosen suitable equation, here a single exponential, a*e(-kx) +c where k is the reaction rate constant. The time needed for half of the hydrophobin multimers in solution to exchange is described as $t_{1/2}$ and was calculated as ln(2)/k (IV).

2.3.3 Size exclusion chromatography

Size exclusion chromatography (SEC) was used in order to examine concentration dependency of hydrophobin multimerization. Superdex 75 column and Äkta explorer (GE, USA) was used (II, IV).

2.4 Size measurements

2.4.1 Differential centrifugal sedimentation

Differential centrifugal sedimentation, DCS measures particle size distribution using centrifugal sedimentation within an optically clear spinning disc filled with fluid and here determines nanoparticle size on a nanometre level based on the sedimentation time of a particle through a glucose gradient (CPC disc centrifuge DC24000, CPS Instruments, USA). DCS measures apparent diameter size which makes it necessary to correct for changes in density of e.g. adsorbed protein layers on a nanoparticle by a core shell model in order to attain accurate size determination of protein shell coated nanoparticles. DSC meas-

urements are calibrated in order to apply the core-shell model $\frac{(\rho_c - \rho_s)}{(\rho_c - \rho_f)}\frac{D_c^3}{D_s} + \frac{(\rho_s - \rho_f)}{(\rho_c - \rho_f)}D_s^2 = D^2$, where ρ_c and D_c describes density and diameter of a core particle with a shell of density ρ_s and thickness D_s placed in a rotating disc filled with a fluid of density ρ_f giving the measured diameter D. (I, (Monopoli et al. 2011)

2.4.2 Dynamic light scattering and zeta potential

Dynamic light scattering (DLS) and zeta potential measures size and surface charge in terms of zeta potential, here on nanoparticle and protein dispersions (Zetasizer ZS, Malvern ,UK). Data is reported as average hydrodynamic diameter and a measure of size distribution. Polydispersity, PDI, is also given as a measure of aggregation (II, III).

2.5 Other

2.5.1 Self-assembled monolayers

Self-assembled monolayers (SAMs) are here created by dissolving cleaned gold disks overnight in a solution of long-chained molecules with a head group for anchoring, a tail and a functional end group dissolved in ethanol which self-assemble to attain ordered surfaces (Ulman 1996), here cationic, anionic and nonpolar aliphatic surfaces used for QCM-D measurements. For cationic surfaces N,N,N-trimethyl-(11mercaptoundecyl)ammonium chloride (HS(CH2)11NMe3+Cl–) thiol (TMA) (Prochimia Surfaces, Poland) was used. For hydrophobic surfaces 1-hexanethiol (HEX) (Sigma-Aldrich, USA) was used, and for anionic surfaces 1-mercaptoundecanoic acid (MUA) (Sigma-Aldrich) was used. SAMs were coated on either QCM-D sensor disks (QSX 303, Q-sense, Sweden) or gold coated glass disk (Bionavis, Finland) (II, III)

2.5.2 Dialysis

Dialysis is a method to remove material from a solution, here used in order to remove free or loosely bound hydrophobin from nanoparticles by diffusion through a semipermeable membrane (Float-A-lyzer G2, 1 ml 50 kDa, Spectrum Labs, USA). A sample of nanoparticles and hydrophobin was loaded into the dialysis device floating in 1 L buffer (PBS pH 7.4) at 4° under continuous stirring, after changing to fresh buffer every day the buffer was changed to MQ water in order to avoid aggregation of particles (I).

2.5.3 SDS-PAGE

SDS-PAGE is used to separate proteins based on their size. Polyacrylamide gel electrophoresis (PAGE) using sodium dodecyl sulphate (SDS) which linearizes protein and imparts an even negative charge per unit mass enabling separa-

tion based on size (Shapiro et al. 1967). 4 % stacking gel and 15 % or 8 % resolving gel was used here in order to separate proteins recovered from nanoparticle surfaces (I).

3. Results and discussion

This work initially focuses on hydrophobin assembly onto nanoparticles and the subsequent recruitment of plasma proteins in order to describe the self-assembly and recruiting properties of the hydrophobin proteins (I). In order to further describe hydrophobin interaction with its surrounding, the abilities to form surface films on varying surfaces and interfaces by self-assembly and to selectively recruit proteins to surface films are examined. In order to study the roles and function of charged side chains of the protein, point mutations of the residues on HFBI were produced (II). Following this, the role of the hydrophilic side of hydrophobins replicating anchoring of the proteins on spores and cell walls and thereby rendering them hydrophobic are described as well as the roles of charged residues on the hydrophilic side in terms of interactions with polar surfaces by allowing hydrophobins to assemble onto solid polar hydrophilic surfaces in solution (III). Lastly, hydrophobin solution dynamics is described in terms of hydrophobin solution multimer exchange and how the exchange is affected by the environment on terms of other hydrophobins, proteins and surfactants (IV).

3.1 Hydrophobin self-assembly on surfaces and recruiting of proteins (I)

All hydrophobins adhere to surfaces, and hydrophobins have been shown to play important roles as coatings of fungal spores (Wösten 2001; Linder et al. 2005). Hydrophobin HFBII was allowed to physically adsorb on monodisperse carboxylated (PCOOH) and sulfonated ($PSOSO_3$) polystyrene nanoparticles (NPs) of nominally 100 nm and 200 nm in diameter. The sulfonated NPs can be seen as more hydrophobic. HFBII binding onto NPs was examined with Dynamic light scattering (DLS), Differential centrifugal sedimentation (DCS) and SDS-PAGE and protein binding was seen on both types of particles (I). In order to examine the ability of hydrophobins to recruit other proteins to surfaces, human plasma proteins were allowed to adsorb on the NP-HFB complexes (I).

3.1.1 Form layers on NP surface by self-assembly

HFBII binding to NPs was examined using DLS, DCS and SDS-PAGE. NP size and charge were examined on both pristine (uncoated) particles and on NPs after incubation with HFBII. Hydrophobin coating was done using a dialysis process. Figure 4 shows how HFBII was successfully adsorbed on the two types of NPs of both sizes, seen as a strong and consistent band of 7 kDa.

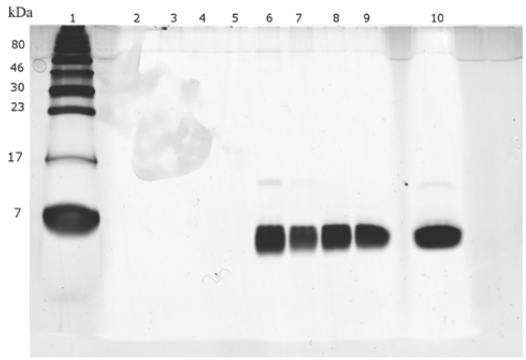

Figure 4. SDS-PAGE gel showing the adsorption of HFBII to 100 and 200 nm carboxylated and sulfonated NPs. Lane 1: ladder; lane 2: 100 nm carboxylated NP; lane 3: 200 nm carboxylated NP; lane 4: 100 nm sulfonated NP; lane 5: 200 nm sulfonated NP; lane 6: 100 nm carboxylated NP with HFBII; lane 7: 200 nm carboxylated NP with HFBII; 8: 100 nm sulfonated NP with HFBII; 9: 200 nm sulfonated NP with HFBII; 10: HFBII control sample.

In DCS measurements, protein adsorption and NP size was measured as a change in density where particle apparent size seen as a change of sedimentation time. A core shell model was applied for accurate size measurement of protein layer thickness using the known density of the protein (I). NPs of 200 nm in size are shown as an example in Figure 5. The results show that NPs of both types and sizes resulted in a shift in apparent size (Table 1) as a result of change of density and/or protein binding. A stronger and more severe shift was observed with sulfonated NPs suggesting stronger binding.

The shell thickness for the 200nm NPs was calculated as 2.3 nm and 1.4 nm for sulfonated and carboxylated respectively (Figure 5). On the sulfonated NPs, a layer of dimensions similar to a theoretical monolayer was thus seen, as the he approximate diameter of a single hydrophobin is about 2 nm. For 100 nm NPs, the shell thickness was calculated to be 1.2 and 0.3 nm for 100 nm sulfonated and carboxylated NPs respectively. This data suggests a more uniform protein layer being formed on sulfonated particles. Looking at approximated diameters on DLS measurements, where a change of hydrodynamic radius is larger on sulfonated NPs, and at 100 carboxylated NPs relatively unchanged, supporting the theory of lower protein binding and less uniform layers being formed on these particles (Table 2).

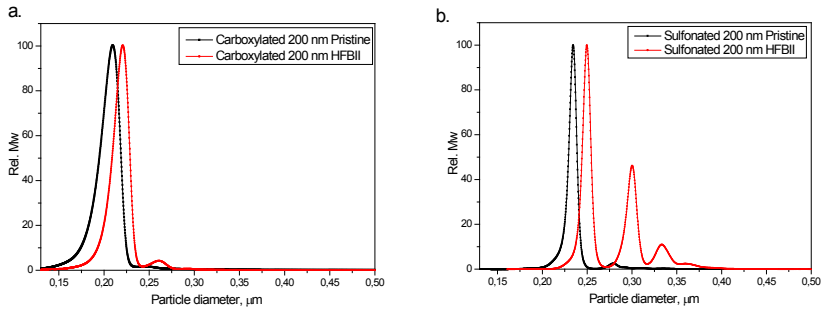

Figure 5. DCS experiments of 200nm carboxylated (a) and sulfonated (b) PS NPs on pristine NPs and on NP- HFBII complexes.

Sample		**Particle apparent size (by DCS)**		**Shell thickness nm**
Surface modification	Particle nominal size [nm]	Pristine [nm]	NP-HFB [nm]	
carboxylated	100	113.2	116.3	0.3
	200	209.6	221.1	1.4
sulfonated	100	96.6	106.1	1.2
	200	234.3	251.4	2.3

Table 1. NP-HFBII: Shell thickness by DCS

The surface charge in terms of zeta potential of NP-HFBII complexes compared to pristine NPs showed similar values in both cases looking at carboxylated NPs. However, the zeta potential of sulfonated NPs was reduced from about 50 mV on pristine NPs to about 30 mV on NP-HFBII complexes of both sizes. This further suggests a more uniform layer being formed on the sulfonated particles, as a thicker layer also was seen in DCS and DLS experiments on these particles. Furthermore, these results also imply that the charged side chains on the hydrophilic side of HFBII can possibly interact and form different type of layers on the two NPs. Hydrophobin HFBI bind differently in terms of orientation on surfaces with varying polarity as is shown in publication III and these differences on surface charge on NP-HFBII complexes suggests that this could be the case also on for HFBII on NPs.

Sample			DLS				
Surface modification	Particle size [nm]	Sample coating	Dm, [nm]	SD	PDI	Zpot [mV]	SD
carboxylated	100	Pristine	111.4	0.6	0.03	-46	0.8
		NP-HFB	111.0	1.7	0.02	-47	1.6
	200	Pristine	196.1	0.8	0.02	-50	1.0
		NP-HFB	202.3	1.9	0.01	-44	0.5
sulfonated	100	Pristine	103.2	0.8	0.04	-50	3.1
		NP-HFB	120.6	1.2	0.09	-28	0.6
	200	Pristine	234.5	1	0.02	-47	0.6
		NP-HFB	302.5	1.4	0.21	-32	1.7

Table 2. NP-HFBII: Z-potential, size by DLS

3.1.2 Recruitment of plasma proteins

In order to examine the recruitment of proteins to a surface via bound hydrophobins, human plasma was allowed to bind onto NP-HFB complexes. A few tens of about 4000 human plasma proteins form a strongly bound protein layer (corona) on NPs, called the hard corona (HC). An external layer of proteins with less affinity, the soft corona, is in exchange with the environment, whereas the HC proteins are in slow exchange. The HC is analysed after separating and washing. The corona of NPs directly in plasma, unwashed and unseparated, is called *in situ* corona (IS).

In HC measurements, the pristine sulfonated NPs generated strong aggregation in presence of plasma making size measurements in DCS difficult. On sulfonated NP-HFBII complexes, aggregation was small, allowing for protein size measurements (Figure 6). Looking at carboxylated NPs, HFBII is reducing the calculated corona thickness compared to pristine NPs (Table 3).

In IS measurements, sulfonated pristine NPs also generated aggregation, but apparent size was however measurable. As was seen in HC measurements, HFBII reduced aggregation dramatically. A hydrophobic coating on both sulfonated and carboxylated NPs of both sizes resulted in a considerate decrease in the corona thickness compared to the corona formed on pristine NPs (Table 3).

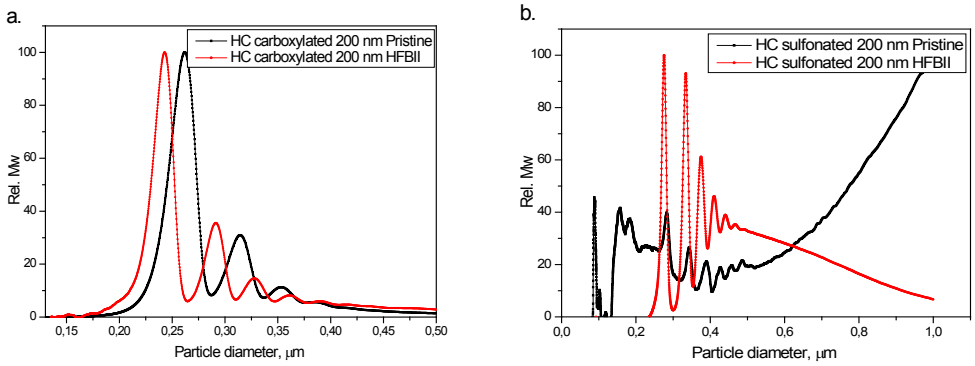

Figure 6. DCS of particles with HC. Performed on pristine NPs and NP – HFBII complexes. Here represented by 200 nm NPs.

Sample			IS			HC		
NP	Particle size [nm]	Sample coating	Plasma corona [nm]	Change [nm]	[%]	Plasma corona [nm]	Change [nm]	[%]
carboxylated	100	Pristine	7.5			6.4		
		NP-HFB	6.3	-1.2	-16	4.7	-1.7	-26.6
	200	Pristine	8.3			7.2		
		NP-HFB	3.7	-4.6	-55	3.1	-4.1	-56.9
sulfonated	100	Pristine	6.9			Agg.		
		NP-HFB	4.5	-2.4	-35	1.6		
	200	Pristine	11			Agg.		
		NP-HFB	6.2	-4.8	-44	3.3		

Table 3. NP Protein Corona thickness by DCS.

In order to examine the HC plasma protein composition, plasma proteins were removed from the particles by reducing and heating in SDS and separated by SDS-PAGE, 15 % and 8 % (Figure 7). SDS-PAGE of IS plasma proteins was not carried out as the result would be inconclusive since non-bound plasma would be seen in the staining. In HC, SDS-PAGE indicated that plasma proteins adsorb on NPs in all cases. All HFBII treated NPs show a clear HFBII band at 7 kDa in the 15 % gel, a band that was missing on all NPs not in contact with hydrophobin. It is noteworthy that HFBII remained strongly associated to all NPs also after incubation in a competitive environment of plasma proteins. In order to look at the HC plasma protein layer composition, an 8 % SDS-PAGE gel was run where proteins of 250-60 kDa have better resolution. Interestingly, the levels of several HC plasma proteins were affected comparing NP-HFBII complexes to pristine NPs, especially in the case of sulfonated particles. The amounts of smaller plasma proteins were altered in the presence of HFBII in all four cases of NPs and sizes. HFBII did thus seem to have not only an effect on the apparent size and calculated corona thickness but also on the composition of the corona.

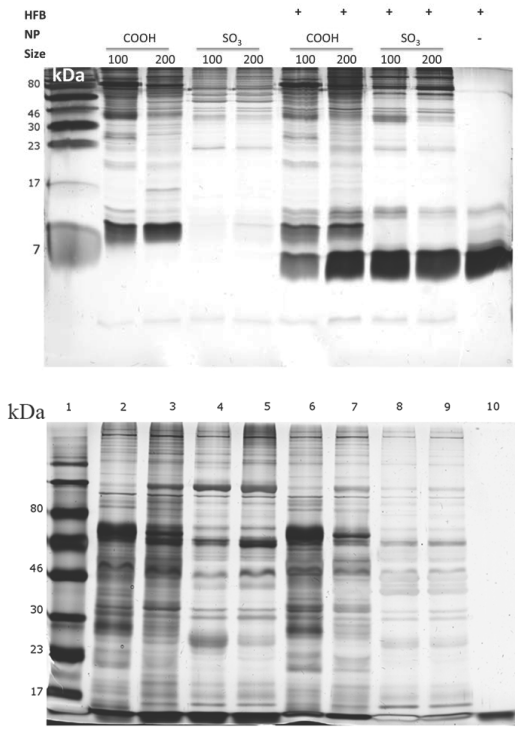

Figure 7. (top) 15 % SDS-PAGE of human plasma proteins free from excess plasma obtained from the hard corona of carboxylated (COOH) and sulfonated (SO_3) nanoparticles. Sample identification is provided on the top of the gel. (bottom) 8 % SDS-PAGE of human plasma proteins free from excess plasma obtained from the hard corona of carboxylated and sulfonated nanoparticles, 100 and 200 nm with pristine and covered with HFBII. Sample order:

1. Ladder, 2. carboxylated 100 nm +HFBII + Corona, 3. carboxylated 200 nm + HFBII + Corona, 4. Sulfonated 100 nm + HFBII + Corona, 5. Sulfonated 200 nm +HFBII + Corona, 6. carboxylated 100 nm + Corona, 7. carboxylated 200 nm + Corona, 8. Sulfonated 100 nm + Corona, 9. Sulfonated 200 nm + Corona, 10. HFBII

HFBII was here shown to strongly adsorb on polystyrene nanoparticles of varying polarity. A stronger binding was seen on the more hydrophobic sulfonated polystyrene NPs where a layer thickness of about a monolayer of 200 nm was observed. Hydrophobin HFBI bind differently in terms of orientation on surfaces with varying polarity as is shown in publication III and differences on surface charge on NP-HFBII complexes suggests that this could be the case also on NPs. The charged side chains on the hydrophilic side of HFBII can possibly interact and form different type of layers on the two nanoparticles.

HFBII was also shown to be tightly bound to the NPs also in competition with human plasma proteins. Adsorption of HFBII on the particles significantly reduced aggregation on sulfonated NPs in plasma suggesting use as an agent to increase bioavailability. Hydrophobins have previously been used to increase bioavailability of Teflon nanoparticles (Lumsdon et al. 2005), and have been suggested to improve dispersions of materials with advantageous electrochemical such as highly oriented pyrolytic graphite (HOPG), two-dimensional crystalline graphene, and single- and multi-walled carbon nanotubes (CNT) (Wösten & Scholtmeijer 2015).

On both types of NPs examined, hydrophobins showed a potential ability to recruit other proteins bound to a surface, as an adsorbed layer of hydrophobin was shown to bind a layer of plasma proteins forming a protein corona different in both composition and mass compared to plasma coronas formed on pristine NPs.

3.2 Interfacial assembly and interactions of other proteins, role of charged residues (II)

In order to further examine hydrophobin interaction with its surrounding, the ability of HFBI to form surface films on surfaces and interfaces by self-assembly and to selectively recruit proteins to surface films was studied. In order to examine the roles of charged side chains of the protein, point mutations of the residues on HFBI were produced (II).

3.2.1 Mutation variants of HFBI

HFBI possesses six charged residues that are exposed on the protein surface (Figure 8). Four of these are located on the face of the protein opposite of the hydrophobic patch (D40, D43, R45 and K50). The remaining two, D30 and K32, are located near the edge of the hydrophobic patch. Mutation variants were produced in four different types by neutralizing charged residues by replacing the charged residues with electrically neutral ones (II). The residues D30 and K32 located near the hydrophobic patch and potentially important for intermolecular interactions (Magarkar et al. 2014) were neutralized to form mutation D30N/D32Q. Neutralized positively charged residues formed the

negatively charged variant R45Q/K50Q, the positively charged variant D40Q/D43N was formed with neutralized negatively charged residues and a neutral variant with all charged residues neutralized was named D40Q/D43N/R45Q/K50Q.

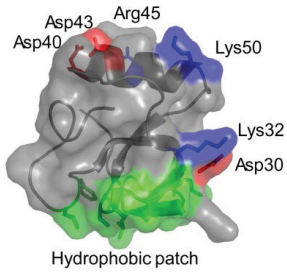

Figure 8. Three-dimensional structure of *T. reesei* hydrophobin HFBI (PDB-ID 2FZ6). Basic and acidic residues are annotated and coloured blue and red, respectively (II).

3.2.2 Behaviour of adhesion, effect of charged residues

HFBI variants and wild-type hydrophobin was allowed to bind onto hydrophobic 1-hexanethiol (HEX) self-assembled monolayer (SAM) surfaces. In order to measure protein adhesion and adsorption of the bound protein layer on the coated surfaces, QCM-D was used to detect frequency and dissipation and convert into bound mass (Figure 9, II). The adsorption into the hydrophobic surface was shown to be very similar among the tested HFBI variants and also in the range of adsorption of wild-type HFBI (Table 4).

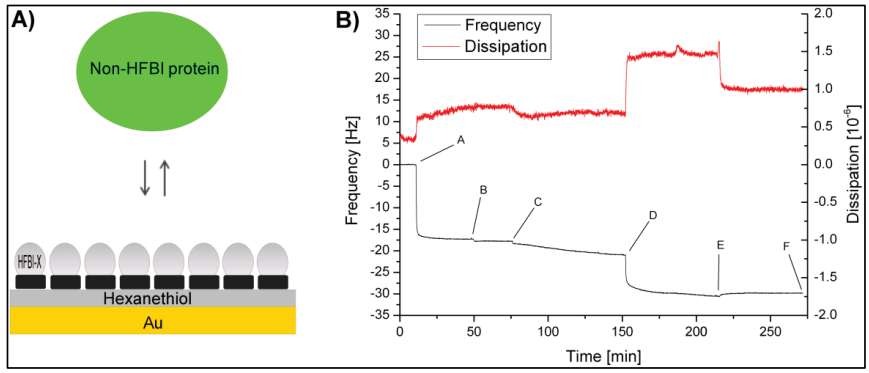

Figure 9. A) Schematic representation of the HFBI coated QCM sensor at which adsorption of non-HFBI proteins was measured; B) Representative protein adsorption QCM experiment at pH 9.0 with HFBI variant D40Q/D43N: (A) Injection of 0.03 mg HFBI-D40Q/D43N in 10 mM Na acetate buffer (pH 5.5), (B) removal of unbound hydrophobin by buffer rinsing, (C) equilibration with 10 mM glycine buffer (pH 9.0), (D) injection of 0.3 mg glucose oxidase at pH 9.0, (E) washing off of unbound glucose oxidase, (F) end of experiment. The adsorbed mass of the non-HFBI protein was calculated using the frequencies at points D and F.

	wild type	D30N/K32Q	D40Q/D43N	R45Q/K50Q	D40Q/D43N/R45Q/K50Q
HAM [ng/cm^2]	223 ± 98	247 ± 35	289 ± 45	217 ± 35	293 ± 56
γ [mN/m]	35.5 ± 1.6	36.5 ± 0.0	31.3 ± 7.5	36.0 ± 0.6	36.6 ± 0.3
t_{DF}	19 ± 3.5	24.3 ± 1.2	32.3 ± 2.5	23.7 ± 3.8	31.3 ± 3.5

Table 4. The hydrophobically adsorbed mass (HAM) was determined from the presented QCM experiments on hexanethiol coated surfaces. (γ) were determined from interfacial HFBI protein layers assembled in a Langmuir trough. (t_{DF}) represents time required for plateau formation of droplet of hydrophobin in solution, measured in triplicate.

3.2.3 Recruitment of other proteins to surfaces

The binding of proteins to self-assembled hydrophobin layers was examined with QCM-D. This was done by adding secreted *T. reesei* enzymes XYNI, XYNII, CBHI and EGII to adsorbed layers of HFBI, wild-type and variants, formed on hexanethiol-coated surfaces. As a reference, Glucose oxidase (GOx) of *A. niger* was in the same matter added to the hydrophobin layer.

GOx was found to interact strongly with the wild-type and all variants, with highest amounts bound at pH 4.7 – 5.7. A second adsorption maximum was measured for variant D40Q/D43N at pH 6-9 (Figure 10A).

No binding was detected with XYNI and EGII (Figure 10B, E). XYNII bound exclusively variant D40Q/D43N, with a binding maximum of 100 ng/cm^2 at around pH 5.2 and around 60 ng/cm^2 in other pHs measured (Figure 10C). In the case of CBHI, wild-type HFBI and variants R45Q/K50Q as well as D40Q/D43N bound between pH 3.9 – 4.7. D40Q/D43N binding of CBHI was considerably higher (570 ng/cm^2 at pH 4.7 than wild-type HFBI (60 ng/cm^2 at pH 3.9) and R45Q/K50Q (20 ng/cm^2 at pH 3.9)(Figure 10D).

Hydrophobins have previously been shown to form protein films and to bind other molecules to this film (Bilewicz et al. 2001; Corvis et al. 2006; Qin et al. 2007; Zhao et al. 2007; Palomo et al. 2003). Furthermore, it has previously been suggested that interactions between hydrophobin and a second layer of proteins are due to electrostatic interactions (Wang et al. 2010). In this work, binding of *T. reesei* enzymes XYNII and CBHI is shown to be very selective in terms of charged residues in HFBI surface. HFBII adsorbed on NPs was shown to adsorb layers of human plasma proteins in different manner when adsorbed on NPs of varying polarity, supporting the conclusion of importance of charged residues (I). Adsorption of hydrophobins on two structurally different anionic surfaces generated very similar results in term so binding and hydrophobicity of bound layer, which compared to a very low binding on anionic surfaces, indicates that specific charge is very important (III). However, hydrophobins might be able to assemble on surfaces in defined orientations related to each other, and to form pores and pockets with structurally defined environments (Figure 11) according to computational modelling. Such pockets can form very selective environments, as has been shown using cyclodextrins (Ling et al. 2008). The structure on the hydrophobin layer can thus have a large effect on the adsorption selectivity. Detailed conclusions on the nature of interactions between hydrophobin layers and a secondary layer of molecules cannot be drawn, but the binding of a secondary layer however seems to be very specific.

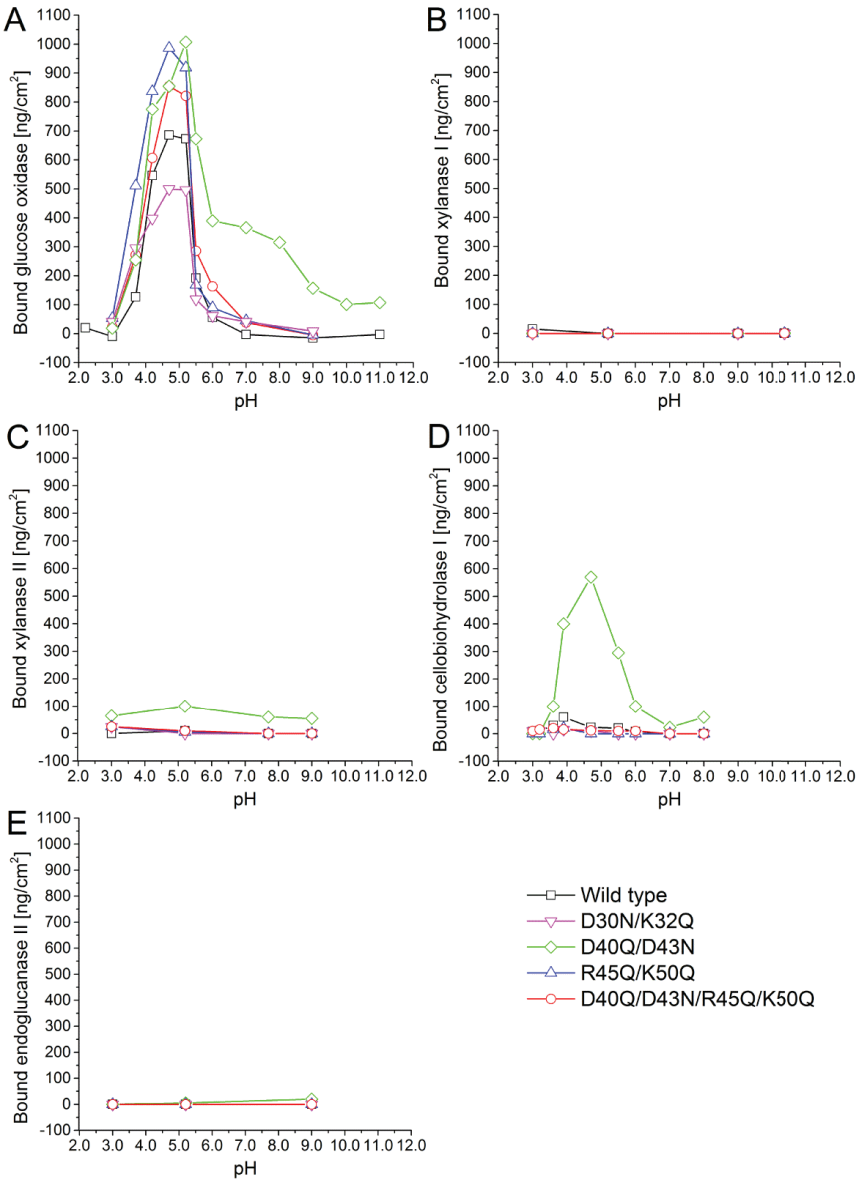

Figure 10. pH-Dependent adsorption of non-HFBI proteins to adsorbed layers of HFBI wild type and HFBI variants D30N/K32Q, D40Q/D34N, D40Q/D34N/R45Q/K50Q and R45Q/K50Q determined by QCM-D. The injected non-HFBI proteins were *Aspergillus niger* glucose oxidase (GOx) (A, pI 4.2) and the *Trichoderma reesei* proteins xylanase I (XYNI) (B), xylanase II (XYNII) (C) cellobiohydrolase I (CBHI) (D) and endoglucanase II (EGII) (E). The adsorption data on glucose oxidase binding to HFBI wild type layers was originally published by (Wang et al. 2010).

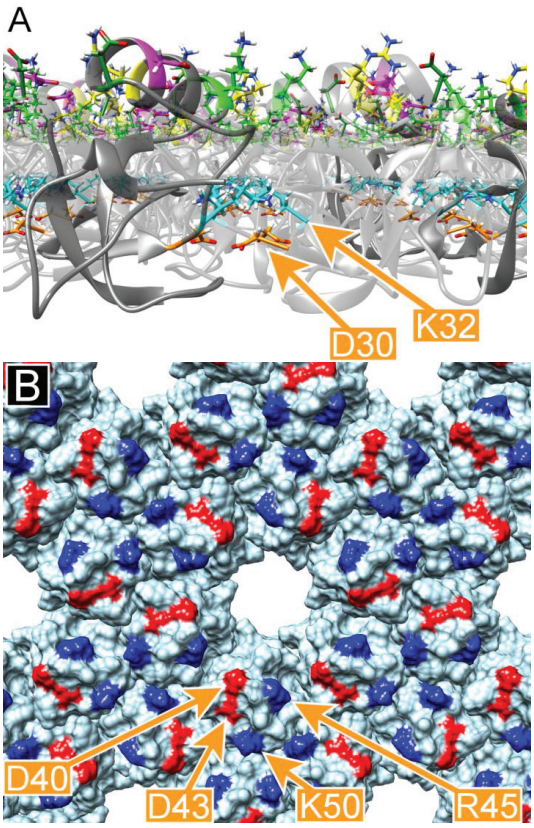

Figure 11. (A) side-view of a computational model of membrane formed by HFBI (Magarkar et al. 2014). Residues D30 and K32 are located within the membrane and are positioned so that they can form ionic bonds between HFBI molecules. (B) HFBI membrane viewed from its hydrophilic face. Residues D40, D43, R45 and K50 are exposed at the surface.

3.2.4 Formation of films at air-water interface

The behaviour of HFBI variants at the air-water interface displayed interesting properties. Firstly, the formation of a flattened plateau on top of a hydrophobin solution droplet was examined (II). The formation of plateau is a characteristic property of HFBI and is likely due to a formation of a hydrophobin monolayer at the air-water interface (Szilvay, Paananen, et al. 2007). All variants produced the same plateau forming effect, but at a varying time scale. For the wild type, the time formation was 19 ± 3.5 min, and for the variants the time was 30 – 70 % longer (Table 4).

Secondly, surface tension reduction upon HFBI layer formation on the air-water interface was measured using a Langmuir through in order to assess the protein concentration in the layers (II). In these measurements, there was little difference between the wild type (35.5 ± 1.6 mN) and the variants (Table 4).

The structure of hydrophobin films at the air-water interface has previously been examined by AFM (Szilvay, Paananen, et al. 2007). The authors showed that the film formed at the air-water interface by HFBI had a well ordered hexagonal structure and was represented by oligomer-like assemblies. The au-

thors further suggested that the hydrophobic patch would be faced towards the air-water interface and the hydrophilic side towards the aqueous environment. In this work, AFM measurements on HFBI variants was carried out similarly by transferring LB films of HFBI onto mica and following AFM measurements (II). All HFBI variants showed ordered structures (Figure 12) comparable to structures of wild-type HFBI (Szilvay, Paananen, et al. 2007). The raft-like structures seen in Figure 12 are likely artefacts of film transfer from larger crystalline domains formed in the air-water interface onto mica.

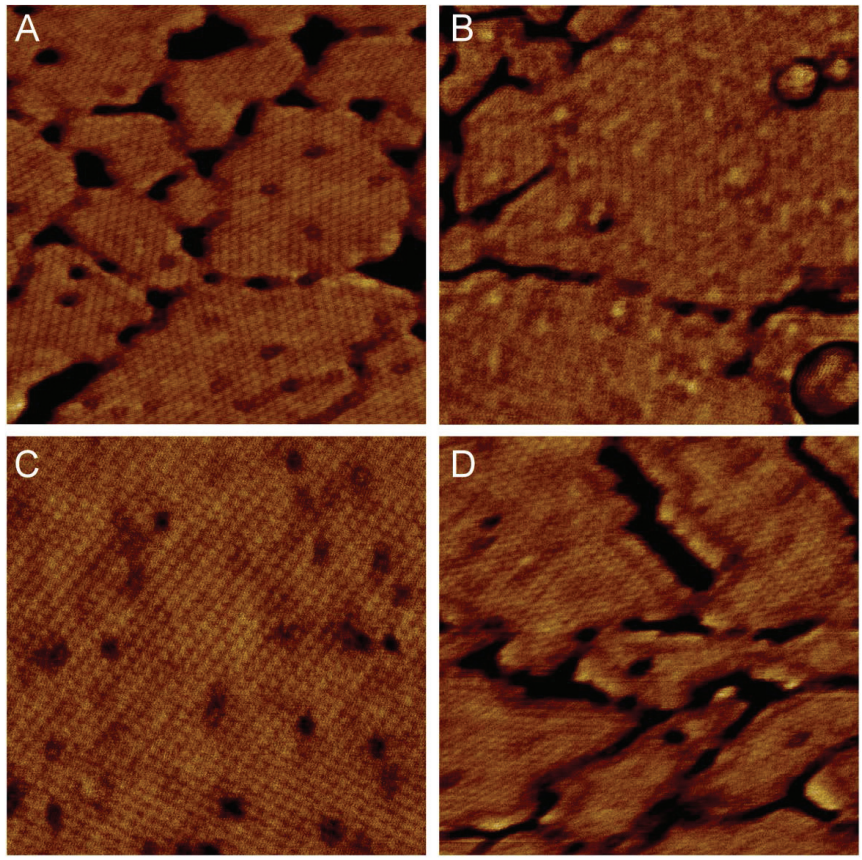

Figure 12. AFM images of LB-films of HFBI that were assembled at the air–water interface and have been transferred to a flat mica substrate, dried and imaged in air using tapping mode. Displayed are typical 200 nm phase images of the HFBI variants D30N/K32Q, D40Q/D43N, R45Q/K50Q and D40Q/D43N/R45Q/K50Q (A–D, respectively).

The clearest differences of hydrophobin films at the air-water interface comparing wild type HFBI and variants were seen examining interfacial rheology properties. The storage modulus (elastic, G′) and loss modulus (viscous, G″) of the hydrophobin layers were determined by interfacial shear rheology measurements (Figure 13). At equilibrium, G′ for the wild-type was 1.04 ± 0.01 N/m, the equilibrium values for variants D30N/K32Q, D40Q/D43N, R45Q/K50Q and D40Q/D43N/R45Q/K50Q were 0.85 ±0.10, 0.62 ±0.01, 1.44 ± 0.03 and 1.09 ± 0.01 N/m respectively (Figure 13A).

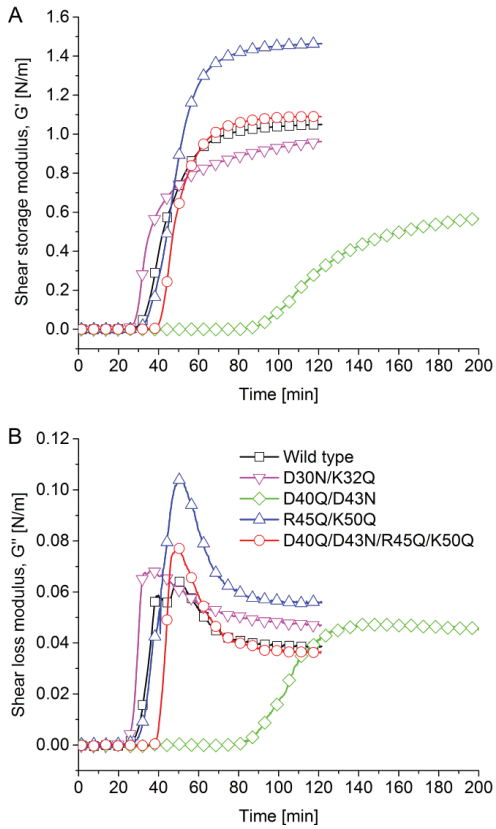

Figure 13. Interfacial rheology data (storage modulus, G' = A; loss modulus, G'' = B) of HFBI wild-type and HFBI variants D30N/K32Q, D40Q/D43N, R45Q/K50Q and D40Q/D43N/R45Q/K50Q at the air-water interface as a function of adsorption time. The interfacial layers are adsorbed from 0.3 μM protein solutions.

The equilibrium shear loss modulus values G″, were less than 0.06 N/m for all hydrophobins, at all cases lower than the G′ values, making them elastic in nature (Figure 13B). Variant R45Q/K50Q showed a ~40 % increase in G′ compared to wild-type. This value is as far as we understand the highest value of storage modulus for a protein film reported compared to literature (Cox et al. 2007). The overall high values of G′ for all variants and wild-type makes the protein films highly elastic. In all cases a remarkably long film formation lag time was detected before onset of significant increase of both G′ and G″. D30N/K32Q displayed the shortest lag time and D40Q/D43N displayed the longest. The overall rate of change was the slowest for D30N/K32Q. The loss modulus also increased the fastest for D30N/K32Q. D30 and K32, neutralized in the D30N/K32Q variant, are located near the hydrophobic patch, on the lateral side of the protein (Figure 8) and could participate in the formation of ionic bonds between molecules (II) . Following this, it is suggested that the residues D30N/K32Q have a role in the mechanism of initial docking in layer formation. Variant D40Q/D43N was showing the longest assembly times and lowest values of G′. Comparing this to the remarkably high G′ value of

R45Q/K50Q, it is interesting to note that the combination of these, where all charged residues have been neutralized, D40Q/D43N/R45Q/K50Q, led to a behaviour in terms of G′ that was close to the wild type and overall behaviour approximately as an average of D40Q/D43N and R45Q/K50Q.

In computational modelling of a membrane (Figure 11) these resiudes are all located on the hydrophilic part of the formed layer and thus not expected to be involved in direct molecular interactions as was suggested for D30N/K32Q. A reason for this could be that the hydrophilic face of the film interacts with other components on the water face. This could possibly be other hydrophobins, further supported by literature where a continuous dynamic state between interface assembled hydrophobin and hydrophobin in solution is presented (Krivosheeva et al. 2013). Furthermore, in publication III is was observed that about 10 % of a self-assembled layer of hydrophobin formed on HEX TMA was removed during washing, which could be composed of hydrophobins in dynamic exchange with the bound layer. As discussed earlier, structure and charge of the hydrophilic face of the hydrophobin layer is having an important role in recruiting a secondary layer of protein when adsorbed on a surface and it is possible that the same face could be interacting with other hydrophobins in solution when forming a layer in the air-water interface.

3.3 Hydrophobin Interactions with polar Surfaces (III)

In publication II it was shown that films formed by hydrophobins selectively bind to proteins and molecules via the hydrophilic side of the film. Furthermore, it has been shown that hydrophobins are involved in making spores and other fungal structures hydrophobic (Nakari-Setälä et al. 1997; Bell-Pedersen et al. 1992). In publication I at was also suggested that hydrophobins bind differently in terms of orientation on spherical surfaces with varying polarity. Following this, it his highly interesting to examine the role of the hydrophilic side of hydrophobins in mediating anchoring of the proteins on spores and cell walls and thereby rendering them hydrophobic, and to further examine the roles of charged residues on the hydrophilic side of the proteins in terms of interactions with polar surfaces. In order to examine these interesting properties, the abilities of hydrophobins to assemble onto solid polar hydrophilic surfaces in solution so that the hydrophobic side of the formed film would face outward towards solution were studied (III).

3.3.1 Interfacial assembly on polar surfaces

Hydrophobin adsorption to both cationic (TMA, PEI) and anionic (MUA) polar hydrophilic surfaces were examined using QCM-D. As a measure of hydrophobicity, the water contact angle (WCA) was measured on all surfaces before and after protein adsorption. The adsorption onto hydrophobic HEX surfaces was also measured. Representative QCM-D adsorption curves are shown in Figure 14.

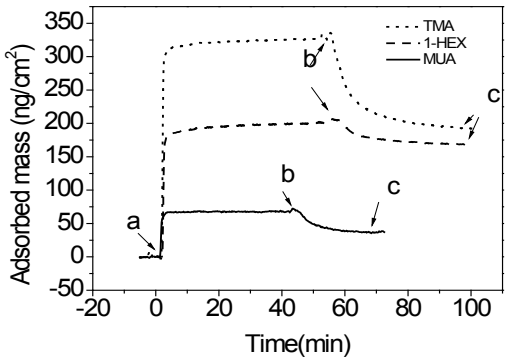

Figure 14. QCM-D sensogram graph showing representative curves of HFBI binding to different self-assembled monolayer (SAM) surfaces. The surfaces used were hydrophobic HEX (at pH 9.5), anionic MUA (at pH 9.0), and cationic TMA (at pH 9.0). Part a corresponds to hydrophobin injection, part b to buffer wash, and part c to end of buffer wash where adsorbed mass and WCA was measured. The adsorbed mass was calculated from resonance frequency change between the initial point (a) and the final point (c).

On cationic TMA surfaces, the protein adsorption of HFBI, HFBII and HFBII was measured by QCM-D over a pH range between 4.0 and 10.5 (Figure 15A). A negative control TMA surface was treated similarly, but without addition of protein. About half of the initially bound mass was typically removed from the surface during washing (Figure 14). The maximum adsorbed mass of HFBI (215 ng/cm^2) was obtained at pH 9.0, a value close to what is expected for a monolayer which has been approximated as 250 ng/cm^2 (Hakanpää 2006). HFBII and HFBII bound to the TMA layer, but at lower levels. The corresponding WCAs before and after hydrophobin coating are seen in Figure 15B. Water drop profiles corresponding to pHs with highest WCAs for each protein are presented in Figure 15D. The TMA surface had a WCA of about 22.3° ±5.7° before coating. All three proteins show a similar pH dependency on WCA, with a maximum peak at pH 8.0 -9.0 with WCAs clearly higher (60- 70°) that the buffer only sample (28 – 30°). Effect of type of buffer used WCA values was examined by measuring WCA on a narrow pH range with different buffers (Figure 15C). A minor buffer related effect was detected, (roughly 5°). The strong pH dependency indicates that electrostatic interactions are important for the interaction between hydrophobin layer and the polar, cationic surface.

Further examining the pH dependency of adsorption, HFBI and HFBII was also allowed to adsorb on hydrophobic HEX SAMs in the same PH range (Figure 16). Here it was expected that the hydrophobins interact with the surface via their hydrophobic patch (Wang et al. 2010) and as result the binding should show low pH dependency. It was observed that hydrophobin adsorbed between 170 and 282 ng/cm in the surface after about 10 % of binding was lost during the washing step. WCAs were measured as 39° and 56° and between38° and 50° for HFBI and HFBII respectively. Comparing these values to an uncoated reference HEX surface under the same condition, the hydrophobin adsorption made the surfaces clearly more hydrophilic indicating binding via the hydrophobic patch. The adsorption was non pH dependant as expected.

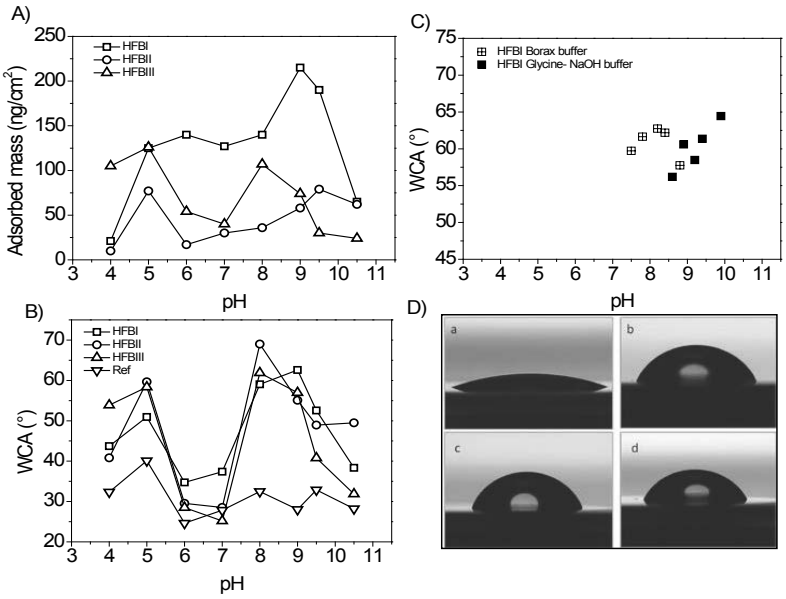

Figure 15. Adsorption of hydrophobins on cationic SAM surfaces. (A) QCM-D derived adsorbed mass of HFBI, HFBII, and HFBIII on TMA SAM surface as a function of pH. (B) WCAs of the same surfaces after hydrophobin adsorption in QCM-D runs as a function of pH. WCAs after HFBI, HFBII, or HFBIII adsorption are shown, as well as a negative control surface (labeled ref) that was treated similarly but without addition of protein. (C) WCA of HFBI on a TMA SAM surface at a narrow pH range. (D) Water drop profile shapes from WCA measurements on TMA SAM surfaces before protein coating (a), after HFBI (at pH 9.0) (b), HFBII (at pH 8.0) (c), and HFBIII (at pH 8.0) (d) coating. The obtained WCAs were 22.3° before deposition, and 62.6°, 69.0°, and 61.9°, after HFBI, HFBII, and HFBIII adsorption, respectively

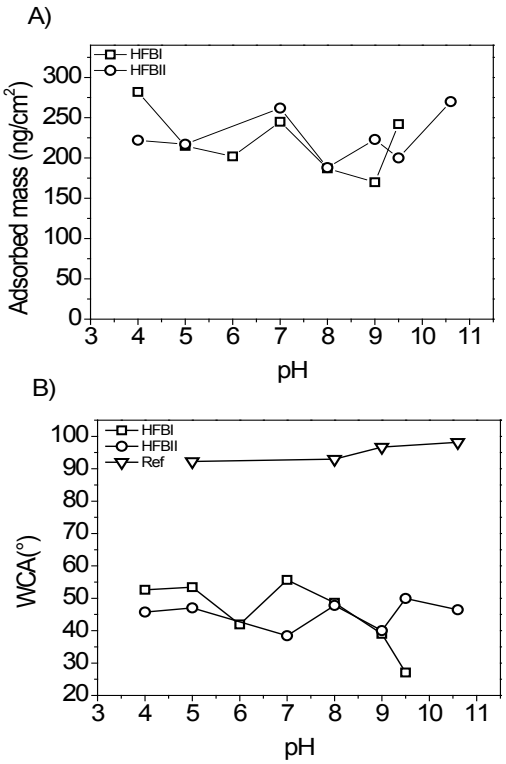

Figure 16. Adsorption of hydrophobins on hydrophobic surfaces. (A) Graph of adsorbed mass of HFBI and HFBII on hydrophobic HEX SAM as a function of pH as observed by QCM-D. (B) WCAs as a function of pH of the HEX SAM coated QCM-D sensors after HFBI or HFBII adsorption. A negative control surface (labeled ref) was treated similarly but without addition of protein. The standard deviation for HFBI on HEX SAM was ±6.7° (N =3) at pH 9.

In order to study the effect of the type of cationic surface, QCM-D and WCA experiments were repeated using HFBI on a structurally different surface, spin-coated cationic polymer PEI (Figure 17). The amount of HFBI adsorbed on the PEI surface (WCA 10° before deposition) as a function of pH shows a peak at pH 5.0 and a maximum binding at pH 10.0 where 260 ng/cm² was adsorbed. Also WCA values show two peaks, a smaller peak at pH 5.0 and a maximum peak at pH 8.0 (50.3°). Hydrophobin adsorption on PEI thus show binding and WCA similar to assembly on TMA as well as a similar pH dependency.

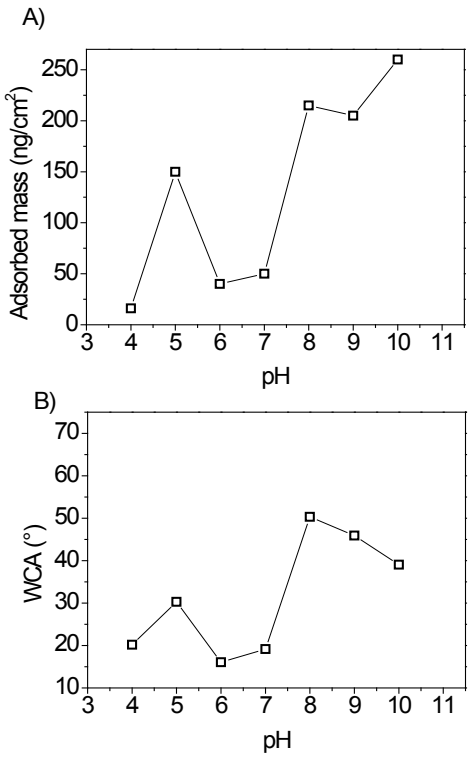

Figure 17. Adsorption of HFBI on cationic PEI surfaces. (A) Mass of adsorbed HFBI on cationic PEI surface as observed by QCM-D at various pHs. (B) WCAs of HFBI coatings on PEI after QCM-D measurements as a function of pH. The WCA of PEI surface before deposition was <10°.

Negatively charged SAM surfaces formed by 1-mercaptounedacanoic acid (MUA) was in a following step studied with QCM-D and WCA measurements to further examine the effect of charge on hydrophobin adsorption (Figure 18). At low pH, there was a significant protein binding with amounts close to a theoretical monolayer, but the binding rapidly decreased with increasing pH. The WCAs were however lower after HFBI adsorption compared to uncoated MUA SAM (31.5° ±3.3°) in the whole pH range. HFBI was thus showed to be inefficient to adsorb in anionic surfaces in order to change their polarity.

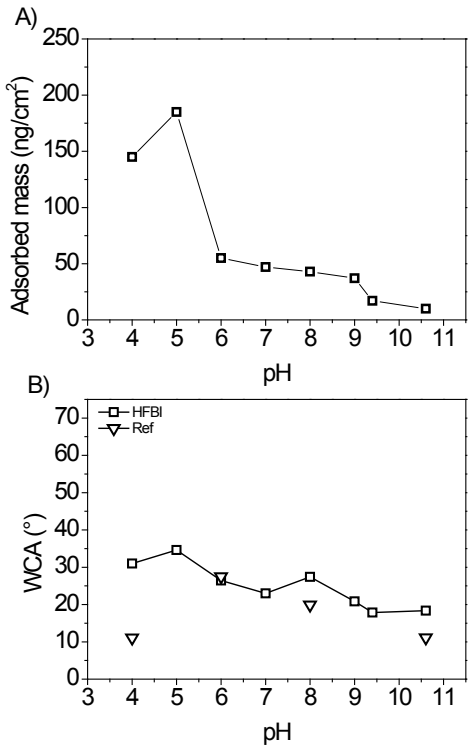

Figure 18. Adsorption of HFBI on anionic MUA SAM. (A) QCM-D derived mass of adsorbed HFBI on MUA as a function of pH. (B) WCAs of the same surface after HFBI adsorption as well as a negative control surface (labelled ref) that was treated similarly but without addition of protein are shown.

In order to further study the nature of interaction of HFBI on polar surfaces and the possible role of electrostatic interactions, HFBI was allowed to adsorb on TMA SAMs at increasing ionic strength using NaCl at different concentrations (0, 10, 25, 50, 75, 100, 500 mM) at pH 9.0 (Figure 19). Both bound mass and WCA was shown to rapidly decrease with increasing ionic strength, further indicating that electrostatic interactions are important for the interaction between hydrophobin layer and polar, cationic surface.

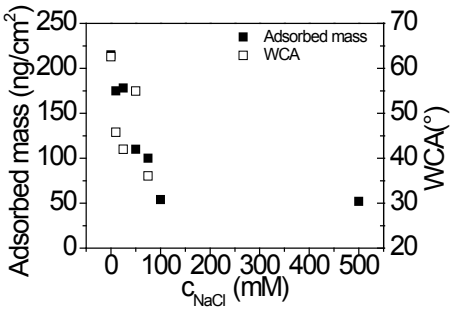

Figure 19. HFBI adsorption to cationic TMA SAMs as a function of NaCl concentration. QCM-D derived adsorbed mass and WCA are shown. The protein adsorption was done at pH 9.0

Hydrophobin was here observed to effectively change the polarity of both hydrophilic and hydrophobic surfaces through self-assembly in solution. Dependency on pH and ionic strength observed when adsorbing hydrophobins on polar cationic surfaces indicates that electrostatic interactions are important for the interaction between a hydrophobin layer and surfaces, especially as a similar pH dependency was not observed when adsorbing hydrophobin on a hydrophobic reference surface. Experiments in two structurally different anionic surfaces (TMA and PEI) generated very similar results and compared to very low binding on anionic surfaces, indicating that in this case, specific charge was very important. Interestingly, in publication II it was suggested that structure is important on recruiting proteins to the hydrophilic side of the film, and holes in the film has been suggested in modelling (II, Figure 11). AFM imaging on films formed on TMA SAM were made but specific features could not be seen other than the formation of a uniform layer (III).

The results shown here indicate that the layers formed by hydrophobins on surfaces with varying polarity are amphiphilic with one side giving a low contact angle and the other a high contact angle. When adsorbing on a hydrophobic surface, the hydrophilic side of the layer is turned towards the solution as has also been suggested previously for layers formed at the air-water interface (Szilvay, Paananen, et al. 2007). The presence of hydrophobin resulted in an increase of WCA of almost 40° after adsorption on a cationic surface suggesting that the hydrophobic patch, and the hydrophobic part of the adsorbed film, would be turned towards solution. Ionisable side chains are present on the hydrophilic part of HFBI, HFBII and HFBII surfaces (III), and the importance of pH and ionic strength seen here is likely a result of how these charged residues interact with the surface through electrostatic interactions. The charged residues of HFBI were shown to selectively bind to proteins and molecules via the hydrophilic side of the film in publication II. The results shown here further indicate that the charged residues are important for how the hydrophobins interact with their environment. Hydrophobins have been shown to be involved in making spores and other fungal structures hydrophobic (Nakari-Setälä et al. 1997; Bell-Pedersen et al. 1992) and the self-assembly in

solution described here is a possible mechanism on how hydrophobins assemble in fungal structures resulting in hydrophobic coatings. In publication I it was also suggested that hydrophobins bind differently in terms of orientation on spherical surfaces with varying polarity. Surface curvature and interactions with other proteins and molecules are likely also important in forming the highly hydrophobic fungal structures observed (Approximately 140°, Figure 1). The effect of poly- and monosaccharides on hydrophobin assembly have been observed (Armenante et al. 2010; Scholtmeijer et al. 2009) and hydrophobins can possibly interact with these to form hydrophobic coatings on fungal structures. Nonetheless it is shown that polar surfaces can act as support for amphiphilic hydrophobin membranes and thereby changing the polarity significantly.

3.4 Dynamics and interactions of hydrophobin assembly in solution (IV)

Little is known on the kinetics and thermodynamics of the self-association of hydrophobins in solution. In this work we examine these properties by stopped-flow fluorescence measurements (SF) and Förster Resonance Energy Transfer (FRET) giving an understanding in the process of hydrophobin solution multimer exchange and how the exchange is affected by environment on terms of other hydrophobins, proteins and surfactants (IV). The different types of multimers formed by class II hydrophobins in solution have been described previously. HFBI and HFBII have been shown to form dimers and tetramers (Torkkeli et al. 2002; Kisko et al. 2008) clustered together through their hydrophobic patches (Hakanpää et al. 2004; Hakanpää 2006). Multimerization of HFBI has been shown to be dependent on hydrophobin concentration and HFBI multimers have been shown to continuously disassemble and reassemble in solution. Furthermore, a continuous dynamic state between interface assembled hydrophobin and hydrophobin in solution has been suggested by (Krivosheeva et al. 2013).

3.4.1 Dynamics of hydrophobin multimer exchange

The dynamics of HFBII multimer exchange in solution was examined by Stopped-Flow spectroscopy (IV). A FRET pair of cy3 and cy5 labelled HFBII-CysC, donor and acceptor was used. The samples were prepared with a 1:10 ratio of labelled HFBII-CysC to unlabelled HFBII where each syringe was loaded with 10 μg/ml labelled HFBII and 90 μg/ml wild-type HFBII, with the cy3 in syringe 1 and cy5 label in syringe 2 resulting in a total HFBII concentration in each syringe of 100 μg/ml. 100 μg/ml total HFBII was set as reference. The addition of wild-type mas made in order to reduce the very high fluorescence signal as performed before (Szilvay et al. 2006) and the concentration dependency of FRET signal was controlled in SEC measurements (IV). Liquid from both syringes were simultaneously injected into a small cuvette after which the flow was stopped and the resulting fluorescence was measured. The

formation of FRET signal followed a single exponential curve showing the time dependence of multimer exchange.

Kinetics of hydrophobin multimer exchange was described with exchange half-life, $t_{1/2}$, and was attained from the FRET signal curve (example in Figure 20) fitted as single exponential, giving a $t_{1/2}$ for the exchange of 0.88 sec at 22°C (Table 5).

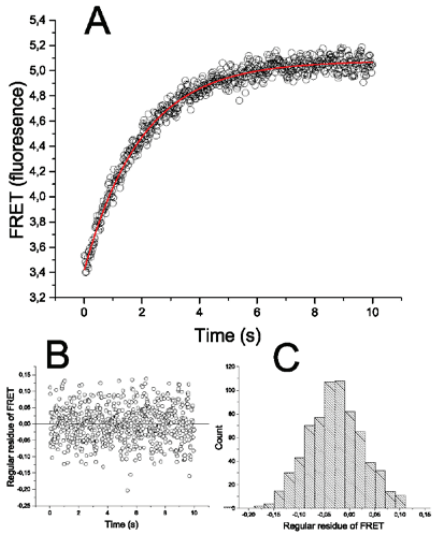

Figure 20. A) Fitting of a single exponential curve of the general form y = A*exp(-x/t1) + y0 to FRET data. B) Residuals show an even distribution throughout the time range of collecting data. C) Residuals have a normal distribution around the fitted curve.

The half-life of protein complexes have been studied previously (Table 5). These can be divided into two groups, a group with $t_{1/2}$ values of milliseconds and those with higher stability with corresponding $t_{1/2}$ values in minutes or hours, reflecting biological functionality. The disassociation of insulin dimers is several times faster, whereas an example of antibody self-association and DNA-binding protein disassociation are slower, with $t_{1/2}$ of about an hour and several minutes respectively. HFBII is placed between somewhere these groups, showing a much faster exchange rate than structural interactions, but still significantly slower than cases where exchange has a biological role. The relatively slow half-life of HFBII multimer exchange is suggested to reflect its biological function, where the multimer driving forces are strong and but still allow dynamic interactions in order to enable the multimer building blocks to take part in growth or surface interactions.

Table 5. Ea, $t_{1/2}$ diss for selected proteins including HFBII

Protein	Ea (kJ/mole)	$t_{1/2}$ diss.	Temp °C
HFBII multimer	92.51	0.88 sec	22
Insulin monomer-dimer (Koren & Hammes 1976)	10.5 ass. 30.9 diss.	6.08* 10^{-9} sec [a]	23
Phosphorylase b, two dimers to tetramer (Muñoz et al. 1983)	12.3 ass.[b] 32.3 diss.[b]	1.5 min [a]	25
Recombinant humanized antibody (rhuMAb) VEGF self-association (Moore et al. 1999)	45.2.	1 h [a]	30
Spectrin dimer – tetramer (Ungewickell & Gratzer 1978)	250.0 ass. 460.0 diss.	10 h [a]	29.5
Intermediate state of folding of Cytochrom C (Yeh et al. 1997)	50.0	0.04 sec [a]	20
Bence-Jones protein Au variable fragment dimerization (Maeda et al. 1978)	N/A	0.005 sec[a]	20
TATA binding protein (TBP) dimer dissacociate (Coleman & Pugh 1997)	N/A	7.4 min	25

Data has been converted to the appropriate units when necessary.[a] Calculated from $k_{diss.}$ assuming first order kinetics ($t_{1/2} = \ln(2)/k_{diss.}$) [b]Approximated using two-point Arrhenius.

Thermodynamics of the hydrophobin multimer exchange was measured by examining the temperature dependency of multimer exchange in SF at three temperatures, (21.5°, 17.5° and 12.5° C). The Arrhenius equation, k=Ae^(-Ea/RT) gives activation energy Ea and frequency factor A by plotting ln(k) vs. 1/T (K), where k is the reaction rate constant from fitting and T temperature (K), example in Figure 21. The activation energy of the HFBII multimer exchange was 92.5 kJ/mole which is in the lower range comparing to other protein complexes (Table 5), but multiple times larger than e.g. an antibody self-association process.

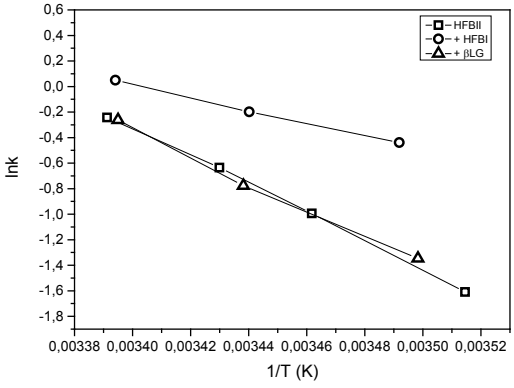

Figure 21. Example of plotting for Arrhenius calculation

3.4.2 Effect on hydrophobin multimer exchange by its surroundings

Addition of HFBI, milk proteins and surfactants was made in order to examine the role of the surroundings on HFBII multimer exchange. The effect on $t_{1/2}$ on

of the multimer exchange by these can be seen in Figure 22, and a comparison using extrapolated values at 20°C is seen in Table 6.

The small surfactant molecules Tween-20 (0.1 %) and Sodium dodecyl sulfate (SDS) (0.01 % in 1:20 labelled : non- labelled HFBII) as well as ethanol (5 %) affected the multimer exchange rate. Ethanol and Tween-20 considerably increased the rate of exchange as seen with lower $t_{1/2}$ values. Tween-20 is likely to interact with the hydrophobic patch of the proteins and ethanol has been shown to dissolve some of the aggregates formed by class II hydrophobins. It is suggested that these molecules are altering hydrophobic interactions in the multimers. The exchange is also shown to be affected by increased ionic strength (NaCl gradient 10, 50, 100 and 200 mM), with larger $t_{1/2}$ observed at higher concentration of NaCl, supporting this conclusion. Furthermore, if electrostatic interactions were involved in e.g. stabilising the complex, a destabilization of the complex and a lower $t_{1/2}$ as a result of salt increase is expected.

Addition of HFBI resulted in a significantly shorter $t_{1/2}$ for exchange in the whole temperature range while a corresponding addition of wild-type HFBII decreased the $t_{1/2}$ by much less, about 10 %. Activation energy also decreased considerably after addition of HFBI (Table 7). This suggests that an interaction between HFBI and HFBII is leading to a destabilization of the HFBII complex making the multimers reassemble at a faster rate. The biological significance of this interaction remains unclear but shows that hydrophobins interact with each other and clearly affect the behaviour of each other. The 10 % decrease in $t_{1/2}$, by doubling the concentration of HFBII indicates that a higher protein concentration to some extent affects how multimers are formed and disassembled, possible due to a shift of size distribution of multimers, e.g. from dimers to tetramers. These may have different rates of formation, but with the methods used here it was not possible to distinguish between these.

β-lactoglobulin and β-casein (1 mg/ml) did not affect the exchange showing that there is little or no interaction between these relative large molecules and the HFBII multimers.

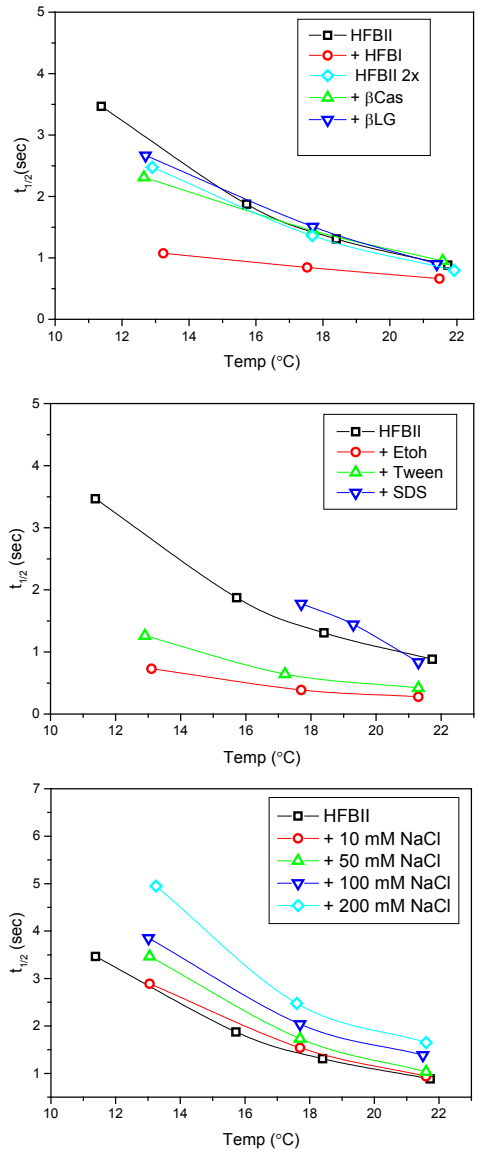

Figure 22. Top: Effect of HFBI,β-casein, β-lactoglobullin and HFBII 2x on t1/2 middle: effect of Tween (0.1 %), ethanol (5 %) and SDS (0.01 % in 1:20 labelled:unlabelled HFBII) on t1/2 bottom: Effect on t1/2 by increasing NaCl concentration.

Table 6. $t_{1/2}$ compared to HFBII reference case using extrapolated data at 20.0° C. Concentrations: Tween (0.1 %), ethanol (5 %) and SDS (0.01 % in 1:20 labelled:unlabelled HFBII) HFBII 100 µg/ml reference is also compared to HFBII 2x (200 µg/ml HFBII, 10 µg/ml labelled HFBII and 190 µg/ml wt HFBII)

	20,0°
HFBII	
+ HFBI	-32 %
HFBII 2x	-10 %
+ βCas	2 %
+ βLG	2 %
+ ethanol	-71 %
+ Tween-20	-55 %
+ SDS	5 %
+ Nacl (mM)	
10	5 %
50	16 %
100	49 %
200	78 %
Extrapolated values	

Table 7. Activation energies, frequency factors. Concentrations: Tween (0.1 %), and ethanol (5 %)

	Ea, kJ/mol	A (Freq. Factor), s^{-1}
HFBII	92.51	1.95E+16
+HFBI	41.38	2.26E+07
HFBII 2x	88.17	3.51E+15
+ βCAS	69.44	1.46E+12
+ βLG	86.83	1.88E+15
+ Etoh	83.38	1.60E+15
+ Tween-20	91.81	3.31E+16
+ Nacl (mM)		
10	92.42	1.77E+16
50	99.33	2.70E+17
100	84.88	5.72E+14
200	92.70	1.17E+16
Note: values for addition of SDS were not possible to obtain due to precipitation in the sample		

In summary the multimerization in solution of HFBII is shown to be a relatively slow exchange process between different multimers. An evident effect of the surroundings on multimer exchange and solution behaviour can be seen as small surfactant molecules as well as increased ionic strength is affecting the exchange rate showing that hydrophobic interactions are important in multimer formation. Commonly used milk proteins casein and β-lactoglobullin do not affect the rate of exchange. The interaction between HFBI and HFBII leads to a destabilization of the HFBII complex making the multimers reassemble at a faster rate, seen as a decrease in $t_{1/2}$, and show that the two hydrophobins interact and clearly affect the behaviour of each other.

4. Conclusions

The results presented here show that hydrophobins function by selectively interacting with their surroundings and that the surroundings in which the proteins exist also affects their function.

Hydrophobins strongly adhere to surfaces of varying polarity and structure by self-assembly, governed by their amphiphilic nature and adsorb with different orientation on hydrophilic and hydrophobic surfaces (I, III). The proteins selectively recruit other proteins and molecules to a self-assembled amphiphilic film of hydrophobin (I, II). Their structure and charged residues are shown to be responsible for these selective interactions. HFBI variants bound to a surface are shown to recruit *T. reesei* enzymes specifically depending on local protein surface charge on the hydrophilic part of the protein (II), and HFBII adsorbed on NPs was shown to adsorb layers of human plasma proteins in different manner when adsorbed on NPs of varying polarity (I). Surface films formed by hydrophobins are highly elastic, and charged residues on the side of the proteins have a role in stabilizing the protein films formed (III). Charged residues located on the hydrophilic part of the formed self-assembled film are suggested as being in a dynamic state with hydrophobins and other proteins and molecules in solution (II, III).

The surroundings in which the proteins exist affect their function. Surfaces of varying polarity in the protein surroundings affect how the proteins self-assemble (I, III). Hydrophobin multimer exchange in solution is shown to be governed by hydrophobic interactions and the multimer exchange behaviour is affected by other proteins and molecules, such as small surfactants and salt interacting with the hydrophobic patch of the proteins, and HFBII and HFBI are shown to interact in solution altering multimer kinetics and thermodynamics considerably (IV).

The specific recruiting and self-assembly behaviour of the proteins depending on polarity shown here gives excellent opportunities for hydrophobin use in specialised coatings on biocompatible implants, self-assembled and anchoring layers on biosensors, and e.g. nanoparticles for drug delivery coated with a hydrophobic coating specifically via secondary binding. Increased knowledge in what type of molecules affect the dynamics of hydrophobin multimer exchange can e.g. be used to make stabilized hydrophobic emulsions in food- and pharmaceutical industry with increased specificity.

The knowledge learned here regarding hydrophobins show that these proteins can be specialised to function as highly selective self-assembling building

blocks, and is enabling development of practical and specific implementations utilizing of a group of common proteins with extraordinary properties.

References

Aimanianda, V. et al., 2009. Surface hydrophobin prevents immune recognition of airborne fungal spores. *Nature*, 460(7259), pp.1117–21. Available at: http://dx.doi.org/10.1038/nature08264 [Accessed March 8, 2015].

Armenante, A. et al., 2010. The Pleurotus ostreatus hydrophobin Vmh2 and its interaction with glucans. *Glycobiology*, 20(5), pp.594–602. Available at: http://www.ncbi.nlm.nih.gov/pubmed/20100692 [Accessed June 1, 2015].

Askolin, S. et al., 2006. Interaction and comparison of a class I hydrophobin from Schizophyllum commune and class II hydrophobins from Trichoderma reesei. *Biomacromolecules*, 7(4), pp.1295–301. Available at: http://www.ncbi.nlm.nih.gov/pubmed/16602752 [Accessed May 31, 2015].

Askolin, S. et al., 2005. The Trichoderma reesei hydrophobin genes hfb1 and hfb2 have diverse functions in fungal development. *FEMS microbiology letters*, 253(2), pp.281–8. Available at: http://www.sciencedirect.com/science/article/pii/S037810970500683X [Accessed May 23, 2015].

Bailey, M.J. et al., 2002. Process technological effects of deletion and amplification of hydrophobins I and II in transformants of Trichoderma reesei. *Applied microbiology and biotechnology*, 58(6), pp.721–7. Available at: http://www.ncbi.nlm.nih.gov/pubmed/12021790 [Accessed May 30, 2015].

Bell-Pedersen, D., Dunlap, J.C. & Loros, J.J., 1992. The Neurospora circadian clock-controlled gene, ccg-2, is allelic to eas and encodes a fungal hydrophobin required for formation of the conidial rodlet layer. *Genes & development*, 6(12A), pp.2382–94. Available at: http://www.ncbi.nlm.nih.gov/pubmed/1459460 [Accessed May 23, 2015].

Bilewicz, R. et al., 2001. Modification of Electrodes with Self-Assembled Hydrophobin Layers. *The Journal of Physical Chemistry B*, 105(40), pp.9772–9777. Available at: http://dx.doi.org/10.1021/jp0113782 [Accessed May 28, 2015].

Bruns, S. et al., 2010. Production of extracellular traps against Aspergillus fumigatus in vitro and in infected lung tissue is dependent on invading neutrophils and influenced by hydrophobin RodA. *PLoS pathogens*, 6(4), p.e1000873. Available at: http://www.pubmedcentral.nih.gov/articlerender.fcgi?artid=2861696&tool=pmcentrez&rendertype=abstract [Accessed May 23, 2015].

Clegg, R.M., 1992. Fluorescence resonance energy transfer and nucleic acids. *Methods in enzymology*, 211, pp.353–88. Available at: http://www.ncbi.nlm.nih.gov/pubmed/1406315 [Accessed April 19, 2015].

Coleman, R.A. & Pugh, B.F., 1997. Slow dimer dissociation of the TATA binding protein dictates the kinetics of DNA binding. *Proceedings of the National Academy of Sciences of the United States of America*, 94(14), pp.7221–6. Available at: http://www.pubmedcentral.nih.gov/articlerender.fcgi?artid=23798&tool=pmcentrez&rendertype=abstract [Accessed June 1, 2015].

Corvis, Y. et al., 2006. Analytical investigation of the interactions between SC3 hydrophobin and lipid layers: elaborating of nanostructured matrixes for immobilizing redox systems. *Analytical chemistry*, 78(14), pp.4850–64. Available at: http://www.ncbi.nlm.nih.gov/pubmed/16841903 [Accessed May 28, 2015].

Corvis, Y. et al., 2005. Preparing catalytic surfaces for sensing applications by immobilizing enzymes via hydrophobin layers. *Analytical chemistry*, 77(6), pp.1622–30. Available at: http://www.ncbi.nlm.nih.gov/pubmed/15762565 [Accessed May 31, 2015].

Cox, A.R. et al., 2007. Surface properties of class II hydrophobins from Trichoderma reesei and influence on bubble stability. *Langmuir*, 23(15), pp.7995–8002.

Cox, A.R., Aldred, D.L. & Russell, A.B., 2009. Exceptional stability of food foams using class II hydrophobin HFBII. *Food Hydrocolloids*, 23(2), pp.366–376. Available at: http://www.researchgate.net/publication/223162311_Exceptional_stability_of_food_foams_using_class_II_hydrophobin_HFBII [Accessed April 7, 2015].

Fan, H. et al., 2006. Molecular dynamics simulations of the hydrophobin SC3 at a hydrophobic/hydrophilic interface. *Proteins*, 64(4), pp.863–73. Available at: http://www.ncbi.nlm.nih.gov/pubmed/16770796 [Accessed May 25, 2015].

Fang, G. et al., 2014. Novel hydrophobin-coated docetaxel nanoparticles for intravenous delivery: in vitro characteristics and in vivo performance. *European journal of pharmaceutical sciences : official journal of the European Federation for Pharmaceutical Sciences*, 60, pp.1–9. Available at: http://www.ncbi.nlm.nih.gov/pubmed/24815943 [Accessed May 31, 2015].

Geisse, N.A., 2009. AFM and combined optical techniques. *Materials Today*, 12(7-8), pp.40–45. Available at: http://www.sciencedirect.com/science/article/pii/S1369702109702019 [Accessed April 12, 2015].

De Groot, P.W. et al., 1997. Isolation of developmentally regulated genes from the edible mushroom Agaricus bisporus. *Microbiology (Reading, England)*, 143 (Pt 6, pp.1993–2001. Available at: http://www.ncbi.nlm.nih.gov/pubmed/9202475 [Accessed May 23, 2015].

Gruner, M.S. et al., 2012. Self-assembly of class II hydrophobins on polar surfaces. *Langmuir*, 28(9), pp.4293–4300. Available at: http://www.ncbi.nlm.nih.gov/pubmed/22315927.

Haas Jimoh Akanbi, M. et al., 2010. Use of hydrophobins in formulation of water insoluble drugs for oral administration. *Colloids and surfaces. B, Biointerfaces*, 75(2), pp.526–31. Available at: http://www.sciencedirect.com/science/article/pii/S0927776509004639 [Accessed May 27, 2015].

Hakanpää, J. et al., 2004. Atomic resolution structure of the HFBII hydrophobin, a self-assembling amphiphile. *The Journal of biological chemistry*, 279(1), pp.534–9. Available at: http://www.ncbi.nlm.nih.gov/pubmed/14555650 [Accessed May 3, 2015].

Hakanpää, J., 2006. Two crystal structures of Trichoderma reesei hydrophobin HFBI--The structure of a protein amphiphile with and without detergent interaction. *Protein Science*, 15(9), pp.2129–2140. Available at: http://www.pubmedcentral.nih.gov/articlerender.fcgi?artid=2242604&tool=pmcentrez&rendertype=abstract [Accessed April 19, 2015].

Hou, S. et al., 2008. Patterning of cells on functionalized poly(dimethylsiloxane) surface prepared by hydrophobin and collagen modification. *Biosensors & bioelectronics*, 24(4), pp.918–22. Available at: http://www.ncbi.nlm.nih.gov/pubmed/18782664 [Accessed May 31, 2015].

Hou, S. et al., 2009. Surface modification using a novel type I hydrophobin HGFI. *Analytical and bioanalytical chemistry*, 394(3), pp.783–9. Available at: http://www.ncbi.nlm.nih.gov/pubmed/19370343 [Accessed May 31, 2015].

Janssen, M.I. et al., 2002. Coating with genetic engineered hydrophobin promotes growth of fibroblasts on a hydrophobic solid. *Biomaterials*, 23(24), pp.4847–54. Available at: http://www.ncbi.nlm.nih.gov/pubmed/12361625 [Accessed May 31, 2015].

Kallio, J.M., Linder, M.B. & Rouvinen, J., 2007. Crystal structures of hydrophobin HFBII in the presence of detergent implicate the formation of fibrils and monolayer films. *The Journal of biological chemistry*, 282(39), pp.28733–9. Available at: http://www.ncbi.nlm.nih.gov/pubmed/17636262 [Accessed May 25, 2015].

Kazmierczak, P. et al., 2005. A Hydrophobin of the chestnut blight fungus, Cryphonectria parasitica, is required for stromal pustule eruption. *Eukaryotic cell*, 4(5), pp.931–6. Available at: http://www.pubmedcentral.nih.gov/articlerender.fcgi?artid=1140098&tool=pmcentrez&rendertype=abstract [Accessed May 23, 2015].

Kisko, K. et al., 2008. Interactions of hydrophobin proteins in solution studied by small-angle X-ray scattering. *Biophysical journal*, 94(1), pp.198–206. Available at: http://www.pubmedcentral.nih.gov/articlerender.fcgi?artid=2134873&tool=pmcentrez&rendertype=abstract [Accessed May 25, 2015].

Kisko, K. et al., 2005. Langmuir–Blodgett films of hydrophobins HFBI and HFBII. *Surface Science*, 584(1), pp.35–40. Available at: http://www.sciencedirect.com/science/article/pii/S0039602805003651 [Accessed May 25, 2015].

Kisko, K. et al., 2007. Self-assembled films of hydrophobin protein HFBIII from Trichoderma reesei. *Journal of Applied Crystallography*, 40(s1), pp.s355–s360. Available at: http://scripts.iucr.org/cgi-bin/paper?aj6012 [Accessed May 25, 2015].

Koren, R. & Hammes, G.G., 1976. A kinetic study of protein-protein interactions. *Biochemistry*, 15(5), pp.1165–1171. Available at: http://dx.doi.org/10.1021/bi00650a032 [Accessed May 2, 2015].

Kostiainen, M.A. et al., 2006. Multivalent dendrons for high-affinity adhesion of proteins to DNA. *Angewandte Chemie (International ed. in English)*, 45(21), pp.3538–42. Available at: http://www.ncbi.nlm.nih.gov/pubmed/16639766 [Accessed May 31, 2015].

Krivosheeva, O. et al., 2013. Kinetic and equilibrium aspects of adsorption and desorption of class II hydrophobins HFBI and HFBII at silicon oxynitride/water and air/water interfaces. *Langmuir : the ACS journal of surfaces and colloids*, 29(8), pp.2683–91. Available at: http://dx.doi.org/10.1021/la3048888 [Accessed May 29, 2015].

Kwan, A.H.Y. et al., 2006. Structural basis for rodlet assembly in fungal hydrophobins. *Proceedings of the National Academy of Sciences of the United States of America*, 103(10), pp.3621–6. Available at:

http://www.pubmedcentral.nih.gov/articlerender.fcgi?artid=1533775&tool=pmcentrez&rendertype=abstract [Accessed May 25, 2015].

Kyte, J. & Doolittle, R.F., 1982. A simple method for displaying the hydropathic character of a protein. *Journal of Molecular Biology*, 157(1), pp.105–132. Available at: http://www.sciencedirect.com/science/article/pii/0022283682905150 [Accessed November 10, 2014].

Laaksonen, P. et al., 2010. Interfacial engineering by proteins: exfoliation and functionalization of graphene by hydrophobins. *Angewandte Chemie (International ed. in English)*, 49(29), pp.4946–9. Available at: http://www.ncbi.nlm.nih.gov/pubmed/20533486 [Accessed May 31, 2015].

Laaksonen, P. et al., 2009. Selective nanopatterning using citrate-stabilized Au nanoparticles and cystein-modified amphiphilic protein. *Langmuir : the ACS journal of surfaces and colloids*, 25(9), pp.5185–92. Available at: http://www.ncbi.nlm.nih.gov/pubmed/19253945 [Accessed May 31, 2015].

Linder, M. et al., 2002. Surface adhesion of fusion proteins containing the hydrophobins HFBI and HFBII from Trichoderma reesei. *Protein Sci*, 11(9), pp.2257–2266. Available at: http://www.ncbi.nlm.nih.gov/pubmed/12192081.

Linder, M. et al., 2001. The hydrophobins HFBI and HFBII from Trichoderma reesei showing efficient interactions with nonionic surfactants in aqueous two-phase systems. *Biomacromolecules*, 2(2), pp.511–7. Available at: http://www.ncbi.nlm.nih.gov/pubmed/11749214 [Accessed April 19, 2015].

Linder, M.B., 2009. Hydrophobins: Proteins that self assemble at interfaces. *Current Opinion in Colloid & Interface Science*, 14(5), pp.356–363. Available at: http://www.sciencedirect.com/science/article/pii/S1359029409000296 [Accessed March 29, 2015].

Linder, M.B. et al., 2005. Hydrophobins: the protein-amphiphiles of filamentous fungi. *FEMS microbiology reviews*, 29(5), pp.877–96. Available at: http://www.sciencedirect.com/science/article/pii/S0168644505000100 [Accessed May 24, 2015].

Ling, X.Y., Reinhoudt, D.N. & Huskens, J., 2008. Reversible Attachment of Nanostructures at Molecular Printboards through Supramolecular Glue. *Chemistry of Materials*, 20(11), pp.3574–3578. Available at: http://dx.doi.org/10.1021/cm703597w [Accessed May 28, 2015].

Lugones, L.G. et al., 1996. An abundant hydrophobin (ABH1) forms hydrophobic rodlet layers in Agaricus bisporus fruiting bodies. *Microbiology (Reading, England)*, 142 (Pt 5, pp.1321–9. Available at: http://www.ncbi.nlm.nih.gov/pubmed/8704971 [Accessed May 23, 2015].

Lugones, L.G. et al., 1999. Hydrophobins line air channels in fruiting bodies of Schizophyllum commune and Agaricus bisporus. *Mycological Research*, 103(5), pp.635–640. Available at: http://www.sciencedirect.com/science/article/pii/S0953756208603172 [Accessed May 23, 2015].

Lugones, L.G. et al., 2004. The SC15 protein of Schizophyllum commune mediates formation of aerial hyphae and attachment in the absence of the SC3 hydrophobin. *Molecular microbiology*, 53(2), pp.707–16. Available at: http://www.ncbi.nlm.nih.gov/pubmed/15228546 [Accessed May 23, 2015].

Lumsdon, S.O., Green, J. & Stieglitz, B., 2005. Adsorption of hydrophobin proteins at hydrophobic and hydrophilic interfaces. *Colloids and surfaces. B, Biointerfaces*, 44(4), pp.172–8. Available at: http://www.ncbi.nlm.nih.gov/pubmed/16085399 [Accessed March 29, 2015].

Mackay, J.P. et al., 2001. The Hydrophobin EAS Is Largely Unstructured in Solution and Functions by Forming Amyloid-Like Structures. *Structure*, 9(2), pp.83–91. Available at: http://www.sciencedirect.com/science/article/pii/S0969212600005591 [Accessed May 31, 2015].

Maeda, H., Steffen, E. & Engel, J., 1978. Kinetics of dimerization of the Bence-Jones protein Au. *Biophysical chemistry*, 9(1), pp.57–64. Available at: http://www.ncbi.nlm.nih.gov/pubmed/753404 [Accessed June 1, 2015].

Magarkar, A. et al., 2014. Hydrophobin film structure for HFBI and HFBII and mechanism for accelerated film formation. *PLoS computational biology*, 10(7), p.e1003745. Available at: http://journals.plos.org/ploscompbiol/article?id=10.1371/journal.pcbi.1003745 [Accessed May 27, 2015].

Mankel, A., Krause, K. & Kothe, E., 2002. Identification of a hydrophobin gene that is developmentally regulated in the ectomycorrhizal fungus Tricholoma terreum. *Applied and environmental microbiology*, 68(3), pp.1408–13. Available at: http://www.pubmedcentral.nih.gov/articlerender.fcgi?artid=123729&tool=pmcentrez&rendertype=abstract [Accessed May 23, 2015].

Misra, R. et al., 2006. Nanoscale reduction in surface friction of polymer surfaces modified with Sc3 hydrophobin from Schizophyllum commune. *Biomacromolecules*, 7(5), pp.1463–70. Available at: http://www.ncbi.nlm.nih.gov/pubmed/16677027 [Accessed May 31, 2015].

Monopoli, M.P. et al., 2011. Physical-chemical aspects of protein corona: relevance to in vitro and in vivo biological impacts of nanoparticles. *Journal of the American Chemical Society*, 133(8), pp.2525–34. Available at: http://dx.doi.org/10.1021/ja107583h [Accessed August 10, 2015].

Moore, J.M., Patapoff, T.W. & Cromwell, M.E., 1999. Kinetics and thermodynamics of dimer formation and dissociation for a recombinant humanized monoclonal antibody to vascular endothelial growth factor. *Biochemistry*, 38(42), pp.13960–13967.

Muñoz, F. et al., 1983. Kinetic and thermodynamic study of the tetramerization equilibrium of phosphorylase b. *Journal of biochemistry*, 94(5), pp.1649–59. Available at: http://www.ncbi.nlm.nih.gov/pubmed/6418736 [Accessed May 30, 2015].

Nakari-Setälä, T. et al., 1997. Differential expression of the vegetative and spore-bound hydrophobins of Trichoderma reesei--cloning and characterization of the hfb2 gene. *European journal of biochemistry / FEBS*, 248(2), pp.415–23. Available at: http://www.ncbi.nlm.nih.gov/pubmed/9346297 [Accessed May 29, 2015].

Paananen, A. et al., 2003. Structural hierarchy in molecular films of two class II hydrophobins. *Biochemistry*, 42(18), pp.5253–8. Available at: http://www.ncbi.nlm.nih.gov/pubmed/12731866 [Accessed May 25, 2015].

Palomo, J.M. et al., 2003. Solid-phase handling of hydrophobins: immobilized hydrophobins as a new tool to study lipases. *Biomacromolecules*, 4(2), pp.204–10. Available at: http://dx.doi.org/10.1021/bm020071l [Accessed May 28, 2015].

Paris, S. et al., 2003. Conidial Hydrophobins of Aspergillus fumigatus. *Applied and Environmental Microbiology*, 69(3), pp.1581–1588. Available at: http://aem.asm.org/content/69/3/1581.abstract [Accessed April 5, 2015].

Qin, M. et al., 2007. Bioactive surface modification of mica and poly(dimethylsiloxane) with hydrophobins for protein immobilization. *Langmuir : the ACS journal of surfaces and colloids*, 23(8), pp.4465–71. Available at: http://www.ncbi.nlm.nih.gov/pubmed/17341100 [Accessed May 28, 2015].

Rillig, M.C., 2005. A connection between fungal hydrophobins and soil water repellency? *Pedobiologia*, 49(5), pp.395–399. Available at: http://www.sciencedirect.com/science/article/pii/S0031405605000351 [Accessed May 23, 2015].

Rillig, M.C. et al., 2007. Role of proteins in soil carbon and nitrogen storage: controls on persistence. *Biogeochemistry*, 85(1), pp.25–44. Available at: http://link.springer.com/10.1007/s10533-007-9102-6 [Accessed May 23, 2015].

Sarlin, T. et al., 2005. Fungal Hydrophobins as Predictors of the Gushing Activity of Malt. *Journal of the Institute of Brewing*, 111(2), pp.105–111. Available at: http://doi.wiley.com/10.1002/j.2050-0416.2005.tb00655.x [Accessed May 31, 2015].

Sarparanta, M. et al., 2012. Intravenous delivery of hydrophobin-functionalized porous silicon nanoparticles: stability, plasma protein adsorption and biodistribution. *Molecular pharmaceutics*, 9(3), pp.654–63. Available at: http://www.ncbi.nlm.nih.gov/pubmed/22277076 [Accessed May 31, 2015].

Scherrer, S. et al., 2000. Interfacial self-assembly of fungal hydrophobins of the lichen-forming ascomycetes Xanthoria parietina and X. ectaneoides. *Fungal genetics and biology : FG & B*, 30(1), pp.81–93. Available at: http://www.ncbi.nlm.nih.gov/pubmed/10955910 [Accessed May 23, 2015].

Scholtmeijer, K. et al., 2009. Assembly of the fungal SC3 hydrophobin into functional amyloid fibrils depends on its concentration and is promoted by cell wall polysaccharides. *The Journal of biological chemistry*, 284(39), pp.26309–14. Available at: http://www.pubmedcentral.nih.gov/articlerender.fcgi?artid=2785318&tool=pmcentrez&rendertype=abstract [Accessed June 1, 2015].

Scholtmeijer, K. et al., 2002. Surface modifications created by using engineered hydrophobins. *Applied and environmental microbiology*, 68(3), pp.1367–73. Available at: http://www.pubmedcentral.nih.gov/articlerender.fcgi?artid=123772&tool=pmcentrez&rendertype=abstract [Accessed May 28, 2015].

Shapiro, A.L., Viñuela, E. & V. Maizel, J., 1967. Molecular weight estimation of polypeptide chains by electrophoresis in SDS-polyacrylamide gels. *Biochemical and Biophysical Research Communications*, 28(5), pp.815–820. Available at: http://www.sciencedirect.com/science/article/pii/0006291X67903919 [Accessed January 10, 2015].

Shibuya, K. et al., 1999. Histopathology of experimental invasive pulmonary aspergillosis in rats: pathological comparison of pulmonary lesions induced by specific virulent factor deficient mutants. *Microbial pathogenesis*, 27(3), pp.123–31. Available at: http://www.ncbi.nlm.nih.gov/pubmed/10455003 [Accessed May 23, 2015].

Spanu, P., 1997. HCF-1, a hydrophobin from the tomato pathogen Cladosporium fulvum. *Gene*, 193(1), pp.89–96. Available at: http://www.ncbi.nlm.nih.gov/pubmed/9249071 [Accessed May 23, 2015].

St Leger, R.J., Staples, R.C. & Roberts, D.W., 1992. Cloning and regulatory analysis of starvation-stress gene, ssgA, encoding a hydrophobin-like protein from the entomopathogenic fungus, Metarhizium anisopliae. *Gene*, 120(1), pp.119–24. Available at: http://www.ncbi.nlm.nih.gov/pubmed/1398117 [Accessed May 23, 2015].

De Stefano, L. et al., 2008. Protein-Modified Porous Silicon Nanostructures. *Advanced Materials*, 20(8), pp.1529–1533. Available at: http://doi.wiley.com/10.1002/adma.200702454 [Accessed May 31, 2015].

De Stefano, L. et al., 2007. Self-assembled biofilm of hydrophobins protects the silicon surface in the KOH wet etch process. *Langmuir : the ACS journal of surfaces and colloids*, 23(15), pp.7920–2. Available at: http://www.ncbi.nlm.nih.gov/pubmed/17580922 [Accessed June 5, 2015].

Stringer, M.A. et al., 1991. Rodletless, a new Aspergillus developmental mutant induced by directed gene inactivation. *Genes & development*, 5(7), pp.1161–71. Available at: http://www.ncbi.nlm.nih.gov/pubmed/2065971 [Accessed May 23, 2015].

Szilvay, G.R., Paananen, A., et al., 2007. Self-assembled hydrophobin protein films at the air-water interface: structural analysis and molecular engineering. *Biochemistry*, 46(9), pp.2345–54. Available at: http://dx.doi.org/10.1021/bi602358h [Accessed May 25, 2015].

Szilvay, G.R., Kisko, K., et al., 2007. The relation between solution association and surface activity of the hydrophobin HFBI from Trichoderma reesei. *FEBS letters*, 581(14), pp.2721–6. Available at: http://www.ncbi.nlm.nih.gov/pubmed/17531982 [Accessed May 31, 2015].

Szilvay, G.R., Nakari-Setälä, T. & Linder, M.B., 2006. Behavior of Trichoderma reesei hydrophobins in solution: Interactions, dynamics, and multimer formation. *Biochemistry*, 45(28), pp.8590–8598.

Tagu, D. et al., 2001. Immunolocalization of hydrophobin HYDPt-1 from the ectomycorrhizal basidiomycete Pisolithus tinctorius during colonization of Eucalyptus globulus roots. *New Phytologist*, 149(1), pp.127–135. Available at: http://doi.wiley.com/10.1046/j.1469-8137.2001.00009.x [Accessed May 23, 2015].

Tagu, D., Nasse, B. & Martin, F., 1996. Cloning and characterization of hydrophobins-encoding cDNAs from the ectomycorrhizal Basidiomycete Pisolithus tinctorius. *Gene*, 168(1), pp.93–97. Available at: http://www.sciencedirect.com/science/article/pii/0378111995007253 [Accessed May 23, 2015].

Takahashi, T. et al., 2005. The fungal hydrophobin RolA recruits polyesterase and laterally moves on hydrophobic surfaces. *Molecular microbiology*, 57(6), pp.1780–96. Available at: http://www.ncbi.nlm.nih.gov/pubmed/16135240 [Accessed May 28, 2015].

Talbot, N.J. et al., 1996. MPG1 Encodes a Fungal Hydrophobin Involved in Surface Interactions during Infection-Related Development of Magnaporthe grisea. *The Plant cell*, 8(6), pp.985–999. Available at: http://www.pubmedcentral.nih.gov/articlerender.fcgi?artid=161153&tool=pmcentrez&rendertype=abstract [Accessed May 23, 2015].

Talbot, N.J., Ebbole, D.J. & Hamer, J.E., 1993. Identification and characterization of MPG1, a gene involved in pathogenicity from the rice blast fungus Magnaporthe grisea. *The Plant cell*, 5(11), pp.1575–90. Available at: http://www.plantcell.org/content/5/11/1575.abstract [Accessed May 23, 2015].

Temple, B. et al., 1997. Cerato-ulmin, a hydrophobin secreted by the causal agents of Dutch elm disease, is a parasitic fitness factor. *Fungal genetics and biology : FG & B*, 22(1), pp.39–53. Available at: http://www.ncbi.nlm.nih.gov/pubmed/9344630 [Accessed May 23, 2015].

Torkkeli, M. et al., 2002. Aggregation and self-assembly of hydrophobins from Trichoderma reesei: low-resolution structural models. *Biophysical journal*, 83(4), pp.2240–7. Available at: http://www.pubmedcentral.nih.gov/articlerender.fcgi?artid=1302312&tool=pmcentrez&rendertype=abstract [Accessed May 25, 2015].

Ulman, A., 1996. Formation and Structure of Self-Assembled Monolayers. *Chemical reviews*, 96(4), pp.1533–1554. Available at: http://www.ncbi.nlm.nih.gov/pubmed/11848802 [Accessed June 2, 2015].

Ungewickell, E. & Gratzer, W., 1978. Self-Association of Human Spectrin. A Thermodynamic and Kinetic Study. *European Journal of Biochemistry*, 88(2), pp.379–385. Available at: http://doi.wiley.com/10.1111/j.1432-1033.1978.tb12459.x [Accessed May 2, 2015].

Valo, H.K. et al., 2010. Multifunctional hydrophobin: toward functional coatings for drug nanoparticles. *ACS nano*, 4(3), pp.1750–8. Available at: http://dx.doi.org/10.1021/nn9017558 [Accessed May 31, 2015].

Wang, X. et al., 2004. Oligomerization of hydrophobin SC3 in solution: from soluble state to self-assembly. *Protein science : a publication of the Protein Society*, 13(3), pp.810–21. Available at: http://www.pubmedcentral.nih.gov/articlerender.fcgi?artid=2286737&tool=pmcentrez&rendertype=abstract [Accessed May 25, 2015].

Wang, Z. et al., 2010. Mechanisms of protein adhesion on surface films of hydrophobin. *Langmuir : the ACS journal of surfaces and colloids*, 26(11), pp.8491–6. Available at: http://dx.doi.org/10.1021/la101240e [Accessed May 28, 2015].

Vejnovic, I., Simmler, L. & Betz, G., 2010. Investigation of different formulations for drug delivery through the nail plate. *International journal of pharmaceutics*, 386(1-2), pp.185–94. Available at: http://www.ncbi.nlm.nih.gov/pubmed/19941943 [Accessed May 31, 2015].

Wessels, J.G. et al., 1991. The thn mutation of Schizophyllum commune, which suppresses formation of aerial hyphae, affects expression of the Sc3 hydrophobin gene. *Journal of general microbiology*, 137(10), pp.2439–45. Available at: http://www.ncbi.nlm.nih.gov/pubmed/1770359 [Accessed May 23, 2015].

Wessels, J.G.H., 1994. Developmental Regulation of Fungal Cell Wall Formation. *Annual Review of Phytopathology*, 32(1), pp.413–437. Available at: http://www.annualreviews.org/doi/abs/10.1146/annurev.py.32.090194.002213 [Accessed April 19, 2015].

Van Wetter, M.A. et al., 2000. Hydrophobin gene expression affects hyphal wall composition in Schizophyllum commune. *Fungal genetics and biology : FG & B*, 31(2), pp.99–104. Available at: http://www.ncbi.nlm.nih.gov/pubmed/11170739 [Accessed May 23, 2015].

Whiteford, J.R. & Spanu, P.D., 2002. Hydrophobins and the interactions between fungi and plants. *Molecular plant pathology*, 3(5), pp.391–400. Available at: http://www.ncbi.nlm.nih.gov/pubmed/20569345 [Accessed May 24, 2015].

Viterbo, A. & Chet, I., 2006. TasHyd1, a new hydrophobin gene from the biocontrol agent Trichoderma asperellum, is involved in plant root colonization. *Molecular plant pathology*, 7(4), pp.249–58. Available at: http://www.ncbi.nlm.nih.gov/pubmed/20507444 [Accessed May 23, 2015].

De Vocht, M.L. et al., 2002. Self-assembly of the hydrophobin SC3 proceeds via two structural intermediates. *Protein science : a publication of the Protein Society*, 11(5), pp.1199–205. Available at: http://www.pubmedcentral.nih.gov/articlerender.fcgi?artid=2373556&tool=pmcentrez&rendertype=abstract [Accessed May 31, 2015].

De Vries, O.M.H. et al., 1999. Identification and characterization of a tri-partite hydrophobin from Claviceps fusiformis . A novel type of class II hydrophobin. *European Journal of Biochemistry*, 262(2), pp.377–385. Available at: http://doi.wiley.com/10.1046/j.1432-1327.1999.00387.x [Accessed May 31, 2015].

Wösten, H., De Vries, O. & Wessels, J., 1993. Interfacial Self-Assembly of a Fungal Hydrophobin into a Hydrophobic Rodlet Layer. *The Plant cell*, 5(11), pp.1567–1574. Available at: http://www.plantcell.org/content/5/11/1567.abstract [Accessed May 23, 2015].

Wösten, H.A., 2001. Hydrophobins: multipurpose proteins. *Annual review of microbiology*, 55, pp.625–46. Available at: http://www.ncbi.nlm.nih.gov/pubmed/11544369 [Accessed May 23, 2015].

Wösten, H.A. et al., 1994. The fungal hydrophobin Sc3p self-assembles at the surface of aerial hyphae as a protein membrane constituting the hydrophobic rodlet layer. *European journal of cell biology*, 63(1), pp.122–9. Available at: http://www.ncbi.nlm.nih.gov/pubmed/8005099 [Accessed May 23, 2015].

Wösten, H.A. & de Vocht, M.L., 2000. Hydrophobins, the fungal coat unravelled. *Biochimica et biophysica acta*, 1469(2), pp.79–86. Available at: http://www.ncbi.nlm.nih.gov/pubmed/10998570 [Accessed April 19, 2015].

Wösten, H.A.B. et al., 1999. How a fungus escapes the water to grow into the air. *Current Biology*, 9(2), pp.85–88. Available at: http://www.cell.com/article/S0960982299800190/fulltext [Accessed May 23, 2015].

Wösten, H.A.B. & Scholtmeijer, K., 2015. Applications of hydrophobins: current state and perspectives. *Applied microbiology and biotechnology*, 99(4), pp.1587–97. Available at: http://www.ncbi.nlm.nih.gov/pubmed/25564034 [Accessed June 1, 2015].

Yeh, S.R. et al., 1997. Ligand exchange during cytochrome c folding. *Nature structural biology*, 4(1), pp.51–6. Available at: http://www.ncbi.nlm.nih.gov/pubmed/8989324 [Accessed May 26, 2015].

Zampieri, F., Wösten, H.A.B. & Scholtmeijer, K., 2010. Creating Surface Properties Using a Palette of Hydrophobins. *Materials*, 3(9), pp.4607–4625. Available at: http://www.mdpi.com/1996-1944/3/9/4607 [Accessed May 23, 2015].

Zhao, Z.-X. et al., 2007. Amperometric glucose biosensor based on self-assembly hydrophobin with high efficiency of enzyme utilization. *Biosensors & bioelectronics*, 22(12), pp.3021–7. Available at: http://www.sciencedirect.com/science/article/pii/S0956566307000048 [Accessed May 28, 2015].

Zhao, Z.-X. et al., 2009. Self-assembled film of hydrophobins on gold surfaces and its application to electrochemical biosensing. *Colloids and surfaces. B, Biointerfaces*, 71(1), pp.102–6. Available at: http://www.sciencedirect.com/science/article/pii/S0927776509000174 [Accessed May 31, 2015].

Publication I

Grunér, Mathias S; Kauscher, Ulrike; Linder, Markus B; Monopoli, Marco P. *An environmental route of exposure affects the formation of nanoparticle coronas in blood plasma*. Accepted for publication in the journal *Journal of Proteomics*, Elsevier B.V. in the year 2015

Journal of Proteomics xxx (2015) xxx–xxx

Contents lists available at ScienceDirect

Journal of Proteomics

journal homepage: www.elsevier.com/locate/jprot

An environmental route of exposure affects the formation of nanoparticle coronas in blood plasma

M.S. Grunér [a,b], U. Kauscher [c,d], M.B. Linder [b], M.P. Monopoli [c]

[a] VTT Technical Research Centre of Finland, Biotechnology, Tietotie 2, FIN-02044 VTT Espoo, Finland
[b] Aalto University, School of Chemical Technology, P.O.Box 16100FI-00076 AALTO, Finland
[c] Centre for BioNano Interactions, School of Chemistry and Chemical Biology and UCD Conway Institute for Biomolecular and Biomedical Research, University College Dublin, Belfield, Dublin 4, Ireland
[d] Imperial College London, London SW7 2AZ, United Kingdom

ARTICLE INFO

Article history:
Received 22 June 2015
Received in revised form 21 October 2015
Accepted 30 October 2015
Available online xxxx

Keywords:
Nanoparticle hydrophobin corona DCS

ABSTRACT

Nanoparticles (NPs) in contact with biological fluids become covered by a tightly bound layer of proteins, the "protein corona", giving a new biological identity to NPs as the cell machinery can engage with the coated surface differently than with the bare one. We here consider the scenario that exposure to nanoparticles occurs through an environmental route, exemplified by using hydrophobins, fungal proteins that are highly adhesive and secreted into the environment in large quantities by fungi. The highly secreted hydrophobin, HFBII of *Trichoderma reesei* is used as a model. In this work we have used a strategy to coat and characterize nanoparticles of different size and surface modification. Hydrophobin coated nanoparticles of varying size and surface modification are shown to strongly increase stability and dispersion of the NPs in human plasma compared to pristine particles. It is also shown that the presence of hydrophobin on the NPs results in a decrease of layer thickness and a change in composition of the protein corona, and that the hydrophobin remained strongly associated to the NPs in competition with plasma proteins. As a conclusion we therefore suggest that the route of exposure of nanoparticles strongly affect their surface properties and possible physiological behavior.

Significance: This work shows how a self-assembling protein, class II hydrophobin HFBII, with interesting biocompatible coating properties, strongly adsorbs on polystyrene nanoparticles. HFBII is also shown to reduce aggregation of the NPs in human plasma which can increase bioavailability of NPs with potential use in biomedical applications. The results here are also of significance for understanding possible interactions of NPS with living organisms. Hydrophobins are secreted in large quantities into the environment by fungi and this work shows how the biological environment of NPs determines the surface and colloidal properties of the particles by forming a protein corona, and that the history of the particle environment, here simulated with hydrophobin exposure, affects both plasma protein corona formation and dispersion behavior. This work thus simulates how alternative exposure routes affect nanoparticle properties, important in understanding the biological fate of NPs.

1. Introduction

Nanoparticles (NPs) have found an increased use in the medical and industrial field with the result that environmental exposure of NPs is largely increasing [1,2]. The fate and transport of NPs through the environment is affected by different biomolecules adsorbing onto the NP surface which may alter the NP identity and following toxicity and interactions with organisms [3,4]. NPs in contact with biological fluid such as human plasma or serum have been shown to be covered by a tightly bound layer of proteins, the "protein corona" [1–10]. Human plasma contains about 4000 different proteins, whose abundance varies in the range of more than ten orders of magnitude [11], and only few tens of these proteins, that are rarely the most abundant ones, are predominantly associated with forming a strongly bound protein corona on nanoparticles, the "hard corona (HC)" [12–17]. While an external layer of proteins with less affinity (the "soft corona" [1]) will be in exchange with the environment [18] the proteins forming the hard corona are so strongly bound that they are in slow exchange [7]. In this work we use the concept of *in situ* corona (IS) to describe a corona that is analyzed in the context of the environment were exposure occurs, in this case blood plasma. The HC in contrast is analyzed by separating and washing the NPs from the unbound and loosely bound proteins which can be found in the media that they were exposed to. The importance of the corona proteins relies on the fact that the cellular machineries engage with the protein corona directly rather than with the pristine surface of the NPs, thus the protein corona composition can strongly influence the biodistribution [19,20], inflammation [21] and intracellular fate of the NPs [22–28]. Designing NPs in order to form defined coronas is significant for applications in nanomedicine and drug delivery [29–33]. However, an understanding is also needed in order to properly

http://dx.doi.org/10.1016/j.jprot.2015.10.028
1874-3919/

evaluate exposure scenarios in safety related issues or the environmental fate of NPs released in nature, either accidentally or purposefully. Consequently, we are interested in how the formation of nanoparticle coronas is affected by sequences of exposure to different environments. We describe how highly expressed fungal proteins, hydrophobins, adsorb onto polymeric NPs and how this in turn affects NP behavior in human plasma.

Hydrophobins are interesting in this context due to two reasons. Firstly, hydrophobins are highly expressed in the environment by fungi where they regulate the surface adhesion and water surface tension in order to grow efficiently. Fungi are found ubiquitously in nature where they have a crucial role in for example the breakdown and turnover of plant material. The amounts of hydrophobins secreted are so high that geological effects such as changes in soil hydrophobicity are anticipated [34,35]. Secondly, fungi also use hydrophobins as coatings on structures such as fruiting bodies and spores. The case of fungal spores is especially interesting as it has been shown that hydrophobin coatings significantly affect how the human immune system responds to the spores. In the case of *Aspergillus fumigatus*, it has been shown that hydrophobin coatings on its spores attenuates the immune response and prevents immunological recognition of them [36].

We can therefore anticipate that an alternative environmental exposure route can lead to the formation of NP coronas of hydrophobins and that this type of coating could have marked effects of the behavior of the particles. Examining these types of exposure routes aims to an increased understanding of risks but also to learning potentially technologically useful functionalization processes.

The functional properties of hydrophobins that lead to coatings and changes of interfacial behavior are quite well understood. [37,38] They possess an amphiphilic structure, *i.e.* one part of the structure is hydrophilic and another part is hydrophobic. They have a size of about 2 nm in diameter and are structurally quite rigid. [39,40] The amphiphilic nature of the hydrophobins allows them to assemble at interfaces between water and air or water and hydrophobic phases. Additionally, interactions between the proteins can lead to membrane-like structures that are mechanically stable, such as the hydrophobic coatings on spores.

2. Materials and methods

2.1. Nanoparticles

Polystyrene sulfonated nanoparticles (Invitrogen Fluospheres YG 100 nm, Polysciences Fluoresbrite YG 200 nm) and carboxylated nanoparticles (Polysciences Fluoresbrite YG 100 nm, 200 nm) were used. All nanoparticles were characterized by measuring their size and zeta-potential in MQ before use.

2.2. Hydrophobin

The class II hydrophobin protein HFBII was purified from *Trichoderma reesei* culture supernatant using two-phase extraction and reversed phase chromatography as described earlier. [41].

2.3. Human plasma

Human plasma was prepared as previously described. [13] When plasma was used for experiments, it was allowed to thaw at room temperature and centrifuged for 3 min at 15 kRCF to remove potential plasma protein aggregates. Thawed plasma was never re-frozen and re-thawed. All data presented are obtained using plasma from one donation session. The blood donation procedure was approved by the Human Research Ethics committee at University College Dublin.

2.4. Buffers

For protein adsorption study, hydrophobin protein was dispersed in phosphate buffered saline (PBS) at pH 6.7, which corresponded to the hydrophobin isoelectric point. After protein adsorption, NP hydrophobin complexes were dialyzed in PBS pH 7.4 prior exposure to plasma. NP dispersion was checked throughout these conditions to evaluate whether the pH change or protein adsorption could induce particle agglomeration.

2.5. Hydrophobin adsorption onto PS NPs

NPs (1 mg/ml) were covered with HFBII in excess (1.5 mg/ml). A theoretical monolayer of hydrophobin was calculated as 92 μg of protein per 1 mg of NP and 46 μg protein per 1 mg of NP for 100 and 200 nm respectively, according to the HFBII dimension determined by X-ray crystallography. [42] NPs and hydrophobin were separately dissolved in PBS pH 6.7. NPs were sonicated for 3 min and HFBII for 10 s prior to use. 500 μl of 2 g/ml NP was mixed with 500 μl 3 mg/ml HFBII. For adsorption, NP + HFBII solution is put in a lab shaker, 500 rpm, 25 °C for 2 h.

2.6. Dialysis

Free or loosely bound hydrophobin was removed from NPs in a dialysis step following hydrophobin adsorption on NPs. Float-A-lyzer G2, 1 ml, 50 kDa (Spectrum Labs, USA) is used as the dialysis device. NP + HFBII solution was put in the device floating in 1 L buffer (PBS pH 7.4) at 4 °C under continuous stirring for 3 days. Every 24 h, buffer was changed. At the final buffer change, MQ water was used instead of buffer in order to avoid aggregation of particles.

2.7. Plasma incubation

The samples were mixed in the order; PBS (pH 7.4) – plasma – NPs. The nanoparticles were incubated with the plasma for 1 h at 37 °C Hard corona, HC: The incubated samples were subjected to centrifugation at 18 kRCF at 4 °C for 40 min. The supernatant was removed and the pellet was resuspended in 300 μl of PBS and then subjected to centrifugation at 18 kRCF at 4 °C for 20 min. This step was repeated three times. After the last centrifugation the supernatant was removed and the pellet was re-suspended carefully with 20 μl SDS-loading buffer. Washes, *i.e.* supernatants, were collected from each washing step. This treatment removed proteins with low affinity for the NP surface (the soft protein corona) with the proteins forming the hard corona still being bound. In situ corona: For *in situ* measurements, no washing step was conducted and the samples were measured directly post plasma protein incubation.

2.8. SDS-page

SDS-PAGE (4% stacking gel and 15% or 8% resolving gel) was used to separate the proteins recovered from the nanoparticle surfaces. After the last centrifugation step in the plasma incubation, the supernatant was removed and the pellet was re-suspended with 20 μl SDS-loading buffer. The samples were loaded into the gel and subjected to electrophoresis at 130 V, 400 mA for about 60 min each, until the proteins reached the end of the gel. The gels were stained using the DAIICHI silver staining kit (Tokyo, Japan).

2.9. Dynamic light scattering and zeta potential

Dynamic light scattering (DLS), and zeta potential measurements of nanoparticle dispersions were carried out using a Malvern Zetasizer ZS (Worcestershire, UK). The presented results are the average of 3 runs each containing 11 individual measurements. The data are reported as

Please cite this article as: M.S. Grunér, et al., An environmental route of exposure affects the formation of nanoparticle coronas in blood plasma, J Prot (2015), http://dx.doi.org/10.1016/j.jprot.2015.10.028

average hydrodynamic diameter and polydispersity index (PDI), which is a measure of the size distribution and polydispersity of the sample, which can be due to the presence of different sized nanoparticles resulting from the synthesis procedure, or possible aggregation (values smaller than 0.3 indicate monodisperse samples with no particle aggregation).

2.10. Protein concentration assay

Protein concentrations were determined using the Micro BCA Protein Assay Kit, Thermo Scientific.

2.11. Differential centrifugal sedimentation

Differential centrifugal sedimentation (DCS) experiments were performed with a CPS Disc Centrifuge DC24000, CPS Instruments, USA to measure NP size and distribution and shell thickness of proteins adsorbed on the surface as previously described. [7] DCS measures particle size distribution using centrifugal sedimentation within an optically clear spinning disc filled with fluid and here determines nanoparticle size on a nanometer level based on the sedimentation time of a particle through a glucose gradient. DCS measures apparent diameter size which makes it necessary to correct for changes in density of *e.g.* adsorbed protein layers on a nanoparticle by a core shell model in order to attain accurate size determination of protein shell coated nanoparticles.

2.12. Gel band densitometry

Gel band densitometry was performed with GeneTools Analysis software (Singene, UK). Gel lane bands were automatically obtained by the software and the background was subtracted using Rolling Disk function. Gel bands from different lanes were visually matched and gel band intensity were plot as shown in Fig. 5b.

3. Results and discussion

3.1. Characterization of pristine NPs and the formation of NP-HFBII complexes

The binding of HFBII to nanoparticles was initially characterized where the protein was physically adsorbed on monodisperse carboxylated (PCOOH) and sulfonated ($PSOSO_3$) polystyrene NPs of nominally 100 nm and 200 nm in diameter. Pristine NPs and NP-HFBII complexes were characterized with differential centrifugal sedimentation (DCS) for size measurement, dynamic light scattering (DLS) and zeta potential measurements to ensure the formation of monodispersed, and stable bio-coated nano-objects as well as SDS-PAGE and protein quantification assay to evaluate plasma and protein adsorption.

Pristine and treated samples were characterized by DLS (Table 1). The results showed that after incubation with HFBII, particle hydrodynamic diameter increased on both sulfonated and carboxylated particles. However the PDI remained almost unchanged which indicates that the protein binds to the surface of the particles without particle agglomeration. HFB protein adsorption resulted in a change in hydrodynamic radius, with the exception of the 100 nm COOH where a change of hydrodynamic size was not observed, possibly due to lower protein binding. On the contrary, the more hydrophobic sulfonated particles, resulted in a stronger change in radius indicating stronger protein binding. This finding is in agreement with the literature where protein adsorption on a more hydrophobic surface is more enhanced [43].

An almost unchanged zeta potential of NP-HFBII complexes compared to the pristine ones was observed for COOH NPs. However, in the case of sulfonated NPs the surface charge reduced from about −50 mV on pristine particles to about −30 mV on NP-HFBII complexes. These results were obtained for sulfonated particles of two different sizes (100 nm and 200 nm diameter). These results from zeta potential measurements imply that HFBII does not only bind with a thicker layer on sulfonated NPs, it also generates a significant drop of surface charge, indicating that a more uniform layer of protein is formed on the sulfonated particles. Additionally, these results imply that HFBII may bind differently in terms of orientation onto the two types of PS particles. This is in agreement with previously published data on flat surfaces of varying polarity [44].

While DLS measurements provided crucial information of the NP dispersion, we have aligned DCS measurements as it represents a high resolution approach. These measurements are not only capable to resolve multiple populations within the same sample, they also provide useful information on particle size distribution of the proteins bound to the surface [7,13]. As DCS measures sedimentation time based on the NP size and density, protein adsorption on the NP surface results in a change in density and size and in a change of the sedimentation time. While DCS measured size provided the apparent size, for accurate size measurement it is necessary to "correct" for such change of density by means of a core shell model, as previously described [13].

Knowing the protein density, we have calculated the protein shell thickness by comparison of the sedimentation changes between pristine and coated particles which can be correlated to protein adsorption and differences in protein binding in relation to the surface curvature and surface modification. Calculated layer thicknesses are shown in Table 2. The results show that all NPs tested resulted in a shift in apparent size as a result of change of density and/or protein binding. In agreement with DLS, a stronger and more severe shift was observed with sulfonated NPs suggesting stronger binding.

This finding is in agreement with the literature where higher protein binding was seen on sulfonated particles [43]. The reason for the difference is likely due to the different surface chemistry and more hydrophobic character of the sulfonated particles [1]. Furthermore, hydrophobins have previously been shown to form layers by self-assembly on hydrophobic surfaces [44–46]. Fig. 1 shows an example of sedimentation curves with 200 nm sulfonated and carboxylated particles. For all particles studied a main peak was detected representing the main particle population. Sulfonated particles also contained two additional peaks with dimensions corresponding to dimer and trimer complexes.

Table 1
NP-HFBII: shell thickness by DLS, Z-potential.

Sample			DLS				
Surface modification	Particle size [nm]	Sample coating	Dm, [nm]	SD	PDI	Zpot [mV]	SD
Carboxylated	100	Pristine	111.4	0.6	0.03	−46	0.8
		NP-HFB	111.0	1.7	0.02	−47	1.6
		Pristine	196.1	0.8	0.02	−50	1.0
	200	NP-HFB	202.3	1.9	0.01	−44	0.5
Sulfonated	100	Pristine	103.2	0.8	0.04	−50	3.1
		NP-HFB	120.6	1.2	0.09	−28	0.6
		Pristine	234.5	1	0.02	−47	0.6
	200	NP-HFB	302.5	1.4	0.21	−32	1.7

Table 2
NP-HFBII: Shell thickness by DCS.

Sample		Particle apparent size (by DCS)		Shell thickness nm
Surface modification	Particle nominal size [nm]	Pristine [nm]	NP-HFB [nm]	
Carboxylated	100	113.2	116.3	0.3
	200	209.6	221.1	1.4
Sulfonated	100	96.6	106.1	1.2
	200	234.3	251.4	2.3

Please cite this article as: M.S. Grunér, et al., An environmental route of exposure affects the formation of nanoparticle coronas in blood plasma, J Prot (2015), http://dx.doi.org/10.1016/j.jprot.2015.10.028

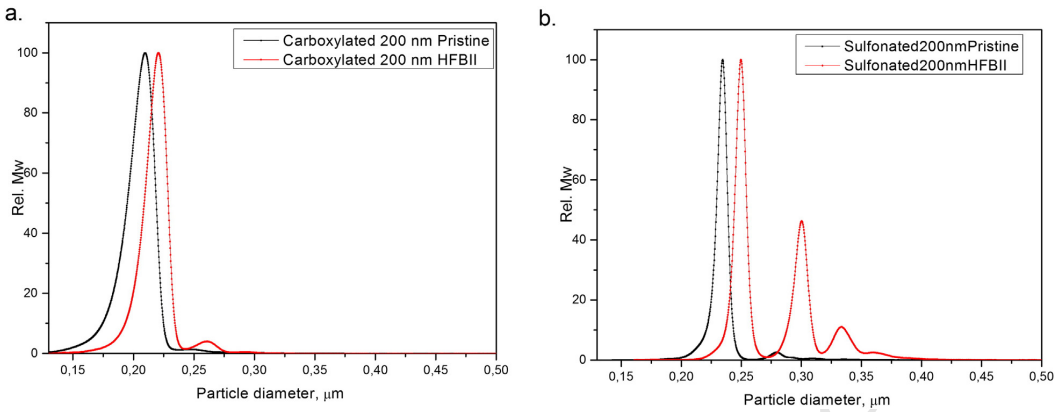

Fig. 1. DCS of NP and HFBII-NP complexes. DCS experiments of 200 nm carboxylated (a) and sulfonated (b) PS nanoparticles on pristine NPs and on NP-HFBII complexes.

The shell thickness for the 200 nm NPs was calculated as 2.3 nm and 1.4 nm for sulfonated and carboxylated NPs respectively. On the 200 nm sulfonated NPs, a layer of dimensions similar to a theoretical monolayer was seen, derived from the approximate diameter of a single hydrophobin, (*i.e.* 2 nm). For 100 nm NPs, the shell thickness was calculated to be 1.2 and 0.3 nm for 100 nm sulfonated and carboxylated NPs respectively, as shown in Table 2. This finding is in agreement with the DLS data where a more attenuated adsorption of HFB was observed on carboxylated NPs.

We note that the change in size has to be carefully evaluated as the module assumes a uniform particle density and the size detected does not represent the true particle size as it is based on the assumption that the particle core material is homogenous in density. [7,13] However the values obtained are particularly useful in comparing relative corona thickness across the different conditions.

Initial analysis by SDS-PAGE. Fig. 2 confirms that HFBII was found associated with all NPs even after extensive dialysis. In the analysis HFBII treated NPs were exposed in high denaturing condition and resolved on a gel. A strong band of 7 kDa, comparable of pure HFBII protein, was detected on SDS-PAGE by silver staining. Fig. 2 shows how HFBII successfully had adsorbed onto the surface of all NPs, seen as a strong and consistent band of 7 kDa, comparable to the band of a HFBII control sample. In order to further confirm successful binding of HFBII on the NP surface, a modified BCA assay was performed to measure protein amounts (Supplementary, Table T1). HFBII was shown to be present on all particles tested.

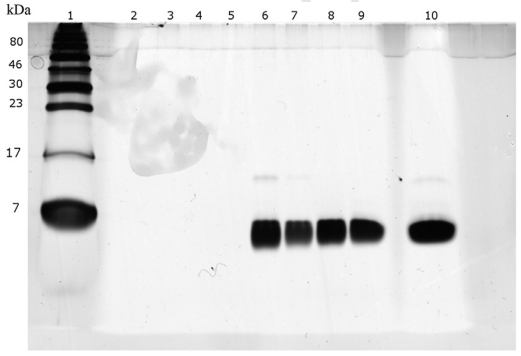

Fig. 2. SDS PAGE of NP and HFBII-NP complexes. SDS-PAGE gel showing the adsorption of HFBII to 100 and 200 nm carboxylated and sulfonated nanoparticles. Lane 1: ladder; lane 2: 100 nm carboxylated NP; lane 3: 200 nm carboxylated NP; lane 4: 100 nm sulfonated NP; lane 5: 200 nm sulfonated NP; lane 6: 100 nm carboxylated NP with HFBII; lane 7: 200 nm carboxylated NP with HFBII; 8: 100 nm sulfonated NP with HFBII; 9: 200 nm sulfonated NP with HFBII; 10: HFBII control sample.

3.2. Binding of plasma proteins to pristine and HFB coated nanoparticles, in situ exposure

The biological environment of NPs determines their surface and colloidal properties by forming a protein corona. The history of the particle environment including alternative exposure routes is here simulated using hydrophobins. The characterization of nanoparticles *in situ, i.e.* without washing the particles, was considerably more challenging than analyzing the HC where particles are washed prior to analysis. However, *in situ* may represent a more realistic state of the NPs during environmental exposure compared to HC. The difficulty of analysis arises as most analytical techniques are not suitable for analysis in the plasma environment. For example SDS-PAGE of particles in plasma would be inconclusive since non-bound plasma would inevitably be seen in the staining. For the analysis of *in situ* the most applicable technique therefore was DCS. The nanoparticles were incubated for 1 h at 37 °C with human plasma solution to mimic the blood stream circulation system and to measure the plasma protein affinity towards pristine NPs and NP-HFBII complexes. DCS of pristine sulfonated NPs generated strong aggregation in presence of human plasma as also previously shown [13], however when HFBII was present, the protein coating reduced aggregation dramatically (Fig. 3, Table 3). Furthermore, a hydrophobin coating on both carboxylated and sulfonated NPs of both sizes resulted in a considerate decrease in the corona thickness compared to the corona formed on pristine NPs. From this point of view HFBII had an effect of altering the structure of the corona. The reduction in thickness of the soft corona was as high as 55% compared to the corona formed on pristine NPs.

3.3. HC

HC complexes of pristine NPs and NP-HFBII complexes were analyzed by DCS to gain information on the dispersion of the NPs and to further evaluate the role of HFB on the plasma protein interactions. Pristine, sulfonated NPs showed severe aggregation during the procedures to obtain the HC and during the washing procedures. However, when these NPs were previously coated with HFBII (NP-HFBII), the aggregation was dramatically reduced. Thus, HFBII binding on the NP surface influences the NP dispersion properties and reduce aggregation of sulfonated NPs. SDS-PAGE (Fig. 5a) indicates that the decreased aggregation of NP-HFBII HC complexes increases total amount of plasma

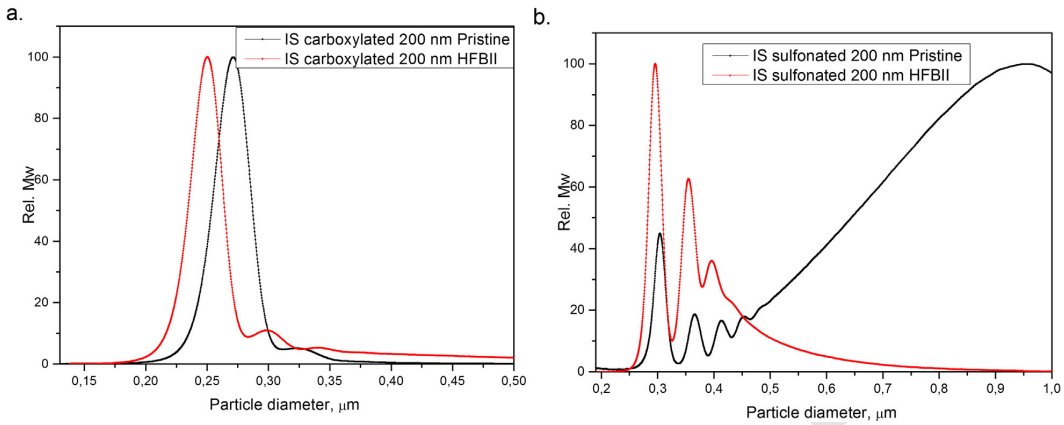

Fig. 3. DCS of particles *in situ*. (a) DCS experiments of carboxylated PS particle — corona complexes *in situ* after incubation of human plasma in PBS. Performed on pristine NPs and on NP–HFBII complexes. (b) DCS experiments of sulfonated PS particle — corona complexes *in situ* after incubation of human plasma in PBS. Performed on pristine NPs and on NP–HFBII complexes. Here represented by 200 nm NPs.

protein bound compared to pristine NP HC complexes suggesting an increased availability of the NP-HFBII.

Pristine and HFBII coated carboxylated NP-HC DCS measurements show similar dispersion properties, the aggregation was however less severe and the size of pristine NP-HC complexes could be measured. Carboxylated NP-HFBII-HC complexes resulted in easily dispersed complexes and a shift in the apparent size was observed indicating differences in different amount of proteins bound to their surface (Fig. 4, Table 3). A comparison of particles treated with HFBII and without, showed that the presence of HFBII on the NPs resulted in an overall reduced final particle diameter and a thinner calculated final layer thickness per particle.

SDS-PAGE was used to evaluate whether HFBII induces differences in blood protein binding (Fig. 5). Quite interestingly all HFBII-coated NPs show a clear HFBII band at 7 kDa (only visible on 15% gel giving optimal resolution for small proteins) indicating that HFBII remained strongly associated to all NPs also after incubation in a competitive environment of plasma proteins and the subsequent washing and centrifugation steps (Fig. 5a). This suggests a strong interaction that is not participating in possible protein exchange. A control sample of HFBII was also run in the same gel confirming that the band detected was hydrophobin and this band was not detected on NPs uncoated with this protein. Furthermore, densitometry of the SDS-PAGE gels confirms HFB binding on the NPs and that the overall composition of the plasma proteins is altered compared to uncoated particles (Fig. 5b).

In order to have more qualitative information of the composition of the protein layer, an additional 8% SDS-PAGE was run where proteins of 250–60 kDa have an optimal resolution (Supplementary, Figure S5) Comparing the lanes we conclude that the level of several plasma proteins in the HC are somewhat affected, especially in the case of sulfonated particles. The amounts of smaller plasma proteins also showed some effect of the presence of HFBII, generating stronger bands in this region in all four cases.

Due to aggregation and varying final volumes at the dialysis step, comparison of band thickness between NP and HFB-NP HC complexes in SDS-PAGE was made difficult. When lowering the concentration of plasma proteins to 10% from 55% in dialysis, final volumes were more similar in all cases and the bands in SDS-PAGE were more easily comparable (Supplementary, Figure S6). In this manner, bands can be seen as generally stronger on NP HC complexes compared to HFB-NP HC complexes and more HFBII can be seen bound on sulfonated particles compared to carboxylated, in agreement with other data.

To further confirm the exchange behavior of hydrophobin during the hard corona preparation, the supernatant of the washing steps, which contained the loosely bound proteins or soft corona, was run in a 15% SDS-PAGE with a resolution of 5–60 kDa. The 7 kDa band was not present in any of the washes, indicating that HFBII was not exchanged during the corona preparation (Supplementary, Figure S7).The gel also showed that three washes were necessary to remove loosely bound plasma proteins, as after the third wash very little protein could be detected.

Nanoparticle safety, exposure routes and environmental fates are likely to depend on how coronas are formed. We show here, using hydrophobins, that the history of the particle environment does have a substantial effect on the formation of the corona and how they are dispersed in solution.

Table 3
NP protein corona thickness by DCS.

Sample			*In situ*	HC
NP	Particle size [nm]	Sample coating	Corona shell thickness [nm]	Corona shell thickness [nm]
Carboxylated	100	Pristine	7.5	6.4
		NP-HFB	6.3	4.7
	200	Pristine	8.3	7.2
		NP-HFB	3.7	3.1
Sulfonated	100	Pristine	6.9	Agg.
		NP-HFB	4.5	1.6
	200	Pristine	11	Agg.
		NP-HFB	6.2	3.3

4. Conclusions

The class II hydrophobin HFBII was herein shown to strongly adsorb on both carboxylated and sulfonated polystyrene NPs. The protein bound with larger layer thickness on sulfonated NPs, generating a hydrophobin layer thickness of about a monolayer on sulfonated particles of 200 nm. On both types of NPs used, a HFBII coating was shown to alter the composition and reduce diameter of a formed protein corona on the NP-HFBII complex. Significantly, adsorption of the protein strongly reduced aggregation of sulfonated PS NPs in human plasma. HFBII-NP complexes covered with both hard (HC) and *in situ* coronas could be made relatively monodisperse compared to complete aggregation in the case of the pristine sulfonated NPs with the same treatment of human plasma. While the difference in aggregation and layer thickness were the most clear effects of HFBII, determining differences in

Please cite this article as: M.S. Grunér, et al., An environmental route of exposure affects the formation of nanoparticle coronas in blood plasma, J Prot (2015), http://dx.doi.org/10.1016/j.jprot.2015.10.028

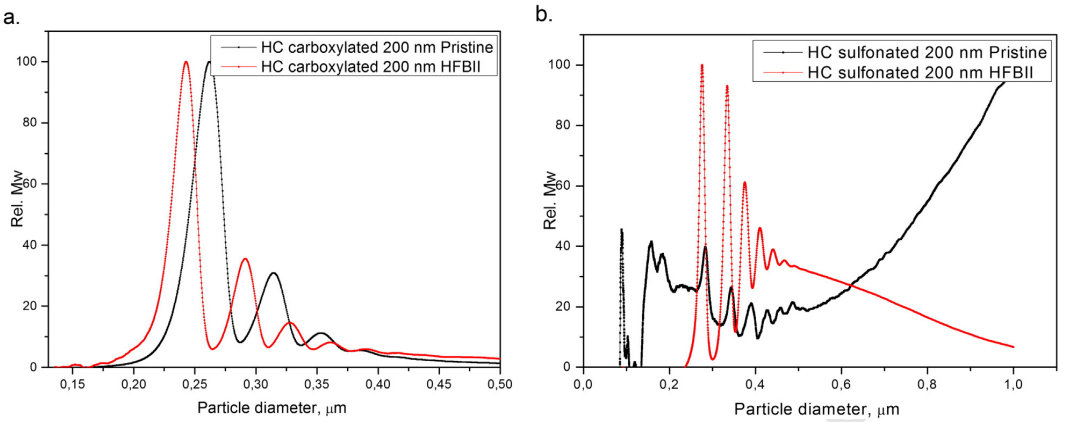

Fig. 4. DCS of particles with HC. Particle diameters of DCS carboxylated PS particle — corona complexes free from excess plasma, after incubation of human plasma in PBS. Performed on pristine NPs and NP–HFBII complexes. Here represented by 200 nm NPs.

the protein composition was more problematic because SDS-PAGE does not allow very detailed conclusions. Furthermore, HFBII was shown to be tightly bound to the NPs also in competition with plasma protein and did not detach in the conditions examined here. We suggest that HFBII can affect bioavailability because the prior formation of a HFBII corona prevents aggregation. These results also indicate a potential use in biomedical applications for increasing the availability of PS NP *in vivo*.

DCS analytical centrifuge has been used and is an emerging, powerful method that can be used for particle characterization as it is capable to resolve subpopulation of particles present in solution [13,49,50]. The use of DCS allowed the characterization of the *in situ* corona and comparing that to the HC and the adsorbed HFBII layer.

The results are of significance for understanding and correctly predicting possible NP interactions with living organisms and are consistent with previous findings, that the biological environment in which the NPs are present largely determines their surface and colloidal properties through the structure of the adsorbed corona. Hydrophobins are important in this context because they are secreted in large quantities by fungi into the environment where fungi have a crucial role in for example the breakdown and turnover of plant material. Especially decaying plant litter and landfills are expected to contain large populations of fungal species and thus secreted hydrophobins. The amounts of hydrophobins and other microbial secreted proteins are estimated to be so large that geological effects such as soil hydrophobicity could be affected [35]. In this work we have evaluated whether the pre-adsorption of environmental relevant molecules has the potential to affect the material properties and we suggest that for understanding the biological fate of nanoparticles such alternative exposure routes and the material life cycle must be taken into account.

Transparency document

The Transparency document associated with this article can be found in the online version. Q5

Uncited references Q6

[47,48]

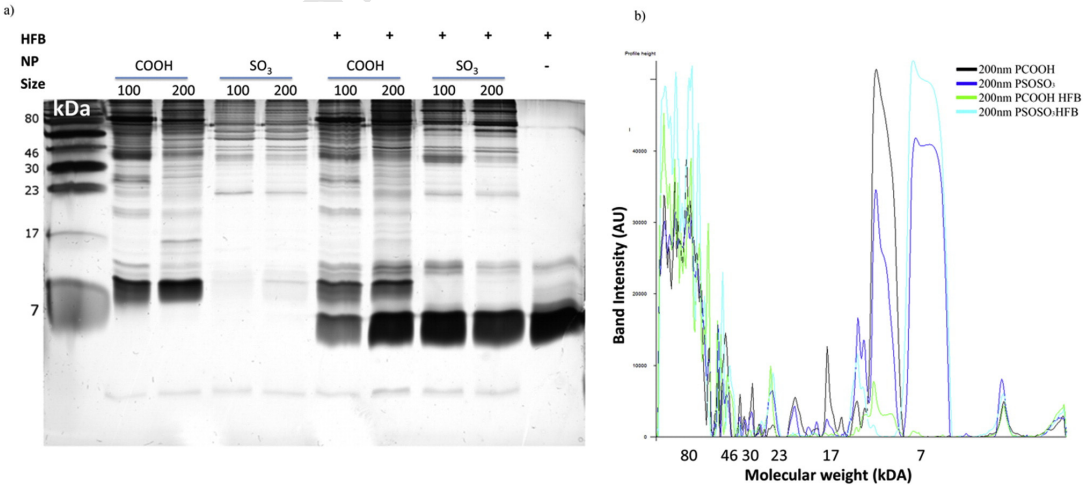

Fig. 5. a) 15% SDS-PAGE of particles with HC. Sample identification is provided on the top of the gel. b) Gel band densitometry of particles with HC. Densitometries refer to the SDS–PAGE of a.

Please cite this article as: M.S. Grunér, et al., An environmental route of exposure affects the formation of nanoparticle coronas in blood plasma, J Prot (2015), http://dx.doi.org/10.1016/j.jprot.2015.10.028

Acknowledgments

Financial support from the following is acknowledged:

STV — Svenska Tekniska Vetenskapsakademien i Finland.

EpitopeMap — Mapping the detailed composition of Surface-Absorbed Protein Layers on Biomaterials and Nanoparticles. Grant 4332.

ISB — National Doctoral Program in Informational and structural biology.

Appendix A. Supplementary data

Supplementary data to this article can be found online at http://dx.doi.org/10.1016/j.jprot.2015.10.028.

References

[1] S. Milani, F. Baldelli Bombelli, A.S. Pitek, K.A. Dawson, J. Radler, Reversible versus irreversible binding of transferrin to polystyrene nanoparticles: soft and hard corona, ACS Nano (2012).

[2] A.E. Nel, L. Madler, D. Velegol, T. Xia, E.M. Hoek, P. Somasundaran, et al., Understanding biophysicochemical interactions at the nano-bio interface, Nat. Mater. 8 (2009) 543–557.

[3] T. Cedervall, I. Lynch, S. Lindman, T. Berggard, E. Thulin, H. Nilsson, et al., Understanding the nanoparticle-protein corona using methods to quantify exchange rates and affinities of proteins for nanoparticles, Proc. Natl. Acad. Sci. U. S. A. 104 (2007) 2050–2055.

[4] M. Lundqvist, J. Stigler, G. Elia, I. Lynch, T. Cedervall, K.A. Dawson, Nanoparticle size and surface properties determine the protein corona with possible implications for biological impacts, Proc. Natl. Acad. Sci. U. S. A. 105 (2008) 14265–14270.

[5] I. Lynch, K.A. Dawson, Protein-nanoparticle interactions, Nano Today 3 (2008) 40–47.

[6] E. Casals, T. Pfaller, A. Duschl, G.J. Oostingh, V. Puntes, Time evolution of the nanoparticle protein corona, ACS Nano 4 (2010) 3623–3632.

[7] D. Walczyk, F.B. Bombelli, M.P. Monopoli, I. Lynch, K.A. Dawson, What the cell "sees" in bionanoscience, J. Am. Chem. Soc. 132 (2010) 5761–5768.

[8] C. Rocker, M. Potzl, F. Zhang, W.J. Parak, G.U. Nienhaus, A quantitative fluorescence study of protein monolayer formation on colloidal nanoparticles, Nat. Nanotechnol. 4 (2009) 577–580.

[9] J. Schaefer, C. Schulze, E.E. Marxer, U.F. Schaefer, W. Wohlleben, U. Bakowsky, et al., Atomic force microscopy and analytical ultracentrifugation for probing nanomaterial protein interactions, ACS Nano 6 (2012) 4603–4614.

[10] M.P. Monopoli, C. Aberg, A. Salvati, K.A. Dawson, Biomolecular coronas provide the biological identity of nanosized materials, Nat. Nanotechnol. 7 (2012) 779–786.

[11] N.L. Anderson, N.G. Anderson, The human plasma proteome: history, character, and diagnostic prospects, Mol. Cell. Proteomics 1 (2002) 845–867.

[12] S. Tenzer, D. Docter, S. Rosfa, A. Wlodarski, J. Kuharev, A. Rekik, et al., Nanoparticle size is a critical physicochemical determinant of the human blood plasma corona: a comprehensive quantitative proteomic analysis, ACS Nano 5 (2011) 7155–7167.

[13] M.P. Monopoli, D. Walczyk, A. Campbell, G. Elia, I. Lynch, F.B. Bombelli, et al., Physical-chemical aspects of protein corona: relevance to in vitro and in vivo biological impacts of nanoparticles, J. Am. Chem. Soc. 133 (2011) 2525–2534.

[14] C.D. Walkey, W.C. Chan, Understanding and controlling the interaction of nanomaterials with proteins in a physiological environment, Chem. Soc. Rev. 41 (2012) 2780–2799.

[15] J. Martel, D. Young, A. Young, C.Y. Wu, C.D. Chen, J.S. Yu, et al., Comprehensive proteomic analysis of mineral nanoparticles derived from human body fluids and analyzed by liquid chromatography-tandem mass spectrometry, Anal. Biochem. 418 (2011) 111–125.

[16] M.A. Dobrovolskaia, A.K. Patri, J. Zheng, J.D. Clogston, N. Ayub, P. Aggarwal, et al., Interaction of colloidal gold nanoparticles with human blood: effects on particle size and analysis of plasma protein binding profiles, Nanomedicine 5 (2009) 106–117.

[17] A. Akesson, M. Cardenas, G. Elia, M.P. Monopoli, K.A. Dawson, The protein corona of dendrimers: PAMAM binds and activates complement proteins in human plasma in a generation dependent manner, RSC Adv. (2012).

[18] G. Caracciolo, D. Caputo, D. Pozzi, V. Colapicchioni, R. Coppola, Size and charge of nanoparticles following incubation with human plasma of healthy and pancreatic cancer patients, Colloids Surf. B: Biointerfaces 123 (2014) 673–678.

[19] H.S. Choi, Y. Ashitate, J.H. Lee, S.H. Kim, A. Matsui, N. Insin, et al., Rapid translocation of nanoparticles from the lung airspaces to the body, Nat. Biotechnol. 28 (2010) 1300–1303.

[20] C. Schleh, B. Rothen-Rutishauser, W.G. Kreyling, The influence of pulmonary surfactant on nanoparticulate drug delivery systems, Eur. J. Pharm. Biopharm. 77 (2011) 350–352.

[21] Z.J. Deng, M. Liang, M. Monteiro, I. Toth, R.F. Minchin, Nanoparticle-induced unfolding of fibrinogen promotes Mac-1 receptor activation and inflammation, Nat. Nanotechnol. 6 (2011) 39–44.

[22] A. Lesniak, F. Fenaroli, M.R. Monopoli, C. Aberg, K.A. Dawson, A. Salvati, Effects of the presence or absence of a protein corona on silica nanoparticle uptake and impact on cells, ACS Nano 6 (2012) 5845–5857.

[23] N.V. Konduru, Y.Y. Tyurina, W.H. Feng, L.V. Basova, N.A. Belikova, H. Bayir, et al., Phosphatidylserine targets single-walled carbon nanotubes to professional phagocytes in vitro and in vivo, PLoS ONE 4 (2009).

[24] M.S. Ehrenberg, A.E. Friedman, J.N. Finkelstein, G. Oberdorster, J.L. McGrath, The influence of protein adsorption on nanoparticle association with cultured endothelial cells, Biomaterials 30 (2009) 603–610.

[25] J. Sund, H. Alenius, M. Vippola, K. Savolainen, A. Puustinen, Proteomic characterization of engineered nanomaterial-protein interactions in relation to surface reactivity, ACS Nano 5 (2011) 4300–4309.

[26] A. Salvati, A.S. Pitek, M.P. Monopoli, K. Prapainop, F.B. Bombelli, D.R. Hristov, et al., Transferrin-functionalized nanoparticles lose their targeting capabilities when a biomolecule corona adsorbs on the surface, Nat. Nanotechnol. 8 (2013) 137–143.

[27] S. Wan, P.M. Kelly, E. Mahon, H. Stockmann, P.M. Rudd, F. Caruso, et al., The "sweet" side of the protein corona: effects of glycosylation on nanoparticle-cell interactions, ACS Nano 9 (2015) 2157–2166.

[28] D. Pozzi, V. Colapicchioni, G. Caracciolo, S. Piovesana, A.L. Capriotti, S. Palchetti, et al., Effect of polyethyleneglycol (PEG) chain length on the bio-nano-interactions between PEGylated lipid nanoparticles and biological fluids: from nanostructure to uptake in cancer cells, Nanoscale 6 (2014) 2782–2792.

[29] M. Ferrari, Cancer nanotechnology: opportunities and challenges, Nat. Rev. Cancer 5 (2005) 161–171.

[30] D. Peer, J.M. Karp, S. Hong, O.C. FarokHzad, R. Margalit, R. Langer, Nanocarriers as an emerging platform for cancer therapy, Nat. Nanotechnol. 2 (2007) 751–760.

[31] M. Sarparanta, L.M. Bimbo, J. Rytkonen, E. Makila, T.J. Laaksonen, P. Laaksonen, et al., Intravenous delivery of hydrophobin-functionalized porous silicon nanoparticles: stability, plasma protein adsorption and biodistribution, Mol. Pharm. 9 (2012) 654–663.

[32] B. Maggio, M.V. Raimondi, D. Raffa, F. Plescia, S. Cascioferro, G. Cancemi, et al., Synthesis and antiproliferative activity of 3-(2-chloroethyl)-5-methyl-6-phenyl-8-(trifluoromethyl)-5,6-dihydropyrazolo[3,4-f][1,2,3,5]tetrazepin-4-(3H)-one, Eur. J. Med. Chem. 96 (2015) 98–104.

[33] M.E. Davis, Z.G. Chen, D.M. Shin, Nanoparticle therapeutics: an emerging treatment modality for cancer, Nat. Rev. Drug Discov. 7 (2008) 771–782.

[34] M.C. Rillig, A connection between fungal hydrophobins and soil water repellency? Pedobiologia 49 (2005) 395–399.

[35] M.C. Rillig, B.A. Caldwell, H.A.B. Wosten, P. Sollins, Role of proteins in soil carbon and nitrogen storage: controls on persistence, Biogeochemistry 85 (2007) 25–44.

[36] V. Aimanianda, J. Bayry, S. Bozza, O. Kniemeyer, K. Perruccio, S.R. Elluru, et al., Surface hydrophobin prevents immune recognition of airborne fungal spores, Nature (London, U. K.) 460 (2009) 1117–1121.

[37] M.B. Linder, Hydrophobins: proteins that self assemble at interfaces, Curr. Opin. Colloid Interface Sci. 14 (2009) 356–363.

[38] M.B. Linder, G.R. Szilvay, T. Nakari-Setaelae, M.E. Penttilae, Hydrophobins: the protein-amphiphiles of filamentous fungi, FEMS Microbiol. Rev. 29 (2005) 877–896.

[39] J. Hakanpaa, G.R. Szilvay, H. Kaljunen, M. Maksimainen, M. Linder, J. Rouvinen, Two crystal structures of *Trichoderma reesei* hydrophobin HFBI — the structure of a protein amphiphile with and without detergent interaction, Protein Sci. 15 (2006) 2129–2140.

[40] J. Hakanpaa, A. Paananen, S. Askolin, T. Nakari-Setala, T. Parkkinen, M. Penttila, et al., Atomic resolution structure of the HFBII hydrophobin, a self-assembling amphiphile, J. Biol. Chem. 279 (2004) 534–539.

[41] M. Linder, K. Selber, T. Nakari-Setala, M. Qiao, M.R. Kula, M. Penttila, The hydrophobins HFBI and HFBII from *Trichoderma reesei* showing efficient interactions with nonionic surfactants in aqueous two-phase systems, Biomacromolecules 2 (2001) 511–517.

[42] J. Hakanpaa, T.A.A. Parkkinen, N. Hakulinen, M. Linder, J. Rouvinen, Crystallization and preliminary X-ray characterization of *Trichoderma reesei* hydrophobin HFBII, Acta Crystallogr. D 60 (2004) 163–165.

[43] A.S. Pitek, D. O'Connell, E. Mahon, M.P. Monopoli, F. Baldelli Bombelli, K.A. Dawson, Transferrin coated nanoparticles: study of the bionano interface in human plasma, PLoS ONE 7 (2012), e40685.

[44] M.S. Gruner, G.R. Szilvay, M. Berglin, M. Lienemann, P. Laaksonen, M.B. Linder, Self-assembly of class II hydrophobins on polar surfaces, Langmuir 28 (2012) 4293–4300.

[45] M. Linder, G.R. Szilvay, T. Nakari-Setala, H. Soderlund, M. Penttila, Surface adhesion of fusion proteins containing the hydrophobins HFBI and HFBII from Trichoderma reesei, Protein Sci. 11 (2002) 2257–2266.

[46] G.G. Martin, G.C. Cannon, C.L. McCormick, Adsorption of a fungal hydrophobin onto surfaces as mediated by the associated polysaccharide schizophyllan, Biopolymers 49 (1999) 621–633.

[47] A.L. Barran-Berdon, D. Pozzi, G. Caracciolo, A.L. Capriotti, G. Caruso, C. Cavaliere, et al., Time evolution of nanoparticle-protein corona in human plasma: relevance for targeted drug delivery, Langmuir 29 (2013) 6485–6494.

[48] S. Tenzer, D. Docter, J. Kuharev, A. Musyanovych, V. Fetz, R. Hecht, et al., Rapid formation of plasma protein corona critically affects nanoparticle pathophysiology, Nat. Nanotechnol. 8 (2013) 772–781.

[49] Ž. Krpetić, A.M. Davidson, M. Volk, R. Lévy, M. Brust, D.L. Cooper, High-resolution sizing of monolayer-protected gold clusters by differential centrifugal sedimentation, ACS Nano 7 (2013) 8881–8890.

[50] N.C. Bell, C. Minelli, J. Tompkins, M.M. Stevens, A.G. Shard, Emerging techniques for submicrometer particle sizing applied to stöber silica, Langmuir 28 (2012) 10860–10872.

Publication II

Lienemann, Michael; Grunér, Mathias S; Paananen, Arja; Siika-Aho, Matti; Linder, Markus B; 2015. *Charge-Based Engineering of Hydrophobin HFBI: Effect on Interfacial Assembly and Interactions*. ACS Publications. *Biomacromolecules*, volume 16, issue 4, pages 1283-1292. DOI: 10.1021/acs.biomac.5b00073

Article

pubs.acs.org/Biomac

Charge-Based Engineering of Hydrophobin HFBI: Effect on Interfacial Assembly and Interactions

Michael Lienemann,[†] Mathias S. Grunér,[†,‡,§] Arja Paananen,[†] Matti Siika-aho,[†] and Markus B. Linder*[,‡]

[†]VTT Technical Research Centre of Finland, Tietotie 2, Fi-02150 Espoo, Finland

[‡]Department of Biotechnology and Chemical Technology, School of Chemical Technology, Aalto University, P.O. Box 16100, Fi-00076 Aalto, Finland

Supporting Information

ABSTRACT: Hydrophobins are extracellular proteins produced by filamentous fungi. They show a variety of functions at interfaces that help fungi to adapt to their environment by, for example, adhesion, formation of coatings, and lowering the surface tension of water. Hydrophobins fold into a globular structure and have a distinct hydrophobic patch on their surface that makes these proteins amphiphilic. Their amphiphilicity implies interfacial assembly, but observations indicate that intermolecular interactions also contribute to their functional properties. Here, we used the class II hydrophobin HFBI from *Trichoderma reesei* as a model to understand the structural basis for the function of hydrophobins. Four different variants were made in which charged residues were mutated. The residues were chosen to probe the role of different regions of the hydrophilic part of the proteins. Effects of the mutations were studied by analyzing the formation and structure of self-assembled layers, multimerization in solution, surface adhesion, binding of secondary layers of proteins on hydrophobins, and the viscoelastic behavior of the air−water interface during formation of protein films; the comparison showed clear differences between variants only in the last two analyses. Surface viscoelasticity behavior suggests that the formation of surface layers is regulated by specific interactions that lead to docking of proteins to each other. One set of mutations led to assemblies with a remarkably high elasticity at the air−water interface (1.44 N/m). The variation of binding of secondary layers of protein on surface-adsorbed hydrophobins suggest a mechanism for a proposed function of hydrophobins, namely, that hydrophobins can act as a specific adhesive layer for the binding of macromolecules to interfaces.

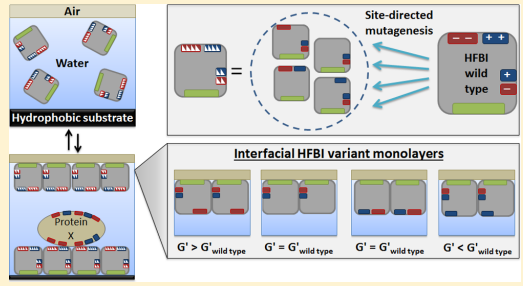

INTRODUCTION

Hydrophobins are extracellular proteins that are unique to filamentous fungi and show functions that are related to the control of interfaces. In various organisms, several different types of interfacial functions have been reported, including adhesion, coatings, and enhancing aerial growth.[1−8] Due to the special properties of hydrophobins and because they can be prepared as pure substances, they have become attractive for use in several types of technical applications. These include dispersion of insoluble drug compounds, production of stable edible foams, protein immobilization, and stabilization of colloidal dispersions.[9−11] Because of the high performance of hydrophobins for these applications, there is also the interesting possibility of studying them as biomimetic models for the development of new surfactants.

Self-assembly has a major role for the structural basis of function in hydrophobins. Characterization and sequence analysis have led to the grouping of hydrophobins into two main classes: class I and class II. Overall, the two classes share the same structural theme, but they differ in the way that they form assembled structures and consequently show differences in the properties of these structures. The following discussion and conclusions relate to class II proteins, and only further work can reveal relations to the behavior of class I members.

Structural analysis based mostly on the hydrophobins HFBI and HFBII from *Trichoderma reesei* have shown that the proteins have a compact globular fold with a large part of the aliphatic hydrophobic side chains collected in one patch on the surface. The patch comprises about 18% of the surface area and leads to an amphiphilic structure.[12] The relatively large size of the hydrophobic patch makes the structure reminiscent of a class of synthetic colloids that are called Janus-particles, which also have a structural division into hydrophobic and hydrophilic parts.[13] One interesting aspect of such large amphiphilic structures relates to the finding that hydrophobicity is a size-dependent phenomenon.[14] Large amphiphiles may therefore have significantly different properties compared to those of smaller amphiphiles. However, when analyzing interfaces of

Received: January 17, 2015
Revised: February 26, 2015
Published: February 27, 2015

DOI: 10.1021/acs.biomac.5b00073
Biomacromolecules 2015, 16, 1283−1292

assembled hydrophobins with AFM and diffraction techniques, it was clearly revealed that the hydrophobins organize into regular structures with defined repeating units.[15] Interestingly, the dimensions of the repeating units were greater than the dimensions of individual protein molecules.[16] The formation of these regular patterns suggests that the functionality of the hydrophobins stem from more complex interactions than mere amphiphilicity and that, for example, intermolecular interactions could play an important role in forming assemblies with several hierarchical levels. Also, some of the functions of hydrophobins, such as their exceptionally high surface elasticity, suggest that intermolecular bonding would contribute to their function.[17]

A detailed structure–function understanding of hydrophobins would have implications for understanding their biological roles as well as understanding their applicability for technical use. Here, one aspect of their study is noteworthy. Fungi have evolved to use hydrophobins for multiple tasks, and most fungal genomes contain multiple copies of hydrophobins that may have different expression profiles. Deletion mutant phenotypes are typically difficult to characterize, apparently because of functional compensation by other hydrophobins. As with their physiological functions, there is not a single characteristic assay that can reveal the functionality of purified hydrophobins in structure–function studies. Instead, the functionality must be inferred from a set of measurements that can include adhesion, formation of multimers in solution, formation of interfacial structures, and others.

In this work, we used point mutations to gain understanding regarding the structure–function relationships in HFBI from *T. reesei*, which belongs to class II hydrophobins. We focused on charged residues because these are most likely to affect the way that the surface-exposed residues interact, and at the same time, these mutations were unlikely to affect the hydrophobic patch. Also, an initial set of variants made with fusion proteins of HFBI and green fluorescent protein (GFP) suggested that such mutations affect protein–protein interactions in HFBI.[18]

MATERIALS AND METHODS

Design of Mutations. The structure of HFBI shows six charged residues that are exposed on its surface (Figure 1A). Four of these are located on the face of the protein that is opposite to the hydrophobic patch (i.e., D40, D43, R45, and K50). The remaining two (D30 and K32) are located near the edge of the hydrophobic patch (see also Supporting Information Figure 2). Because of these structural arrangements, we designed the mutant variants so that the regions were probed separately. The charged residues proximal to the hydrophobic patch (D30 and K32) were also identified in computational studies as being potentially important for intermolecular interactions (Figure 1B).[19] These residues were exchanged for electrically neutral ones in the variant D30N/K32Q. The four charged residues on the face opposite the hydrophobic patch were studied in three different variants. Neutralizing the positively charged residues gave the negatively charged variant R45Q/K50Q, neutralizing the negatively charged residues gave the positively charged variant D40Q/D43N, and all the charged residues on this face were neutralized in the third variant, D40Q/D43N/R45Q/K50Q.

Production of HFBI Variants in *T. reesei*. The *T. reesei* production strain M219 was used for construction of the HFBI variant-producing *Trichoderma* strains. As a first step, the *hfb2* gene was disrupted by insertion of a hygromycin resistance cassette from the plasmid pTNS27[20] in order to prevent copurification of naturally secreted HFBII hydrophobin during HFBI variant purification from the supernatant. The cassette was amplified from plasmid pTNS27 as described previously.[21] Knockout mutants were isolated by initial

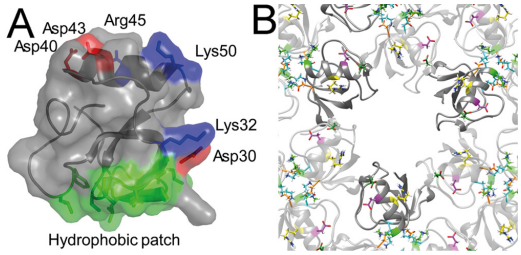

Figure 1. (A) Three-dimensional structure of *T. reesei* hydrophobin HFBI (PDB ID 2FZ6). Basic and acidic residues are annotated and colored blue and red, respectively. The protein binds to hydrophobic substrates and the air–water interface through the hydrophobic patch. The figure was produced using PyMOL.[33] (B) Computational model of an HFBI monolayer with 6-fold symmetry (referred to as β structure by Magarkar et al.[19]). The side chain atoms of the mutated residues are shown as sticks, oxygen, in red, and nitrogen, in blue. The positions of the mutated side residues in the HFBI sequence are indicated by coloring of the side chain carbon atoms (e.g., orange, D30; cyan, K32, dark green, D40; magenta, D43; yellow, R45; light green, K50). Individual HFBI molecules of the pore-forming hexamer complex are highlighted by shading. The pores in the protein layer are flanked by the negatively charged side chains of residues D40 and D43 as well as the positively charged side chain of R45. The figure was produced using the UCSF Chimera package.[34]

plating on hygromycin-containing top agar (150 μg/mL) and consecutive transfer to agar plates containing 0.1% (w/v) Triton X-100 and hygromycin (125 μg/mL). *hfb2* gene disruption was confirmed by PCR (Phire Plant Direct PCR kit) (Thermo, Finnzymes) using two probes that were complementary to the *hph* resistance marker (hph_sekv 1:5′-ATT CTT CGC CCT CCG AGA GC-3′) and the *hfb2* region located upstream of the deletion cassette insertion (Mil73_fw: 5′-GAA TCA TGC TGG AGT GAA GG-3′). In addition, the absence of HFBII in the culture supernatant was confirmed by western blotting (4–20% acrylamide Criterion gradient gel, Bio-Rad, with HFBII-specific polyclonal antibodies). The *T. reesei hfb2::hph* strain was named VTT D-121447.

Variant-producing strains were made using VTT D-121447 by insertion of the mutated *hfb1* gene into the genome by homologous recombination. The HFBI gene insertion was performed into the highly expressed *cbh1* gene using plasmids that contained an insertion cassette consisting of the acetamide resistance gene *amdS* and a HFBI variant gene for one of the variants (e.g., pMil003, D40Q/D43N/R45Q/K50Q; pMil004, D40Q/D43N; pMil005, R45Q/K50Q; and pMil006, D30N/K32Q). The insertion resulted in disruption of the *cbh1* gene and placement of the HFBI variant genes under the control of the *cbh1* promoter. Homologous recombination and clone selection was performed as described above with the exception that acetamide (10 mM) was used as a selective antibiotic. Acetamide-resistant clones were analyzed for HFBI variant gene insertion by sequencing using primers that bind to the CBHI promoter (T010_Cbh1 prom 5′ sekv: 5′-CAA CTC AGA TCC TCC AGG AGA C-3′) and CBHI terminator (T043_Cbh1_term_R sekv: 5′-TCA TGA TAC GGG CTC ACC AAG-3′). These genetic modifications yielded four novel *T. reesei* strains that were named D-121448 (D40Q/D43N/R45Q/K50Q), D-121449 (D40Q/D43N), D-121450 (R45Q/K50Q), and D-121451 (D30N/K32Q). The production of the four HFBI variants was performed in 1 L of minimal medium (TrMM, pH 5.2), which had the following composition: 0.11 M KH_2PO_4, 38 mM $(NH_4)_2SO_4$, 2.4 mM $MgSO_4$, 4.1 mM $CaCl_2$, 0.18 mM $FeSO_4 \cdot 7\ H_2O$, 95 μM $MnSO_4 \cdot H_2O$, 49 μM $ZnSO_4 \cdot H_2O$, 0.16 mM $CoCl_2 \cdot 6\ H_2O$, and 2% (w/v) glucose) supplemented with 4% (w/v) lactose and 2% (w/v) spent grain extract. The fungal cultivation was performed in shake flasks for 7 days at 28 °C with 200 rpm shaking, after which the culture liquid was stored frozen until further processing.

DOI: 10.1021/acs.biomac.5b00073
Biomacromolecules 2015, 16, 1283–1292

Purification of HFBI Variants from *T. reesei* Culture Supernatant. Purification of the HFBI variants was performed using a combination of protein separation in an aqueous two-phase system (ATPS) and reversed-phase chromatography essentially as described previously.[22] Initially, the frozen fungal culture liquid was thawed in a water bath at 22 °C for 1 h, and insoluble material was removed by centrifugation at 4400*g* for 25 min and gravity filtration of the supernatant through grade 597-1/2 quantitative folded filter paper with pore size of 4−7 μm (Whatman PLC, UK). The pH of the filtered solution was adjusted to 5 by addition of 1 M sodium acetate solution. Berol 532 detergent (Akzo Nobel N.V., The Netherlands) was added to the supernatant to a final concentration of 2% (w/v). The solution was mixed by gentle shaking and allowed to separate in a separation funnel. The detergent phase was isolated followed by addition of 20 mL of 50 mM sodium acetate buffer (pH 5.15) containing 40 mM EDTA and 0.18 mL of isobutanol. The mixture was mixed gently, and the phases were allowed to separate in a separation funnel. The lower phase was purified further by preparative reversed-phase chromatography using a Vydac C4 (1 × 20 cm) column and a gradient elution from an aqueous solution containing 0.1% (v/v) trifluoroacetic acid to 100% acetonitrile containing 0.1% (v/v) trifluoroacetic acid. HFBI variant proteins eluting as fractions with a high absorption at λ = 230 nm were pooled and lyophilized.

Reagents and Chemicals. *T. reesei* endoglucanase II EGII (Tr CelSA) was purified as described previously,[23] xylanases XYNI and XYNII were purified according to a published method,[24] but in the case of TrXYNI the last gel filtration step was omitted, and cellobiohydrolase I CBHI (Tr Cel7A) was prepared as previously described.[25] Glucose oxidase from *Aspergillus niger* (GOx) and 1-hexanethiol were obtained from Sigma-Aldrich Chemie GmbH (Germany).

Measurement of Zeta Potential. The samples were prepared by dissolving lyophilized wild type and variants of HFBI in water at a concentration of 0.1 mg/mL, and the pH was titrated to values between 1.5 and 9.5 depending on the variant using 100 mM and 1.0 M HCl and 10 and 100 mM NaOH. The zeta potential was measured using a Zetasizer Nano-ZS instrument (Malvern, UK) and a sample volume of 1.0 mL.

Size-Exclusion Chromatography (SEC). HFBI variants dissolved in 100 μL of buffer were injected at a series of concentrations onto a Superdex 75 column (GE, Sweden) and eluted with 10 mM Na-acetate at pH 5.5 containing 0.2 M NaCl using an Äkta Explorer (GE, Sweden) chromatography system. Protein elution was detected at λ = 230 nm. Standard proteins were injected to calibrate the elution time against the protein molecular weight. The references used were vitamin B-12 (1.4 kDa, Sigma), aprotinin (6.5 kDa, Sigma), ribonuclease A (13.7 kDa, GE, Sweden), and ovalbumin (43.0 kDa, GE, Sweden).

Drop Flattening Measurements. The time required for the formation of a flat plateau on top of a drop of an aqueous solution of hydrophobin was measured with an optical contact angle and surface tensiometer (CAM 200, KSV NIMA, Finland). The experiment was done by dissolving the protein in water and placing 50 μL of this solution on Parafilm. This technique, which addresses a characteristic feature in hydrophobins, was earlier described and discussed in ref 15. Images were taken with 60 s intervals in order to register the time at which the drop started to flatten on the top. Triplicate experiments were performed for each variant.

Formation and Static Analysis of HFBI Monolayers. Formation of HFBI variant monolayers was analyzed in a humidified atmosphere using a Langmuir trough and presoaked 20.6 mm perimeter Wilhelmy paper plates (KSV NIMA, Finland). Surface pressure was monitored by probing 20 mL of 5 mM Na-acetate (pH 5.5) in a glass beaker of 4.7 cm diameter that had been equilibrated to room temperature. The sample protein was dissolved at a concentration of 0.85−1.0 μM by short magnetic stirring (1.5−2 min), and the change of surface pressure was monitored until equilibrium was reached (typically, after 30 min to 1 h). In the experiment, the Wilhelmy plate was submerged prior to protein addition.

HFBI Layer Compression Assay Using the Langmuir Trough. Monolayers of HFBI variants were assembled, and their structural properties were measured using a KSV Minimicro trough (KSV NIMA, Finland). Protein layers were prepared at the air−water interface by injecting 20 μg of dissolved protein into 55 mL of 5 mM Na-acetate buffer (pH 5.5) at 21 °C. This solution was left for 45 min in order to allow the hydrophobin proteins to reach equilibrium. Compression/expansion cycle isotherms were recorded while moving the barriers at a constant rate of 2 mm/min and switching to expansion at 35 mN/m surface pressure.

Interfacial Rheology. The interfacial shear rheological properties of wild-type HFBI and HFBI variants at the air−water interface were measured at RT using a DHR-2 rheometer (TA Instruments, UK) equipped with a Pt−Ir du Noüy ring (13 mm diameter, Krüss, Germany, flamed prior to use) in oscillatory mode. The concentrations of stock solutions of HFBI and HFBI variants were determined by UPLC. A 0.3 μM solution (≈ 2.3 μg/mL = 0.00023% (w/v)) of HFBI (or variant) in water was prepared to a 50 mL volumetric flask and allowed to temper to RT (22 °C) for 1 h prior to experiments. The solution was placed in a 60 mm diameter glass dish, and the du Noüy ring was placed onto the surface according to the manufacturer's instructions. The interfacial shear elastic (storage) modulus, G', and viscous (loss) modulus, G'', were monitored at constant frequency of 0.1 Hz and constant strain of 0.1% during film formation for at least 2 h to reach equilibrium. The chosen frequency and strain were measured to be in the linear viscoelastic region. Each measurement was replicated at least twice.

Atomic Force Microscopy (AFM). A NanoScopeV Multimode8 AFM (E scanner, Bruker) and NCS15/AlBS cantilevers (μMasch, USA) were used in all measurements. All images were recorded in tapping mode in air with scan rates in the range of 0.7−1 Hz (free amplitude about, 0.68 V; damping ratio, 0.7−0.8). Images were flattened only to remove possible tilt in the image data (NanoScope Analysis), and no further processing was done. A scanning probe image processor (SPIP, Image Metrology, Denmark) was used for image analysis. The topography and phase contrast images were captured simultaneously. The phase contrast image shows the phase difference between the oscillations of the cantilever driving piezo and the detected oscillations. It is thought that image contrast is derived from surface properties such as stiffness and viscoelasticity (hard tapping) or hydrophilicity/hydrophobicity (light tapping), but it also shows enhanced edge structures.

Protein Adsorption Using Quartz Crystal Microbalance with Dissipation Monitoring QCM-D. Hydrophobin adhesion and adsorption of sample proteins to HFBI variant layers at various pH values were monitored by QCM-D through measurement of frequency and dissipation (D4-QCM system, Biolin Scientific AB, Sweden). QCM sensors with a hydrophobic sensor surface were prepared by first cleaning gold-coated QCM sensor disks (model QSX301, Biolin Scientific AB, Sweden) in an UV/ozone chamber for 10 min and exposing them for another 10 min to a 5:1:1 mixture of water, H_2O_2, and an aqueous ammonia solution (25% w/w) at ∼75 °C. This was followed by thorough rinsing with water, drying under a stream of N_2, and incubating for 2 min in ethanol (94% w/v). The prewetted sensors disks were immersed in a 50 mM 1-hexanethiol solution in ethanol and left to react at room temperature overnight. As a final step, unreacted 1-hexanethiol was washed off with ethanol and water, and the sensor was dried under a flow of N_2. The QCM-D measurements were performed at 23 °C, and buffer/sample injection was performed at a rate of 0.1 mL/min. All buffers were degassed by vacuum filtration before use. HFBI variant adsorption was carried out by injection of 300 μL of protein sample solution at a concentration of 0.1 mg/mL. Unbound protein was removed from the sensor surface by rinsing at pH 5.5 using 10 mM Na-acetate buffer.

RESULTS

Production of HFBI Variants. Secretion of HFBI variants was confirmed by western blot analysis using polyclonal HFBI-specific antibodies. The selected *T. reesei* strains produced the

DOI: 10.1021/acs.biomac.5b00073
Biomacromolecules 2015, 16, 1283−1292

HFBI variants in the supernatant at high concentrations, allowing purification by ATPS and yielding 100−500 mg of protein per liter (D30N/K32Q, 244.7 mg/L; D40Q/D43N, 98.5 mg/L; R45Q/K50Q, 390 mg/L; and D40Q/D43N/R45Q/K50Q, 504 mg/L). Zeta-potential measurements showed that the introduced amino acid substitutions resulted in changes of the isoelectric point, as expected, according to the type of the modified acid (Figure 2 and Table 1). The solubility

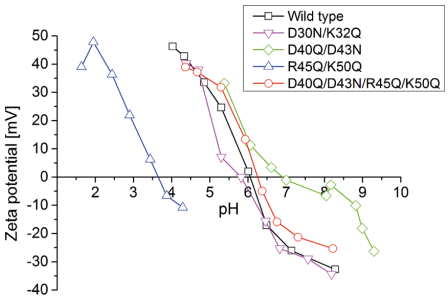

Figure 2. Zeta potential of wild-type HFBI and variants D30N/K32Q, D40Q/D43N, R45Q/K50Q, and D40Q/D43N/R45Q/K50Q measured in 0.1 mg/mL protein solutions. From this plot, the isoelectric points were determined to be 6.1, 5.8, 7.0, 3.6, and 6.2, respectively.

of all of the variants was very good and was similar to that of the wild type at least up to the highest tested concentrations of several milligrams per milliliter.

Size-Exclusion Chromatography (SEC). The concentration-dependent multimerization of the four HFBI variants was analyzed by dissolving the protein at concentrations ranging between 3 μM and 1 mM, followed by separating over a SEC column and monitoring their elution. At concentrations below 30 μM, the four HFBI variants and the wild type eluted at similar elution times corresponding to a molecular weight of around 5 kDa as the monomer state (7.5 kDa). Larger complexes were formed when the hydrophobin concentration was increased above 100 μM (Figure 3). The concentration range at which the transition between these two states occurred was indistinguishable when comparing the wild type and the four variants and shows that the formation of complexes is a concentration-dependent equilibrium driven by high protein concentration.

Assembly of Hydrophobin Variant Layers at the Air−Water Interface. The formation of a flattened plateau on the

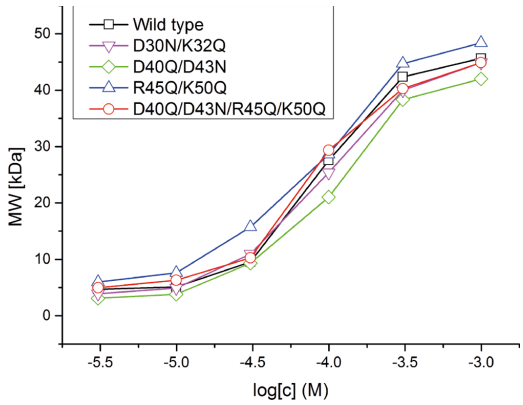

Figure 3. Concentration-dependent multimerization of HFBI variants, as determined by SEC. The calculated molecular weights of the main elution peaks are plotted against the concentration of the solution of the injected HFBI variant.

top of a hydrophobin solution droplet is a characteristic property for HFBI. This is likely due to the formation of a hydrophobin monolayer at the air−water interface. In order to test the ability of the HFBI variants to show similar function, droplets of hydrophobin solution were left to evaporate, and the time necessary for plateau formation was determined using the surface tensiometer apparatus. All variants produced the same plateau effect, although the rate at which the plateau was formed showed some delay compared to that of the wild type. For the wild type, the time for formation was 19 ± 3.5 min, and for the variants, the time was typically 30−70% longer.

In order to assess the protein concentration in these layers on a macroscopic scale, surface tension (γ) reduction upon HFBI variant layer formation at the air−water interface was measured using a Langmuir trough. These measurements showed that the four variants produced very similar layers (see Table 1) that resembled the wild-type layer (35.5 ± 1.6 mN/m) closely. The molecular area that was occupied in the interfacial layers by the tested HFBI proteins was determined by repeated compression−expansion cycles. The protein layer densities of the HFBI variants were determined from the second compression isotherm and were found to be indistinguishable from that of the wild-type HFBI (3.23 ± 0.51 nm^2; Table 1).

Table 1. Experimental and Calculated Parameters for HFBI and the Different Variants[a]

	wild type	D30N/K32Q	D40Q/D43N	R45Q/K50Q	D40Q/D43N/R45Q/K50Q
MW (Da)	7535	7533	7546	7506	7517
IEP	6.1 (5.7)	5.8 (5.7)	7.0 (8.2)	3.6 (3.9)	6.2 (5.5)
HAM (ng/cm^2)	223 ± 98	247 ± 35	289 ± 45	217 ± 35	293 ± 56
MA (Å^2)	323 ± 51	322 ± 52	323 ± 34	324 ± 55	343 ± 38
γ (mN/m)	35.5 ± 1.6	36.5 ± 0.0	31.3 ± 7.5	36.0 ± 0.6	36.6 ± 0.3
t_{DF} (min)	19.0 ± 3.5	24.3 ± 1.2	32.3 ± 2.5	23.7 ± 3.8	31.3 ± 3.5

[a]MW, experimentally determined molecular weight according to MALDI-TOF mass spectrometry; IEP, isoelectric point determined from duplicate measurements with theoretical value based on amino acid sequence given in brackets; HAM, hydrophobically adsorbed mass, which was determined from the presented QCM experiments on hexanethiol coated surfaces; MA, molecular area; and γ, surface tension of HFBI variant solutions, which was determined from interfacial HFBI protein layers assembled in a Langmuir trough. Time required for plateau formation on hydrophobin variant droplets (t_{DF}) was measured in triplicate.

DOI: 10.1021/acs.biomac.5b00073
Biomacromolecules 2015, 16, 1283−1292

Interfacial Rheology of Hydrophobin Variant Layers. The adsorption of wild-type HFBI and HFBI variants to the air−water interface was monitored and viscoelastic properties were determined by interfacial shear rheology measurements. The storage modulus (elastic, G') and loss modulus (viscous, G'') of the interfacial hydrophobin layers are shown in Figure 4A,B, respectively. At equilibrium, the shear storage modulus,

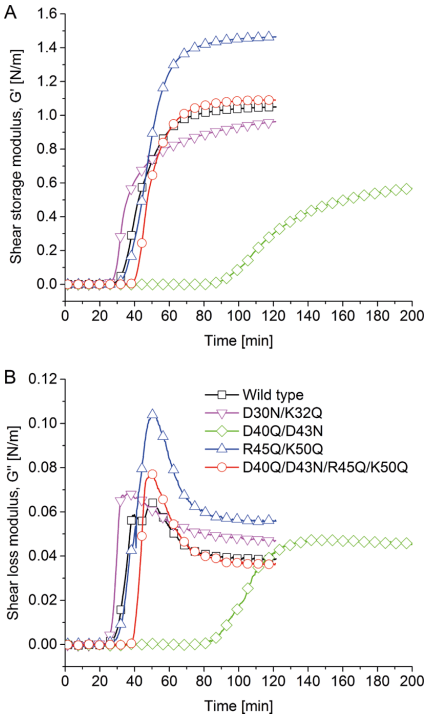

Figure 4. Interfacial rheology data of wild-type HFBI and HFBI variants D30N/K32Q, D40Q/D43N, R45Q/K50Q, and D40Q/D43N/R45Q/K50Q at the air−water interface as a function of adsorption time: (A) storage modulus, G', and (B) loss modulus, G''. The interfacial layers are adsorbed from 0.3 μM protein solutions.

G', for wild-type HFBI reached a value of 1.04 ± 0.01 N/m, which is comparable to previously reported values for HFBI (0.7 N/m in ref 17). The corresponding values for HFBI variants D30N/K32Q, D40Q/D43N, R45Q/K50Q, and D40Q/D43N/R45Q/K50Q are 0.85 ± 0.10, 0.62 ± 0.01, 1.44 ± 0.03, and 1.09 ± 0.01 N/m, respectively. The G' values are in a similar range or less than that for wild-type HFBI, except for the high value for R45Q/K50Q variant that showed a ∼40% increase in the elastic modulus. The equilibrium shear loss modulus values, G'' (Figure 4B), for all hydrophobins were less than 0.06 N/m. Tan δ values at equilibrium were very low, less than 0.1, for all hydrophobins, showing dominance of the G' values in all cases.

AFM Imaging of Langmuir−Blodgett Films. AFM images of Langmuir−Blodgett films (LB films) of all HFBI variants showed regular ordered raft-like structures (Figure 5A−D). It is possible that at the air−water interface all protein films consisted of larger crystalline domains, which broke down

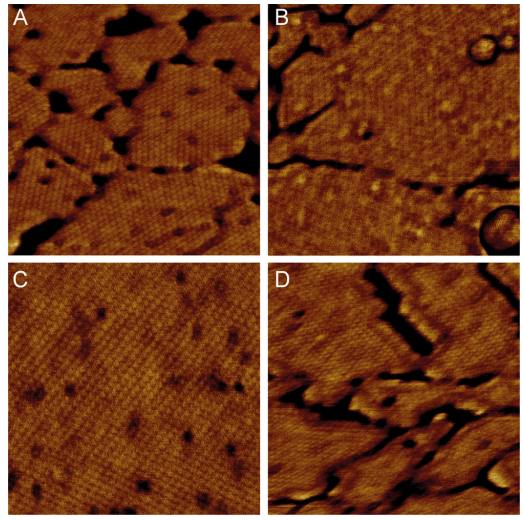

Figure 5. AFM images of LB films of HFBI variants that were assembled at the air−water interface, transferred to a flat mica substrate, dried, and imaged in air using tapping mode. Displayed are typical 200 nm phase images of HFBI variants D30N/K32Q, D40Q/D43N, R45Q/K50Q, and D40Q/D43N/R45Q/K50Q (A−D, respectively).

to smaller rafts during film transfer onto mica. The crystallinity of the protein films was confirmed by Fourier transformation of the phase contrast image data. The oblique structures of all HFBI variants possessed unit cell vector dimensions of 5.4 ± 0.9 nm for a and b and 120 ± 12° for γ. The values for wild-type HFBI were 5.6 ± 0.5 nm for a and b and 120 ± 7° for γ. The deviation of the lattice constants from pure hexagonal packing ($a = b$ and $\gamma = 120°$) and differences between different samples are within the expected error limits set by scanner hysteresis, creep, and drift in the AFM. These errors can potentially lead to small differences in self-assembled structures of the HFBI variants going unnoticed.

QCM Measurements of pH-Dependent Binding of Soluble Proteins to HFBI Variants. The binding of proteins to hydrophobin layers was investigated by QCM in order to determine whether the regular charge pattern of a HFBI monolayer (Figure 1B) was recognized by other proteins. This was done by adding secreted carbohydrate-active *T. reesei* enzymes and, as a reference, *A. niger* glucose oxidase to adsorbed layers of wild-type hydrophobin and the four variants, as outlined in Figure 6A,B. The adsorption to a hydrophobic hexanethiol-coated surface was found to be very similar among the tested HFBI variants (Table 1) and in the range of wild-type HFBI adsorption (223 ± 98 ng/cm^2).

Adsorbed layers of wild-type HFBI and variants bound the highest GOx amounts between pH 4.7 and 5.2 (Figure 7A). When compared to the wild type, the D30N/K32Q substitution resulted in a lower amount of adsorbed GOx, whereas layers of the other three variants bound more GOx than that of the wild type. In addition to this common GOx adsorption peak, a second GOx adsorption maximum at pH 6−9 was measured for variant D40Q/D43N.

Adsorbed layers of variants D30N/K32Q and D40Q/D43N/R45Q/K50Q did not bind the *T. reesei* enzymes XYNI (pI 9),

DOI: 10.1021/acs.biomac.5b00073
Biomacromolecules 2015, 16, 1283−1292

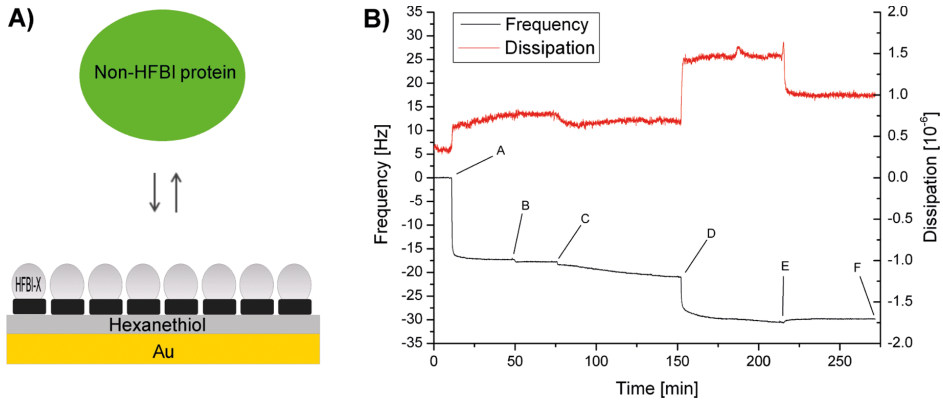

Figure 6. (A) Schematic representation of the HFBI coated QCM sensor at which adsorption of non-HFBI proteins was measured. (B) Representative protein adsorption QCM experiment at pH 9.0 with HFBI variant D40Q/D43N: (A) injection of 0.03 mg of HFBI-D40Q/D43N in 10 mM Na-acetate buffer (pH 5.5), (B) removal of unbound hydrophobin by buffer rinsing, (C) equilibration with 10 mM glycine buffer (pH 9.0), (D) injection of 0.3 mg of glucose oxidase at pH 9.0, (E) washing off of unbound glucose oxidase, and (F) end of experiment. The adsorbed mass of the non-HFBI protein was calculated using the frequencies at points D and F.

XYNII (pI 5.5), CBHI (pI 3.7−4.2), and EGII (pI 5.2) within the pH range of the experiments (Figure 7B−E). Similarly, wild-type HFBI and variants D40Q/D43N and R45Q/K50Q did not bind XYNI, EGII, and, in the case of wild type and variant R45Q/K50Q, also XYNII (Figure 7B,C,E). In the case of CBHI, however, binding to wild-type HFBI and variants D40Q/D43N and R45Q/K50Q was detected between pH 3.9 and 4.7 (Figure 7D) and was much higher for D40Q/D43N (570 ng/cm^2 at pH 4.7) than that for the wild type (60 ng/cm^2 at pH 3.9) and R45Q/K50Q (20 ng/cm^2 at pH 3.9). XYNII did bind exclusively variant D40Q/D43N and exhibited a binding maximum of 100 ng/cm^2 at around pH 5.2, whereas basal adsorption of around 60 ng/cm^2 was measured throughout the probed pH range with this variant (Figure 7C).

DISCUSSION

High-resolution imaging, modeling, and exceptional properties suggest that structurally defined interactions and specific molecular docking play important roles in the formation of the interfacial layers of HFBI and similar hydrophobins. Here, point mutations were made in order to perturb molecular interactions and thereby gain insight into the structural basis of the function of HFBI. We made mutations with different combinations of charged residues that were changed into sterically related noncharged homologues. Three of the variants of HFBI probed the surface region opposite the hydrophobic patch (e.g., D40Q/D43N, R45Q/K50Q, and D40Q/D43N/R45Q/K50Q). In a fourth variant (D30N/K32Q), the two charged residues close to the hydrophobic patch were investigated (Figure 1A).

Many of the methods used for functional characterization did not reveal any differences between variants. For instance, gel filtration showed that multimerization depends on the solution concentration of protein and did not differ significantly between wild type and variants. Additionally, all mutated variants formed interfacial films in a similar way, as shown both by how such films are formed spontaneously on the top of a drop as well as in the Langmuir trough. By high-resolution AFM, the films of the variants had the same distinct structural patterns as have been demonstrated previously for wild type. When we studied how wild type and variants bound to solid surfaces, we obtained nearly identical binding capacities as well as viscoelastic properties for the adsorbed layers. When comparing expression levels of the variants and wild type, we noted that expression levels of the variants in solution tended to be somewhat higher than seen for the wild type. Zeta-potential measurements showed differences in the isoelectric points between variants that were in line with the change of charge due to mutations, but they did not indicate any direct functional difference. For D40Q/D43N, the difference in predicted pI and zero zeta potential was the largest. Such differences can indicate that the local environment in the protein affects the ionization state of the side chains and that this may have an effect on the function of these side chains. As noted below, this particular variant shows some significant functional differences that may be linked to this observation.

However, in two clearly different and quantifiable sets of experiments, differences between variants and wild type were seen. One was the interfacial rheology properties, and the other was in how immobilized surface films of the variants interact with other proteins. By interfacial rheology, we were able to follow events leading to the formation of films at the air−water interface (Figure 4). A characteristic feature of the film formation was the remarkably long lag time before the onset of significant increase in G' and G''. This lag time and the order in which the variants performed was reproducible, i.e., the time of the onset of an increase in G' and G'' was reproducibly the shortest for D30N/K32Q and longest for D40Q/D43N. Although the D30N/K32Q variant showed a shorter time before the onset of an increase in G' and G'' than that of the other variants, the overall rate of change was slower than that for the wild type and the other variants. However, the loss modulus increased most rapidly for D30N/K32Q. As shown in Figure 8A, results from structural analysis show that D30 and K32 are located on the lateral sides of adjacent HFBI molecules, where they can participate in forming ionic bonds between molecules.[19] The location of these residues and the effect on function, therefore, suggests that these residues have a role in the mechanism of initial docking of the proteins and also

DOI: 10.1021/acs.biomac.5b00073
Biomacromolecules 2015, 16, 1283−1292

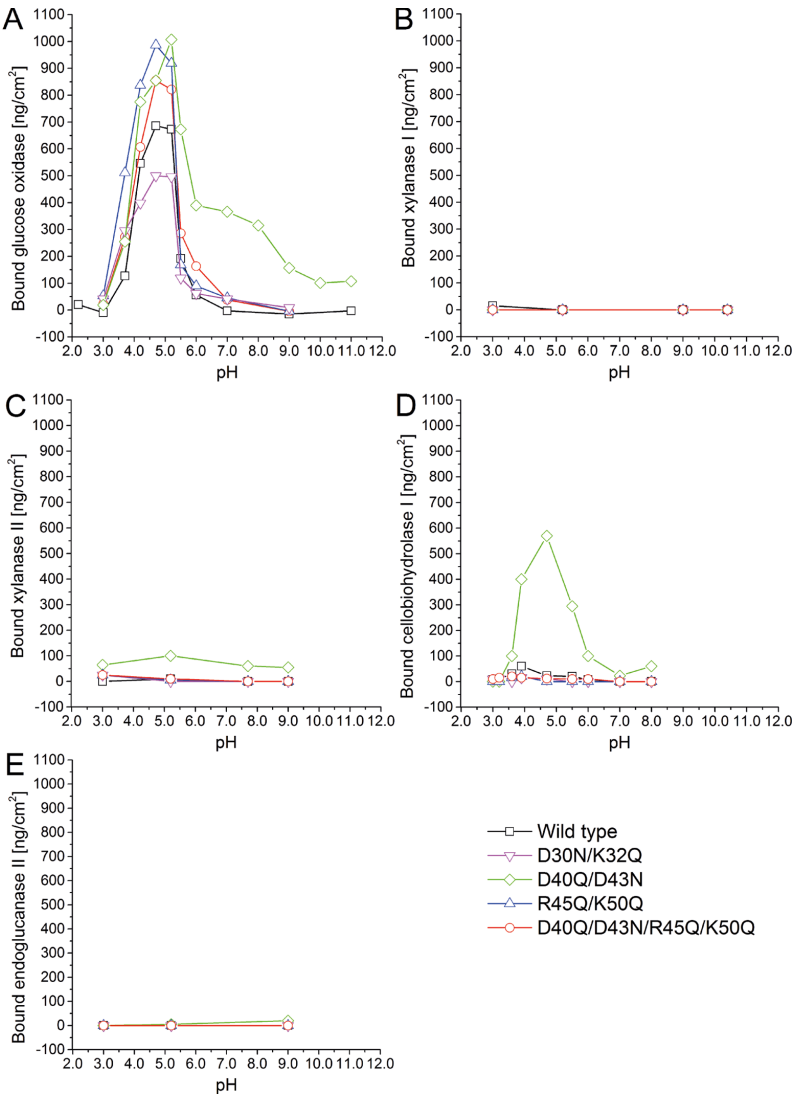

Figure 7. pH-dependent adsorption of non-HFBI proteins to adsorbed layers of wild-type HFBI and HFBI variants D30N/K32Q, D40Q/D34N, D40Q/D34N/R45Q/K50Q, and R45Q/K50Q determined by QCM-D. The injected non-HFBI proteins were *Aspergillus niger* glucose oxidase (GOx) (A; pI 4.2) and the *Trichoderma reesei* proteins xylanase I (XYNI) (B; pI 9), xylanase II (XYNII) (C; pI 5.5), cellobiohydrolase I (CBHI) (D; pI 3.7−4.2), and endoglucanase II (EGII) (E; pI 5.2). The adsorption data on glucose oxidase binding to wild-type HFBI layers was originally published in ref 28.

on the lateral coherence of the molecules, as indicated by the relatively high G'' compared to G'. This also implies that molecular recognition events kinetically control the mechanism by which elastic surface films form. The development of G'' for the wild type also showed an interesting behavior in having a local minimum at around 40 min, but this minimum was missing from all of the variants. This indicates a mechanism in which intermediate forms exist and structural rearrangements occur during the assembly process.

The R45Q/K50Q mutant is interesting because it followed the behavior of the wild type but reached higher absolute values. The final value for G' was very high (1.44 N/m), which, to our understanding, is the highest value for a protein film reported in the literature.[17] Variant D40Q/D43N was clearly different than the rest, being significantly slower to assemble and not reaching the G' values of the wild type. However, surprisingly, a combination of these two variants in D40Q/D43N/R45Q/K50Q again compensated and led to a behavior that was close to the wild type and behaved approximately as an

DOI: 10.1021/acs.biomac.5b00073
Biomacromolecules 2015, 16, 1283−1292

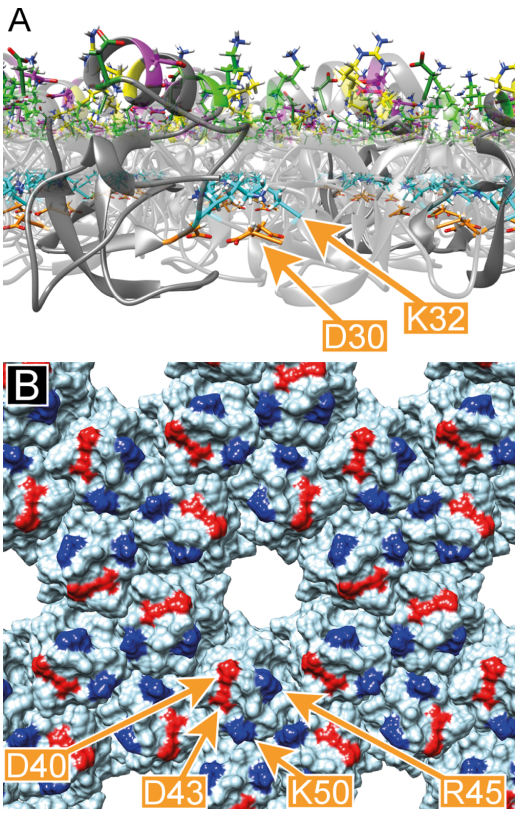

Figure 8. (A) Side-view of a model for the membrane formed by HFBI.[19] Residues D30 and K32 are located within the membrane and are positioned so that they can form ionic bonds between HFBI molecues. (B) View of the same HFBI membrane from its hydrophilic face. Residues D40, D43, R45, and K50 are exposed on the surface.

average of the two sets of mutations. As shown in Figure 8B, structural analysis shows that all of these residues are located on the hydrophilic part of the membrane and are not expected to be involved in direct molecular interactions between protein molecules. In principle, this result could be interpreted in two ways. The mutations may result in small conformational changes that are distant from the point of the mutation but fortuitously lead to changes in the fit between protein molecules. An alternative is that the mutations affect the way in which the hydrophilic face interacts with some other components in the water phase. We find it likely that these other components are other hydrophobin molecules. Earlier studies suggested that there is a continuous dynamic state between interface assembled hydrophobin and hydrophobin in solution.[26] It is also easy to imagine that the mutations on the water-exposed face would affect such dynamic interactions, making this perhaps a more likely scenario than that of a fortuitous change in the three-dimensional structure leading to an increased fit.

The second way in which the variants showed a behavior differing from that of the wild type was in the way in which surface films of hydrophobin interacted with other proteins. As earlier suggested, the prevention or promotion of adhesion of secondary layers of proteins to hydrophobin may form an important part of their functions *in vivo*.[27−29] One demonstration of such function is the recruitment of enzymatic functionalities on surfaces, leading to enhanced enzymatic activities on solid substrates.[30] Another function is related to the role of hydrophobins as an adhesive for fungal mycelium to adhere to various structures.[7] In both cases, an interaction must occur between the underlying hydrophobin film and subsequent layers. To study this interaction, we used a range of enzymes that are naturally produced by *T. reesei* (Figure 7). We did not expect that there would necessarily exist a natural interaction between the hydrophobin layer and these proteins, but they were chosen because they all are produced by the fungus and are known to be extracellular, highly soluble, and stable. The wild type and variants all interacted with GOx, as also previously shown for the wild type. The efficiency of the interaction depended on the variant, but, overall, we can conclude that GOx interacts strongly with HFBI and that the mutations generally did not change this behavior. Variant D40Q/D43N, however, showed interactions over a broader range of pH. For the other proteins studied (XYNI, XYNII, CBHI, EGII), only CBHI showed a differing behavior with one of the variants, D40Q/D43N. We conclude that structural changes in the film formed by this variant allowed an efficient interaction with CBHI. Interestingly, the change in adhesiveness among mutations was very selective, with only variant D40Q/D43N showing differing behavior and only with two proteins, CBHI and GOx. Although we cannot draw detailed conclusions on the nature of the interactions, these data suggest that interactions between hydrophobin layers and secondary adsorption can be very specific. The specificity of the interactions has a plausible structural basis in the fact that hydrophobins can arrange on interfaces to produce very organized structures (e.g., as in Figures 5 and 8B). When proteins assemble on these surfaces in defined orientations related to each other, they also form pores or pockets with structurally defined environments. It is well-known from, for example, work with cyclodextrins that such binding pockets can form very selective environments for specific interactions.[31] We therefore suggest that the behavior of the variants indicates that the nanoscale structural environment provided by the hydrophobin layers have a role for the selectiveness of interactions for proteins binding to them. The finding that changing the charge landscape of the protein did not result in a predictable shift in adsorption optimum for the secondary protein layer also suggests that the structure of the hydrophobin layer forms an important contribution to its adsorption selectivity.

The results discussed above support a view of HFBI and similar hydrophobins in which molecular interactions lead to self-assembled structures. Sequence comparison between closely related hydrophobins shows several locations with charged residues that have a high degree of conservation, such as around the 30 and 32 positions (see sequence alignment in Supporting Information, Figure 3). Asp30 is part of a conserved negatively charged loop that may contain up to four aspartates, as in the recently described class II hydrophobin NC2.[32] More variation is seen around the region that forms an α-helix in HFBI and also contains charged residues in locations 40, 43, 45, and 50 in HFBI. On the basis of the current work, we can expect that these homologous hydrophobins will show an overall behavior in forming solution multimers, films at the air−water interface, and adsorption on solid surfaces that are very

DOI: 10.1021/acs.biomac.5b00073
Biomacromolecules 2015, 16, 1283−1292

close to that of HFBI. Properties such as how surface-bound layers will interact with other proteins may show differences. Perhaps more noticeable effects were initially expected because in a previous study we had identified that corresponding mutations in a GFP-HFBI fusion protein did result in strongly changed multimerization behavior.[18] There is a strong difference in multimerization behavior of hydrophobins with and without fusion partners, where fusion proteins are much more sensitive to changes. Therefore, it clear that the linking of fusion partners affects the structural basis of interactions in hydrophobins.

Since most functional characterizations did not reveal differences between variants, it is suggested that the basic amphiphilic architecture dictates their functions to a large extent. However, details of adhesive and interfacial behavior were affected. One especially remarkable function of HFBI and its variants is the extraordinary surface elasticity of films of these proteins at the air−water interface. Mutations affected mechanisms in subtle ways, but the end state was still formed in a very robust way. Therefore, it is likely that the functions arise from the formation of multiple interactions. The presence of multiple interactions together with the several ways in which hydrophobins show functionality (i.e., forming coatings, adhesion, surface tension) results in a very complex system where precise molecular interactions play an important role but where alternative arrangements and mechanisms are found.

CONCLUSIONS

The structural basis for the functions of HFBI was probed by site-directed mutagenesis. The overall behavior of HFBI was surprisingly robust with very small differences noted in properties between wild type and variants by most of the methods of analysis. Changes were found in the surface elasticity of air−water films and in the way surface-bound films interacted with other proteins. This is significant because these are two properties that are characteristic of HFBI; no other molecules give rise to such high surface elasticity, and surface adhesion has an important biological function. The changes in surface elasticity can be interpreted as showing that there are interactions between proteins assembled at the air−water interface and other molecules in the water phase. The results also show that there are other interactions between side chains that affect lateral interactions between molecules at the air−water interface. The effects of mutations on how other molecules in solution interact with hydrophobin bound to solid surfaces support earlier findings that hydrophobins function as specific adhesive layers. We suggest a role of structurally defined surface pockets formed by the surface-bound hydrophobins.

Finally, we note that some mutations caused a qualitative difference or enhancement in these functions, suggesting that the natural performance of these is finely tuned to match a specific function. This also suggests that it is possible to use molecular engineering to further tune these functions for new applications.

ASSOCIATED CONTENT

Supporting Information

Figure S1: Mycelium of the grown fungus. Figure S2: Full sequence of HFBI with signal sequence. Figure S3: Sequence alignment with homologous proteins. This material is available free of charge via the Internet at http://pubs.acs.org.

AUTHOR INFORMATION

Corresponding Author

*Tel.: +358-09 47001; E-mail: markus.linder@aalto.fi.

Present Address

[§](M.S.G.) Bimelix Ab, Torggatan 10, AX-22100 Mariehamn, Åland, Finland.

Notes

The authors declare no competing financial interest.

ACKNOWLEDGMENTS

This work was supported by the Academy of Finland through its Centres of Excellence Programme (2014−2019) and project nos. 131055 and 126572. Drs. Tiina Nakari-Setälä and Markku Saloheimo are thanked for providing vector pTNS27 and *T. reesei* strain M219, respectively, and for participating in helpful discussions related to strain development. Riitta Suihkonen, Päivi Matikainen, Heini Lehtonen, and Riitta Nurmi are thanked for excellent technical assistance. Dr. Dilek Ercili-Cura and Martina Lille are thanked for fruitful discussions related to interfacial rheology. Yoshijuki Takatsuji and Ryota Yamasaki are thanked for performing QCM-D measurements in which GOx binding to HFBI variant layers was quantified. Dr. Géza R. Szilvay is thanked for helpful discussions on the Class II hydrophobin protein sequence alignment. Anneloes Oude Vrielink is thanked for carrying out useful tests with a tensiometer.

ABBREVIATIONS

GFP, green fluorescent protein; ATPS, aqueous two-phase system; SEC, size-exclusion chromatography; QCM-D, quartz crystal microbalance with dissipation monitoring; AFM, atomic force microscopy; GOx, glucose oxidase; XYNI, xylanase I; XYNII xylanase II; CBHI, cellobiohydrolase I; EGII, endoglucanase II

REFERENCES

(1) Aimanianda, V.; Bayry, J.; Bozza, S.; Kniemeyer, O.; Perruccio, K.; Elluru, S. R.; Clavaud, C.; Paris, S.; Brakhage, A. A.; Kaveri, S. V.; Romani, L.; Latge, J. P. Surface hydrophobin prevents immune recognition of airborne fungal spores. *Nature* **2009**, *460*, 1117−1121.

(2) Bayry, J.; Aimanianda, V.; Guijarro, J. I.; Sunde, M.; Latge, J. P. Hydrophobins—unique fungal proteins. *PLoS Pathog.* **2012**, *5*, e1002700.

(3) Hektor, H. J.; Scholtmeijer, K. Hydrophobins: proteins with potential. *Curr. Opin. Biotechnol.* **2005**, *16*, 434−439.

(4) Kershaw, M. J.; Talbot, N. J. Hydrophobins and repellents: proteins with fundamental roles in fungal morphogenesis. *Fungal Genet. Biol.* **1998**, *23*, 18−33.

(5) Linder, M. B. Hydrophobins: proteins that self assemble at interfaces. *Curr. Opin. Colloid Interface Sci.* **2009**, *14*, 356−363.

(6) Sunde, M.; Kwan, A. H. Y.; Templeton, M. D.; Beever, R. E.; Mackay, J. P. Structural analysis of hydrophobins. *Micron* **2008**, *39*, 773−784.

(7) Wösten, H. A. B.; Schuren, F. H. J.; Wessels, J. G. H. Interfacial self-assembly of a hydrophobin into an amphipathic protein membrane mediates fungal attachment to hydrophobic surfaces. *EMBO J.* **1994**, *13*, 5848−5854.

(8) Wösten, H. A. B.; van Wetter, M. A.; Lugones, L. G.; van der Mei, H. C.; Busscher, H. J.; Wessels, J. G. H. How a fungus escapes the water to grow into the air. *Curr. Biol.* **1999**, *9*, 85−88.

(9) Valo, H. K.; Laaksonen, P. H.; Peltonen, L. J.; Linder, M. B.; Hirvonen, J. T.; Laaksonen, T. J. Multifunctional hydrophobin: toward functional coatings for drug nanoparticles. *ACS Nano* **2010**, *4*, 1750−1758.

DOI: 10.1021/acs.biomac.5b00073
Biomacromolecules 2015, 16, 1283−1292

(10) Cox, A. R.; Aldred, D. L.; Russell, A. B. Exceptional stability of food foams using class II hydrophobin HFBII. *Food Hydrocolloids* **2009**, *23*, 366−376.
(11) Lumsdon, S. O.; Green, J.; Stieglitz, B. Adsorption of hydrophobin proteins at hydrophobic and hydrophilic interfaces. *Colloids Surf., B* **2005**, *44*, 172−178.
(12) Kallio, J. M.; Linder, M. B.; Rouvinen, J. Crystal structures of hydrophobin HFBII in the presence of detergent implicate the formation of fibrils and monolayer films. *J. Biol. Chem.* **2007**, *282*, 28733−28739.
(13) Walther, A.; Müller, A. H. E. Janus particles: synthesis, self-assembly, physical properties, and applications. *Chem. Rev.* **2013**, *113*, 5194−5261.
(14) Chandler, D. Interfaces and the driving force of hydrophobic assembly. *Nature* **2005**, *437*, 640−647.
(15) Szilvay, G. R.; Paananen, A.; Laurikainen, K.; Vuorimaa, E.; Lemmetyinen, H.; Peltonen, J.; Linder, M. B. Self-assembled hydrophobin protein films at the air−water interface: structural analysis and molecular engineering. *Biochemistry* **2007**, *46*, 2345−2354.
(16) Kisko, K.; Szilvay, G. R.; Vuorimaa, E.; Lemmetyinen, H.; Linder, M. B.; Torkkeli, M.; Serimaa, R. Self-assembled films of hydrophobin proteins HFBI and HFBII studied in situ at the air/water interface. *Langmuir* **2009**, *25*, 1612−1619.
(17) Cox, A. R.; Cagnol, F.; Russell, A. B.; Izzard, M. J. Surface properties of class II hydrophobins from *Trichoderma reesei* and influence on bubble stability. *Langmuir* **2007**, *23*, 7995−8002.
(18) Lienemann, M.; Gandier, J.-A.; Joensuu, J. J.; Iwanaga, A.; Takatsuji, Y.; Haruyama, T.; Master, E.; Tenkanen, M.; Linder, M. B. Structure−function relationships in hydrophobins: probing the role of charged side chains. *Appl. Environ. Microbiol.* **2013**, *79*, 5533−5538.
(19) Magarkar, A.; Mele, N.; Abdel-Rahman, N.; Butcher, S.; Torkkeli, M.; Serimaa, R.; Paananen, A.; Linder, M.; Bunker, A. Hydrophobin film structure for HFBI and HFBII and mechanism for accelerated film formation. *PLoS Comput. Biol.* **2014**, *7*, e1003745.
(20) Askolin, S.; Penttilä, M.; Wösten, H. A. B.; Nakari-Setälä, T. The *Trichoderma reesei* hydrophobin genes hfb1 and hfb2 have diverse functions in fungal development. *FEMS Microbiol. Lett.* **2005**, *253*, 281−288.
(21) Penttilä, M.; Nevalainen, H.; Ratto, M.; Salminen, E.; Knowles, J. A versatile transformation system for the cellulolytic filamentous fungus *Trichoderma reesei*. *Gene* **1987**, *61*, 155−164.
(22) Paananen, A.; Vuorimaa, E.; Torkkeli, M.; Penttilä, M.; Kauranen, M.; Ikkala, O.; Lemmetyinen, H.; Serimaa, R.; Linder, M. B. Structural hierarchy in molecular films of two class II hydrophobins. *Biochemistry* **2003**, *42*, 5253−5258.
(23) Suurnäkki, A.; Tenkanen, M.; Siika-Aho, M.; Niku-Paavola, M. L.; Viikari, L.; Buchert, J. *Trichoderma reesei* cellulases and their core domains in the hydrolysis and modification of chemical pulp. *Cellulose* **2000**, *7*, 189−209.
(24) Tenkanen, M.; Puls, J.; Poutanen, K. Two major xylanases of *Trichoderma reesei*. *Enzyme Microb. Technol.* **1992**, *14*, 566−574.
(25) Rahkamo, L.; Siika-Aho, M.; Vehviläinen, M.; Dolk, M.; Viikari, L.; Nousiainen, P.; Buchert, J. Modification of hardwood dissolving pulp with purified *Trichoderma reesei* cellulases. *Cellulose* **1996**, *3*, 153−163.
(26) Krivosheeva, O.; Dedinaite, A.; Linder, M. B.; Tilton, R. D.; Claesson, P. M. Kinetic and equilibrium aspects of adsorption and desorption of class II hydrophobins HFBI and HFBII at silicon qxynitride/water and air/water interfaces. *Langmuir* **2013**, *29*, 2683−2691.
(27) von Vacano, B.; Xu, R.; Hirth, S.; Herzenstiel, I.; Ruckel, M.; Subkowski, T.; Baus, U. Hydrophobin can prevent secondary protein adsorption on hydrophobic substrates without exchange. *Anal. Bioanal. Chem.* **2011**, *400*, 2031−2040.
(28) Wang, Z. F.; Lienemann, M.; Qiau, M.; Linder, M. B. Mechanisms of protein adhesion on surface films of hydrophobin. *Langmuir* **2010**, *26*, 8491−8496.
(29) Corvis, Y.; Walcarius, A.; Rink, R.; Mrabet, N. T.; Rogalska, E. Preparing catalytic surfaces for sensing applications by immobilizing enzymes via hydrophobin layers. *Anal. Chem.* **2005**, *77*, 1622−1630.
(30) Takahashi, T.; Maeda, H.; Yoneda, S.; Ohtaki, S.; Yamagata, Y.; Hasegawa, F.; Gomi, K.; Nakajima, T.; Abe, K. The fungal hydrophobin RolA recruits polyesterase and laterally moves on hydrophobic surfaces. *Mol. Microbiol.* **2005**, *57*, 1780−1796.
(31) Ling, X. Y.; Reinhoudt, D. N.; Huskens, J. Reversible attachment of nanostructures at molecular printboards through supramolecular glue. *Chem. Mater.* **2008**, *20*, 3574−3578.
(32) Ren, Q.; Kwan, A. H.; Sunde, M. Solution structure and interface-driven self-assembly of NC2, a new member of the Class II hydrophobin proteins. *Proteins* **2013**, *82*, 990−1003.
(33) DeLano, W. L. *The PyMOL Molecular Graphics System*; DeLano Scientific: San Carlos, CA, 2002.
(34) Pettersen, E. F.; Goddard, T. D.; Huang, C. C.; Couch, G. S.; Greenblatt, D. M.; Meng, E. C.; Ferrin, T. E. UCSF chimera—a visualization system for exploratory research and analysis. *J. Comput. Chem.* **2004**, *25*, 1605−1612.

DOI: 10.1021/acs.biomac.5b00073
Biomacromolecules 2015, 16, 1283−1292

Publication III

Grunér, Mathias S; Szilvay, Géza R; Berglin, Mattias; Lienemann, Michael; Laaksonen, Päivi; and Linder, Markus B. 2012. *Self-assembly of Class II Hydrophobins on Polar Surfaces*. American Chemical Society. *Langmuir*, volume 28, issue 9, pages 4293–4300. DOI:10.1021/la300501u

Langmuir

Article

pubs.acs.org/Langmuir

Self-assembly of Class II Hydrophobins on Polar Surfaces

Mathias S. Grunér,[†] Géza R. Szilvay,[†] Mattias Berglin,[‡] Michael Lienemann,[†] Päivi Laaksonen,[†] and Markus B. Linder*[,†]

[†]VTT Technical Research Centre of Finland, Biotechnology, Tietotie 2, FIN-02044 VTT, Espoo, Finland

[‡]Department of Cell and Molecular Biology, Interface Biophysics, Göteborg University, SE-40530 Göteborg, Sweden

ABSTRACT: Hydrophobins are structural proteins produced by filamentous fungi that are amphiphilic and function through self-assembling into structures such as membranes. They have diverse roles in the growth and development of fungi, for example in adhesion to substrates, for reducing surface tension to allow aerial growth, in forming protective coatings on spores and other structures. Hydrophobin membranes at the air−water interface and on hydrophobic solids are well studied, but understanding how hydrophobins can bind to a polar surface to make it more hydrophobic has remained unresolved. Here we have studied different class II hydrophobins for their ability to bind to polar surfaces that were immersed in buffer solution. We show here that the binding under some conditions results in a significant increase of water contact angle (WCA) on some surfaces. The highest contact angles were obtained on cationic surfaces where the hydrophobin HFBI has an average WCA of 62.6° at pH 9.0, HFBII an average of 69.0° at pH 8.0, and HFBIII had an average WCA of 61.9° at pH 8.0. The binding of the hydrophobins to the positively charged surface was shown to depend on both pH and ionic strength. The results are significant for understanding the mechanism for formation of structures such as the surface of mycelia or fungal spore coatings as well as for possible technical applications.

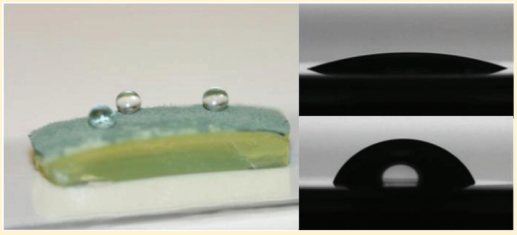

1. INTRODUCTION

Hydrophobins are structural proteins that fulfill many different tasks in the growth and development of filamentous fungi. They were first discovered as highly expressed genes and have subsequently been found in all filamentous fungi studied.[1] Sequence analysis suggested that hydrophobins could be divided into two classes, class I and class II.[2] Analysis of the properties of hydrophobins has shown that the division is useful since it reflects some clear functional differences. Both classes readily assemble into different types of supramolecular structures, most notably into membrane structures at interfaces. The clearest difference between the classes is that the structures formed by class I members are often very stable and can be disassembled only by using harsh conditions such as strong acids. In both classes the membranes seem to have multiple functions such as adhesion, formation of coatings on spores or fruiting bodies, and even to facilitate the formation of aerial structures.[3]

The determination of the three-dimensional structure of a class II hydrophobin, HFBII from *Trichoderma reesei*, suggested a mechanism for membrane formation.[4] HFBII has an almost globular structure that is highly cross-linked by disulfide bonds. One face of the protein shows nearly exclusively aliphatic hydrophobic residues. The rest of the protein shows typical hydrogen-bonding and charged residues which makes the molecule amphiphilic. Another class II hydrophobin HFBI showed an almost identical structure[5] whereas the class I EAS[6] hydrophobin protein had the same overall fold but did not have such a distinct amphiphilic structure. Furthermore, the EAS hydrophobin showed more loop-structures possibly reflecting the involvement of additional interactions on the route to self-assembly.

The amphiphilic structure explains the localization of hydrophobins to interfaces between polar and nonpolar substances such as the air−water interface and on hydrophobic surfaces in water.[7−12] There are also several observations indicating that molecular interactions between hydrophobin molecules in the plane of the interfacial layer play a significant role in stabilizing it. One such observation is the very high elasticity of membranes at the air−water interface,[12] and another observation is the highly organized two-dimensional crystalline structures observed at these interfaces.[13−15]

Self-assembly at interfaces is one of the most special properties demonstrated for hydrophobins. It is interesting that assembly occurs at different interfaces for apparently different reasons. The assembly at the air−water interface is related to the formation of aerial structures in moist or submerged conditions.[8] The assembly at hydrophobic interfaces can be related to adhesion of fungi to different substrates.[16] They also have the property to "recruit" other proteins to surfaces.[17] It has also been shown that hydrophobins are involved in making spores or other structures hydrophobic.[18,19] Both adhesion to hydrophobic surfaces[10,11,20−22] and assembly at the air−water interface[7,8,14,15,23,24] have been studied extensively, but mechanisms

Received: July 12, 2011
Published: February 9, 2012

   dx.doi.org/10.1021/la300501u | *Langmuir* 2012, 28, 4293−4300

for the assembly of hydrophobins on polar (hydrophilic) surfaces under aqueous conditions has not been well studied to date. However, understanding the mechanisms that allow hydrophobins to form hydrophobic coatings on hydrophilic surfaces is of great importance for understanding the interactions of fungi with their environment and the formation of hydrophobic hyphae[8,25] and spores.[18]

Observations of filamentous fungi show that the structures formed by their mycelia can be very hydrophobic (see Figure 1), and it is interesting to consider the role of hydrophobins in forming this hydrophobicity.[25] This mechanism is important to understand when investigating the interactions of fungi with their environment, as demonstrated for example by the finding that hydrophobin coatings are critical for the infective pathways of fungi.[26] There may also be interesting applications for coating materials emerging from the understanding of such routes.

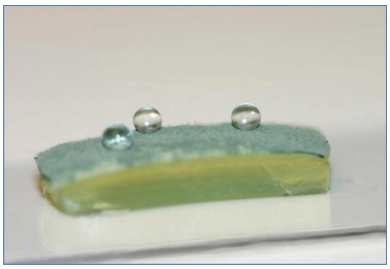

Figure 1. Surface of a mycelial mat of *T. reesei* growing on agar is highly hydrophobic as shown by water drop contact angles of about 140°.

In this work, we were interested in how class II hydrophobins in aqueous solution could assemble on a solid polar hydrophilic surface so that the hydrophobic side of the membrane would face outward significantly reducing the polarity of the surface. It is already known quite well how hydrophobin layers are formed on hydrophobic surfaces.[27,28] The mass of such layers corresponds to a monomolecular layer of protein, suggesting that the hydrophobin binds with its hydrophobic patch to the hydrophobic surface and exposes its hydrophilic side out toward the hydrophilic surroundings. Interestingly, it was found that this hydrophilic side has some unexpected properties. It was found that other proteins could readily bind to the assembled hydrophobin layer from the water exposed side.[11] However, binding was highly dependent on pH and experiments showed that the hydrophilic side of the membrane exposes charges in such a way that efficient electrostatic interactions are formed with molecules in solution under suitable conditions. The binding properties of the hydrophobin layers are likely to be linked to the organized and repetitive structure of the hydrophobin layers. The biological role of this function is not known, but it suggests a way in which the hydrophilic side of the protein membrane could interact with other molecules or structures. One function could be to recruit other proteins to surfaces or to mediate anchoring of hydrophobins on spores or cell walls. This led us to investigate if a similar mechanistic study could show how membranes of class II hydrophobins could form on polar charged surfaces.

2. MATERIALS AND METHODS

Reagents and Chemicals. The class II hydrophobin proteins HFBI, HFBII, and HFBIII, were purified from *T. reesei* mycelium or culture supernatant using two-phase extraction and reversed phase chromatography as described earlier.[29,13]

The buffers used for protein adsorption experiments at different pHs were 10 mM sodium acetate (pH 4.0, 5.0), sodium phosphate (pH 6.0, 7.0), Tris-HCl (pH 8.0), and glycine−NaOH (pH 9.0, 9.5, 10.5). Hydrophobin adsorption was studied at a narrow pH range using buffers 10 mM Na−borate (pH 7.5−8.8) and glycine−NaOH (pH 8.6−9.9). For ionic strength experiments, the following buffers were used: 10 mM Na−borate at pH 8.9 with 10−500 mM NaCl.

Preparation of SAM Layers. Self-assembled monolayers (SAMs)[30] were prepared to form cationic, anionic, and nonpolar aliphatic surfaces. For preparing cationic surfaces *N,N,N*-trimethyl-(11-mercaptoundecyl)ammonium chloride ($HS(CH_2)_{11}NMe_3^+Cl^-$) thiol (TMA) (pK_a 9.76[31]) (Prochimia Surfaces, Poland) was used, for hydrophobic surfaces 1-hexanethiol (HEX) (Sigma-Aldrich, USA) was used, and for anionic surfaces 1-mercaptoundecanoic acid (MUA) (pK_a 4.80[32]) (Sigma-Aldrich) was used.

The SAM coatings were prepared either on gold coated quartz crystal microbalance with dissipation monitoring (QCM-D) sensor disks (QCX 301, Q-Sense AB, Sweden) or on gold coated glass disks (with a chromium adhesion layer) (Bionavis, Finland). The procedure for coating was as follows: The substrates were cleaned in a UV/ozone chamber (Procleaner, Bioforce) for 10 min followed by a 10 min heating in a mixture of $H_2O/NH_3/H_2O_2$ (5:1:1) at 75 °C. Disks where then cleaned thoroughly with Milli-Q (Millipore) followed by a second UV/ozone cleaning. The discs where then immersed overnight at ambient temperature (21 °C) in 10 mM SAM reagents dissolved in ethanol. Before use, the substrates were rinsed with ethanol and Milli-Q water and dried with N_2 (g).

Preparation of Cationic Polymer Surfaces. For forming cationic polymer surfaces, the polymer polyethylenimine (PEI) (Sigma-Aldrich) was spin coated on SiO_2 QCM-D sensor discs (QSX 303, Q-Sense AB, Sweden). A 40 μL drop of 1 g/L PEI in Milli-Q was spin coated on the SiO_2 discs in atmospheric pressure for 90 s at 3000 rpm and dried.

Hydrophobin Adsorption Measured Using QCM-D. QCM-D was used to measure resonance frequency and dissipation simultaneously and to thereby calculate the mass of the bound protein layer (D4-QCM system, Q-Sense AB, Sweden). The adsorbed mass per areal unit was calculated from the resonance frequency changes using the Sauerbrey relation, $\Delta m = -C\Delta f/n$, where Δm is adsorbed mass, Δf is frequency change, C = 17.7 ng·Hz·cm^{-2}, and using the third overtone (n = 3). By combining the frequency measurements with dissipation measurements, it becomes possible to determine whether the bound protein layer is rigid or soft (water rich).[33] The dissipation value (D) is a measure of how rapidly the oscillations decay, describing the viscoelastic properties of the protein layer. A rigid material results in low dissipation values, whereas a softer renders higher values.

Hydrophobins (HFBI, HFBII, and HFBIII) were dissolved in buffer at 0.1 mg/mL. Protein solution (300 μL) was pumped through the measuring chamber with a flow rate of 100 μL/min. The sensors were left to stabilize after adsorption for 30−80 min until a stable signal was achieved and were then washed with the running buffer.

Hydrophobin Adsorption onto Submerged Substrates. Hydrophobin protein HFBI was diluted to 0.1 mg/mL in different buffer solutions with varying pH. SAM coated glass disks (Bionavis), described above, were immersed in the protein solution for about 45 min. The disks were then washed with buffer and left to soak in an excess of buffer for 10 min. The disks were then washed thoroughly in Milli-Q water before being dried with N_2 (g).

Water Contact Angle Measurements. For water contact angle (WCA) measurements, an optical contact angle and surface tension meter (CAM 200, KSV NIMA, Finland) was used. A 6 μL drop of Milli-Q water was applied on the surface under study and the average contact angle was calculated from a series of 15 pictures taken with a 5 s interval. The WCA was measured before and after each protein

adsorption experiment. The reported WCA values were determined as the average of three measurements.

Surface Characterization by Impedance Measurements. Impedance measurements were made using a z-LAB instrument (Layerlab AB, Sweden). This device is based on resonance enhanced surface impedance technology (RESI) and is here used to monitor changes in impedance in order to distinguish between loose and dense layers as well as the insulating properties of a protein layer. An increase in capacitance value indicates the formation of a less insulating layer.[34] Gold coated surfaces (ZO-PADS, Layerlab) were used in all experiments. The sensors were coated with SAMs as described above. For SAM coating, the sensors were first cleaned in a $H_2O/NH_3/H_2O_2$ mixture (5:1:1) at 75 °C for 10 min. The discs were then immersed overnight at room temperature in SAM reagent as described above. Before experiments, the sensors were sonicated in pure ethanol, cleaned with Milli-Q water, and dried with N_2 (g). Measurements were done using HFBI (0.1 mg/mL) in 50 mM glycine−NaOH at pH 8.9. The sample was injected (75 μL at a flow rate 25 μL/min for 3 min), and the sensor was allowed to stabilize for 10−30 min until a stable baseline was obtained. The sensors were then washed with buffer at 25 μL/min. All measurements were done in triplicate. The capacitance of the protein layer, $C_{Protein}$, was calculated from the SAM capacitance, C_{SAM} which is measured just before protein injection, and the total capacitance, $C_{Total,}$ which is measured after wash, using the formula: $C_{Protein} = 1/((1/C_{Total}) - (1/C_{SAM}))$.

Atomic Force Microscopy (AFM). For AFM imaging protein layers were prepared on flame annealed gold chips (Arrandee, Germany) coated with HEX or TMA SAMs as described above for hydrophobin adsorption onto submerged substrates. After protein adsorption and washing, the samples were immediately imaged in water without drying in between. Imaging was done in water using a NanoScope IIIa Multimode AFM ("E" scanner; Digital Instruments/Bruker) as described earlier[14] using silicon nitride cantilevers (NP-S, Veeco) with a force constant of 0.32 N m^{-1}. Roughness analysis was performed using the software Scanning Probe Image Processor, SPIP (Image Metrology, Denmark).

3. RESULTS

Adsorption of Hydrophobins to Surfaces. Hydrophobin adsorption to hydrophobic, cationic, and anionic surfaces was investigated using QCM-D. Figure 2 shows representative adsorption curves of HFBI binding on SAM surfaces of TMA (cationic) at pH 9.5, HEX (hydrophobic) at pH 9.0, and MUA (anionic) at pH 9.0. The WCA was measured on all QCM-D sensor chips before and after the QCM-D adsorption experiments. After protein adsorption had reached a maximum, the surfaces were rinsed with buffer to remove any loosely bound protein. Control experiments were made by identical treatments of the surfaces but leaving out the protein.

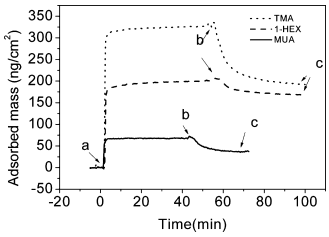

Figure 2. QCM-D sensograms showing representative curves of HFBI binding to different SAM surfaces. The surfaces used were hydrophobic HEX (at pH 9.5), anionic MUA (at pH 9.0), and cationic TMA (at pH 9.0). Part a corresponds to hydrophobin injection, part b to buffer wash, and part c to end of buffer wash where adsorbed mass and WCA was measured. The adsorbed mass was calculated from resonance frequency change between the initial point (a) and the final point (c).

Hydrophobic Surfaces. The mass of HFBI and HFBII adsorption on hydrophobic HEX SAM was observed by QCM-D (Figure 3). The measured values of adsorbed mass on the HEX SAM surface were between 170 and 282 ng/cm^2 depending on pH (Figure 3A). The adsorption reached maximum levels within minutes and washing with buffer typically removed only about 10% of adsorbed protein. Dissipation changes were typically below 0.2 in all experiments indicating a rigid layer. The WCA was measured for all QCM-D sensor chips before and after the QCM-D adsorption experiments. The WCA of the freshly prepared HEX SAM was 92.0 ± 6.3° before deposition. After protein adsorption, the surfaces were clearly more hydrophilic with WCA values between 39° and 56°, and between 38° and 50°, for HFBI and HFBII, respectively (Figure 3B). To confirm results, we also tested the possible effect of having longer chain SAMs by using undecanethiol SAM surfaces. On the undecanethiol surface, the mass of bound HFBI was 262 ng/cm^2 and resulting WCA 34.9 ± 3° at pH 9 showing that chain length did not affect binding.

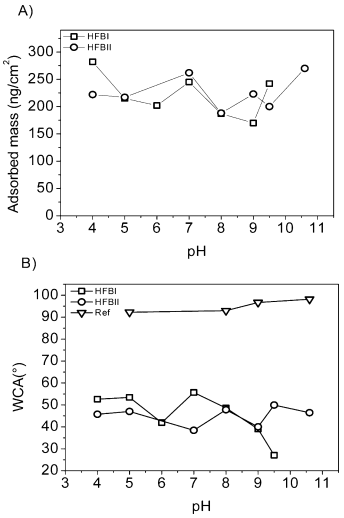

Figure 3. Adsorption of hydrophobins on hydrophobic surfaces. (A) Graph of adsorbed mass of HFBI and HFBII on hydrophobic HEX SAM as a function of pH as observed by QCM-D. (B) WCAs as a function of pH of the HEX SAM coated QCM-D sensors after HFBI or HFBII adsorption. A negative control surface (labeled ref) was treated similarly but without addition of protein. The standard deviation for HFBI on HEX SAM was ±6.7° (N = 3) at pH 9.

Cationic Surfaces. The binding of HFBI, HFBII, and HFBIII was studied on two types of cationic surfaces; TMA SAM and spin coated polymer PEI. The protein adsorption to the TMA SAM surface was measured using QCM-D over a pH range between 4.0 and 10.5 (Figure 4A). The corresponding WCAs were measured on QCM-D sensors before and after protein adsorption, and are shown in Figure 4B. Before deposition, the TMA SAM had a WCA of about 22.3° (±5.7°). For hydrophobin adsorbing on a TMA SAM, close to half of the initially bound mass was typically removed from the surface during the wash step (Figure 2). The dissipation changes were

dx.doi.org/10.1021/la300501u | Langmuir 2012, 28, 4293−4300

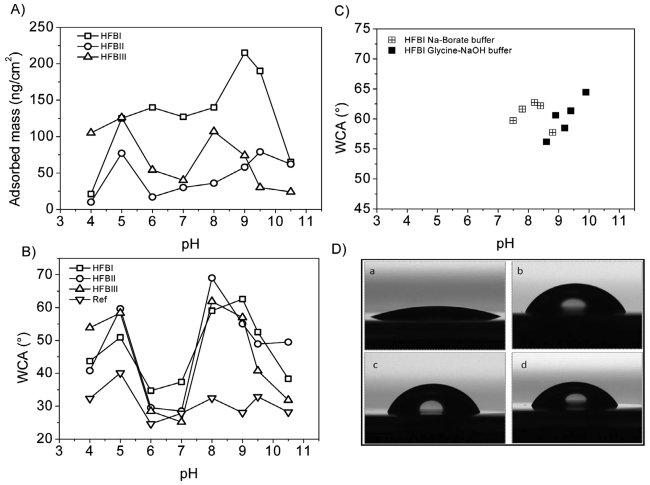

Figure 4. Adsorption of hydrophobins on cationic SAM surfaces. (A) QCM-D derived adsorbed mass of HFBI, HFBII, and HFBIII on TMA SAM surface as a function of pH. (B) WCAs of the same surfaces after hydrophobin adsorption in QCM-D runs as a function of pH. WCAs after HFBI, HFBII, or HFBIII adsorption are shown, as well as a negative control surface (labeled ref) that was treated similarly but without addition of protein. (C) WCA of HFBI on a TMA SAM surface at a narrow pH range. (D) Water drop profile shapes from WCA measurements on TMA SAM surfaces before protein coating (a), after HFBI (at pH 9.0) (b), HFBII (at pH 8.0) (c), and HFBIII (at pH 8.0) (d) coating. The obtained WCAs were 22.3° before deposition, and 62.6°, 69.0°, and 61.9°, after HFBI, HFBII, and HFBIII adsorption, respectively.

below 0.2 in all experiments indicating that all the layers formed had a rigid structure. For HFBI, the maximum of adsorbed mass (215 ng/cm^2) was obtained at pH 9.0. The value is close to what is expected for a monolayer based on an approximate calculation using the dimensions of the protein (2.2 nm × 2.2 nm) which gives a weight for a monolayer of about 250 ng/cm^2.[5]

WCA as a function of pH for HFBI, HFBII, and HFBIII as well as a buffer control on TMA are shown in Figure 4B. All three proteins show a similar dependency of WCA on pH with a smaller peak at pH 4.0−5.0 and a maximum WCA peak at pH 8.0−9.0. The smaller WCA peak at pH 4.0−5.0 had a very similar shape for all three hydrophobins and the negative control. However, at the maximum peak around pH 8.0−9.0, the WCAs of hydrophobin samples are clearly higher (60−70°) than the buffer only sample (28−30°). HFBI has a maximum value of WCA of 62.6° at pH 9.0, HFBII, a maximum of 69.0° at pH 8.0, and HFBIII, a maximum of 61.9° at pH 8.0. The influence of the type of buffer used was examined by changing the 10 mM phosphate buffer for experiments at pH 6 and 7 for HFBI and HFBII on TMA SAM to Na-citrate (10 mM, pH 6) or Tris-HCl (10 mM, pH 7). The WCA values showed moderate changes with WCA values for HFBI increasing from 34.7° to 39.1° at pH 6 and 37.4° to 44.3° at pH 7. For HFBII, the values were changed from 29.5° to 32.2° at pH 6 and 28.5° to 38.8° at pH 7.

To confirm results and study the effect of the type of buffer used we investigated the binding to TMA SAM at a selected narrow pH range in more detail (Figure 4C). A pH range of 7.5−9.9 was probed using 10 mM Na−borate (pH 7.5−8.8) and glycine−NaOH (pH 8.6−9.9) buffers in room temperature. Using the Na−borate buffer, the WCA has a maximum at pH 8.2 with a 62.7° WCA. There are variations between the two used buffers as seen in the samples with overlapping pHs. Some of this variation (roughly 5°) could be due to experimental variation, but a small buffer related effect is likely to exist.

Water drop profiles at pHs on cationic surfaces with the highest average WCA for each protein are shown in Figure 4D. The cationic surface without protein shows a low contact angle (Figure 4D, a), but after hydrophobin treatment, the WCA markedly increases (Figure 4D, b−d for HFBI, HFBII, and HFBIII, respectively).

Cationic PEI Surfaces. To study the effect of the underlying charged surface on the assembly of hydrophobin the adsorption, QCM-D, and WCA experiments were repeated using a cationic polymer (PEI) instead of the cationic TMA SAM as the underlying layer. The amount of adsorbed HFBI mass on PEI as a function of pH and the corresponding WCAs are shown in Figure 5. The spin-coated PEI surface had a WCA below 10° before deposition. The amount of adsorbed HFBI as a function of pH shows a peak at pH 5 where 150 ng/cm^2 is adsorbed and an increased binding at basic pHs with a maximum value of 260 ng/cm^2 adsorbed protein at pH 10. The pH dependency of HFBI binding to PEI was very similar to the binding to TMA. The adsorption of HFBI on the PEI surface generates two peaks of WCA as a function of pH. The resulting WCA values as a function of pH (Figure 5B) show two peaks: the smaller peak measured at pH 5.0 with a 30.3° WCA and a second, maximum peak at pH 8 with a WCA of 50.3°.

Adsorption on Anionic Surfaces. The effect of surface charge was studied by using an anionic and highly hydrophilic MUA SAM and following the binding of HFBI as well as a negative control without protein (buffer only) to this surface (Figure 6). Before protein deposition, the MUA SAM had a WCA of about 31.5° (±3.3°). At low pH, there was significant protein binding with amounts close to a monolayer, but the binding rapidly decreased with increasing pH. For both HFBI and the buffer control, the WCAs were lower than before adsorption on the MUA SAM over the whole pH range. The

dx.doi.org/10.1021/la300501u | Langmuir 2012, 28, 4293−4300

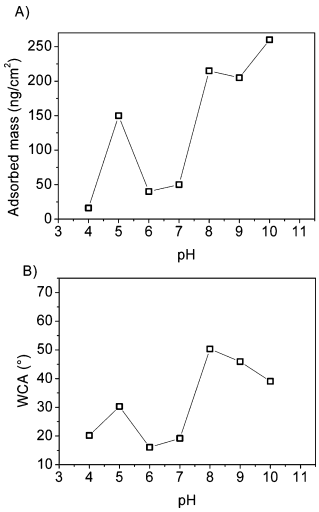

Figure 5. Adsorption of HFBI on cationic PEI surfaces. (A) Mass of adsorbed HFBI on cationic PEI surface as observed by QCM-D at various pHs. (B) WCAs of HFBI coatings on PEI after QCM-D measurements as a function of pH. The WCA of PEI surface before deposition was <10°.

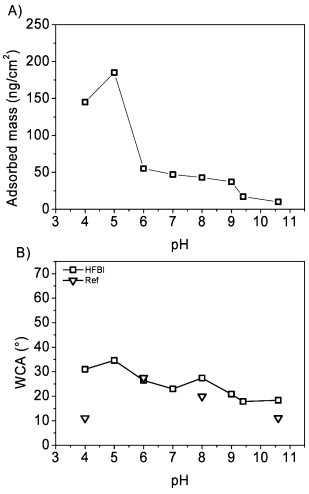

Figure 6. Adsorption of HFBI on anionic MUA SAM. (A) QCM-D derived mass of adsorbed HFBI on MUA as a function of pH. (B) WCAs of the same surface after HFBI adsorption as well as a negative control surface (labeled ref) that was treated similarly but without addition of protein are shown.

results show that HFBI interactions with anionic surfaces were very different from interactions with cationic surfaces.

Effect of Ionic Strength. The nature of the interaction between the cationic TMA SAM and HFBI was studied by following binding and WCA with increasing ionic strength. A 10 mM glycine buffer at pH 9.0 with NaCl at different concentrations (0, 10, 25, 50, 75, 100, 500 mM) was used. The results show that both bound mass and WCA rapidly decrease with increasing ionic strength, which indicates a role for ionic interactions in the layer formation (Figure 7). However, HFBI

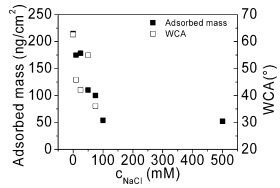

Figure 7. HFBI adsorption to cationic TMA SAMs as a function of NaCl concentration. QCM-D derived adsorbed mass and WCA are shown. The protein adsorption was done at pH 9.0.

adsorption to the cationic surface could not be completely inhibited even at 500 mM NaCl, and it is possible that at such high ionic strengths the hydrophobic interactions between the SAM and HFBI are promoted.

Characterization by Capacitance. The capacitance of the HFBI layer was measured for both cationic TMA and hydrophobic HEX SAMs at pH 8.9. The capacitance of HFBI on the HEX SAM surface was 5.0 ± 0.8 μF/cm^2 while the capacitance of HFBI on the cationic TMA SAM was 73.7 ± 29.3 μF/cm^2. The much lower capacitance value on the hydrophobic surface compared to the cationic surface indicates that the binding of HFBI on the hydrophobic surface is denser and results in an insulating layer, while the binding to the cationic surface results in a surface which is less insulating and possibly less structured. The capacitance values of the underlying HEX and TMA SAM were 2.16–2.63 and 4.66–4.94 μF/cm^2, respectively.

Characterization by AFM. The HFBI layers were imaged using AFM to see if there are differences in morphology between the protein layers on HEX and TMA surfaces. The layers on both substrates had a very similar appearance and were covering the substrate evenly without observable defects. Specific features on the molecular scale could not be identified. The rms roughness (standard deviation of the height values) of the protein layers on TMA and HEX was 2.2 and 1.2 nm, respectively.

4. DISCUSSION

In this work we have shown that class II hydrophobins can bind to polar surfaces that are immersed in aqueous solution under controlled pH and salinity. Hydrophobins did bind to cationic, but not anionic, surfaces and resulted in a significant decrease in polarity of the surface, measured as an increase in water contact angle (WCA). The binding was highly dependent on pH with the largest increase in WCA occurring between pH 8 and 9. At these pH values the hydrophobin layer had a mass corresponding to a monomolecular layer of protein. The binding and resulting WCA values were highly dependent on the ionic strength of the solution, which together with the strong pH dependency indicates that electrostatic forces were important for the interaction between the hydrophobin and the polar surface.

The WCAs of hydrophobin layers on the cationic surfaces were at their highest about 70° (Figure 4B). In control experiments surfaces were treated with the same solutions but not containing protein which resulted in WCAs of about 30°. Thus the presence of hydrophobin gave an approximate 40°

dx.doi.org/10.1021/la300501u | Langmuir 2012, 28, 4293–4300

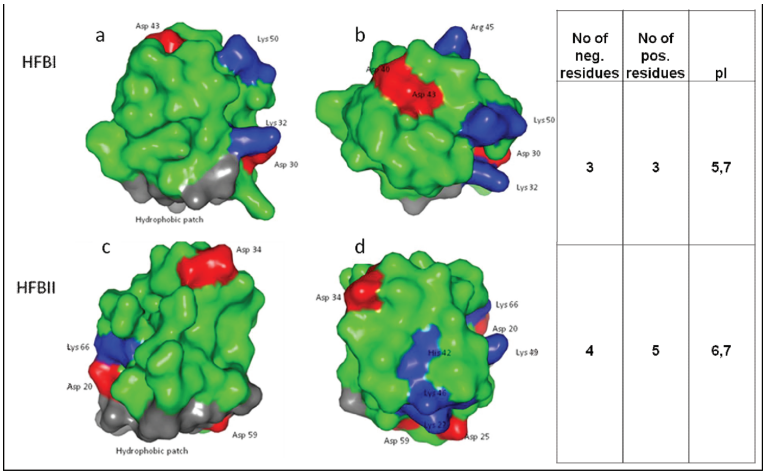

	No of neg. residues	No of pos. residues	pI
HFBI	3	3	5,7
HFBII	4	5	6,7

Figure 8. Structure of HFBI and HFBII. Part a or c shows the protein with the hydrophobic patch (gray) at the bottom, and part b or d show a top view of a or c. The ionizable side chains are shown where red is negative and blue is positive charge in neutral pH. The number of charged residues and pI of the proteins are also shown.

increase in WCA. The behavior is in clear contrast to the binding of hydrophobin to hydrophobic surfaces (Figure 3), where the hydrophobin layer resulted in a drop of contact angle from slightly over 90° to 40−50°, i.e. a decrease of 40−50°. Our interpretation of these data is that the layers that the hydrophobins form are amphiphilic with one side giving a low contact angle and the other giving a higher contact angle. On the hydrophobic surface, the hydrophilic side of the layer is turned toward the solution and on the cationic surface the more hydrophobic side of the layer is turned toward the solution. Previous reports support this view as it has been shown that hydrophobins form layers that have a thickness corresponding to a monomolecular layer on surfaces and interfaces.[14,27] Previously it was also shown that these layers are oriented so that the hydrophilic part of the protein is turned toward the aqueous side at the air−water interface.[14]

We suggest that the process for forming layers with higher contact angles has a biological significance since it could form a part of a mechanism by which hydrophobins participate in the formation of hydrophobic structures in fungi such as mycelium or spores. However, the WCA of the membranes formed in our experiments were still significantly more polar than measured for fungal mycelia (approximately 140°; Figure 1). There are several possible causes for this difference. On the surface of mycelia, it is expected that structural arrangements with other cell wall components as well as geometrical effects such as curvature can play an essential role for its surface properties. The formation of the hydrophobicity of mycelium may also require the participation of additional components. We can also expect that the formation of cell wall structures during fungal growth is a concerted event involving several components.

Nonetheless, it is noteworthy that in the procedure used here the hydrophobin must overcome a substantial energy barrier in order to increase the WCA by assembly in a fully submerged aqueous environment. The driving force for this energetically unfavorable process must be coupled to the self-assembly process that forms surface layers of hydrophobin. In comparison the self-assembly process should then be more favorable. An indication for the mechanism involved came from the observation in experiments on cationic surfaces that the initial amount of protein was initially large and then decreased during extensive washing. As seen in Figure 2, the initial binding on TMA was almost twice of that amount which is left after rinsing. In comparison, the corresponding initial amount bound on HEX or MUA was much smaller. The behavior on TMA could be explained by initial binding as a double layer with a subsequent removal of the outer layer, leaving only the single adsorbed layer after washing. Therefore, a high contact angle surface would not necessarily be formed while exposed to water but could initially form as the base part of a bilayer and being exposed only after the outer layer has been washed off.

To get a deepened understanding of the structure of the adsorbed membranes, they were analyzed by impedance spectroscopy, QCM, and AFM. The QCM and AFM did not reveal any differences when hydrophobin on cationic TMA SAM surface was compared to the corresponding layers on hydrophobic HEX SAM surface. In QCM the dissipation value indicated a rigid layer in both cases and the change in resonance frequency indicated a similar mass. Comparing AFM images of the two layers showed smooth surfaces in both cases but with the hydrophobin−TMA surface having a slightly higher roughness. The images did not show molecular details as previously have been obtained for layers on atomically smooth surfaces such as mica and graphite.[13,14] The reason for this is that the relative roughness of underlying gold case posed limitations for the image resolution. The data obtained by impedance spectroscopy indicated that the hydrophobin layers on the cationic surface were less insulating than the layers formed on hydrophobic surfaces. An interpretation of these data is that the hydrophobin on the cationic surfaces in some manner contains more defects or irregularities. As such irregularities were not identified by AFM, they probably occur more on the molecular or nanoscale and are structurally not easily characterized.

To verify the role of cationic charge on surfaces, we conducted experiments to compare the TMA SAM and a

structurally very different spin coated PEI polymer surface (Figure 5). Experiments using either surface showed very similar results, although the final WCAs on PEI were slightly lower (Figure 5). These results indicate that the charge of the surface is more important than the structural composition of the underlying surface. However, charge was very important as noted by the completely different results obtained on anionic surfaces (Figure 6) which resulted in very low binding and low differences in WCA.

The molecular details of how the hydrophobins interact with polar surfaces are still unknown. We note however that the hydrophilic side of both HFBI and HFBII show ionizable side chains.[4,5] HFBI has three positively and three negatively charged groups while HFBII has five positively and four negatively changed groups, and their pI values are 5.7 and 6.7 respectively (Figure 8). The lowest binding of both proteins occurred at their respective pI values, although it should be noted that pI represents an average for the whole protein while electrostatic interactions may affect more local environments. The structure of HFBIII is currently unknown but a homology model of HFBIII structure (data not shown) shows that HFBIII has four positively and five negatively charged groups on its hydrophilic side.

In the literature, there are reports describing the difference in polarity of the different sides of layers of class I hydrophobins.[10,20,21,35−37] In these studies, a very different route for forming layers was used. First, membranes were allowed to form at the air−water interface. Then they were deposited on a support typically by drying on polar surfaces such as filter paper. These studies show that hydrophobic membranes can efficiently be formed in this way and the resulting membranes have had high contact angles, sometimes up to 120° (class I hydrophobins). However, preorganization at the air−water interface is unlikely the explanation for how hydrophobins assemble in fungal structures, for example on spores.

Previously Martin et al.[28,38] showed that the class I hydrophobin SC3 could assemble on hydrophilic mica in solution, but this required the presence of the polysaccharide schizophyllan. Both SC3 and schizophyllan are produced by the same organism, *Schizophyllum commune*. In the presence of schizophyllan, the protein layer became highly insoluble and changed the surface contact angle of mica from about 0° to 20−30°, i.e. a much smaller change than found in this study, suggesting a different type of arrangement. The interactions with schizophyllan led to the suggestion that the polysaccharide has a role in stabilizing and ordering the SC3 protein prior to assembly. The effect of poly- and monosaccharides on hydrophobin assembly has been observed in other studies as well.[39,40]

Although our data in the present study using class II hydrophobins shows different details than Martin et al. found for SC3, both studies emphasize the importance of interactions of the hydrophilic part of the protein with other components. However, in nature the polymer−protein interactions can be much more complex and specific and structural features such as surface curvature can play a large role. Nonetheless we show that polar surfaces can act as supports for the formation of hydrophobin membranes. The formation of molecular membranes on different types of interfaces appears to be central to most of the biological functions of hydrophobins as well as for a number of emerging technical applications. Studying these interactions leads to the possibility to understand the molecular structure of fungal spores, cell walls, or fruiting bodies. Also since hydrophobins have received much attention as industrially useful proteins,[3] the hydrophilic assembly can pave the way for new inventions and applications.

AUTHOR INFORMATION

Corresponding Author

*E-mail: markus.linder@vtt.fi.

Notes

The authors declare no competing financial interest.

ACKNOWLEDGMENTS

Riitta Suihkonen is thanked for technical assistance. Olof Andersson and Julia Hedlund at Layerlab are thanked for help with impedance measurements. Financial support from the Academy of Finland is acknowledged. A researcher visit was supported by COST TD0906 Biological Adhesives.

REFERENCES

(1) Linder, M. B.; Szilvay, G. R.; Nakari-Setala, T.; Penttila, M. E. Hydrophobins: the protein-amphiphiles of filamentous fungi. *FEMS Microbiol Rev* **2005**, *29* (5), 877−96.

(2) Wessels, J. G. H. Developmental Regulation of Fungal Cell-Wall Formation. *Ann. Rev. Phytopathol.* **1994**, *32*, 413−437.

(3) Linder, M. B. Hydrophobins: Proteins that self assemble at interfaces. *Curr. Opin. Colloid Interface Sci.* **2009**, *14* (5), 356−363.

(4) Hakanpaa, J.; Paananen, A.; Askolin, S.; Nakari-Setala, T.; Parkkinen, T.; Penttila, M.; Linder, M. B.; Rouvinen, J. Atomic resolution structure of the HFBII hydrophobin, a self-assembling amphiphile. *J. Biol. Chem.* **2004**, *279* (1), 534−9.

(5) Hakanpaa, J.; Szilvay, G. R.; Kaljunen, H.; Maksimainen, M.; Linder, M.; Rouvinen, J. Two crystal structures of Trichoderma reesei hydrophobin HFBI--the structure of a protein amphiphile with and without detergent interaction. *Protein Sci.* **2006**, *15* (9), 2129−40.

(6) Kwan, A. H.; Winefield, R. D.; Sunde, M.; Matthews, J. M.; Haverkamp, R. G.; Templeton, M. D.; Mackay, J. P. Structural basis for rodlet assembly in fungal hydrophobins. *Proc. Natl. Acad. Sci. USA* **2006**, *103* (10), 3621−6.

(7) Wösten, H. A.; Asgeirsdottir, S. A.; Krook, J. H.; Drenth, J. H.; Wessels, J. G. The fungal hydrophobin Sc3p self-assembles at the surface of aerial hyphae as a protein membrane constituting the hydrophobic rodlet layer. *Eur. J. Cell Biol.* **1994**, *63* (1), 122−9.

(8) Wösten, H. A.; van Wetter, M. A.; Lugones, L. G.; van der Mei, H. C.; Busscher, H. J.; Wessels, J. G. How a fungus escapes the water to grow into the air. *Curr. Biol.* **1999**, *9* (2), 85−8.

(9) Talbot, N. J. Fungal biology. Coming up for air and sporulation. *Nature* **1999**, *398* (6725), 295−6.

(10) Lugones, L. G.; Bosscher, J. S.; Scholtmeyer, K.; de Vries, O. M.; Wessels, J. G. An abundant hydrophobin (ABH1) forms hydrophobic rodlet layers in Agaricus bisporus fruiting bodies. *Microbiology* **1996**, *142* (Pt 5), 1321−9.

(11) Wang, Z.; Lienemann, M.; Qiau, M.; Linder, M. B. Mechanisms of protein adhesion on surface films of hydrophobin. *Langmuir* **2010**, *26* (11), 8491−6.

(12) Cox, A. R.; Cagnol, F.; Russell, A. B.; Izzard, M. J. Surface properties of class ii hydrophobins from Trichoderma reesei and influence on bubble stability. *Langmuir* **2007**, *23* (15), 7995−8002.

(13) Paananen, A.; Vuorimaa, E.; Torkkeli, M.; Penttila, M.; Kauranen, M.; Ikkala, O.; Lemmetyinen, H.; Serimaa, R.; Linder, M. B. Structural hierarchy in molecular films of two class II hydrophobins. *Biochemistry* **2003**, *42* (18), 5253−8.

(14) Szilvay, G. R.; Paananen, A.; Laurikainen, K.; Vuorimaa, E.; Lemmetyinen, H.; Peltonen, J.; Linder, M. B. Self-assembled hydrophobin protein films at the air-water interface: structural analysis and molecular engineering. *Biochemistry* **2007**, *46* (9), 2345−54.

(15) Kisko, K.; Szilvay, G. R.; Vuorimaa, E.; Lemmetyinen, H.; Linder, M. B.; Torkkeli, M.; Serimaa, R. Self-assembled films of

hydrophobin proteins HFBI and HFBII studied in situ at the air/water interface. *Langmuir* **2009**, *25* (3), 1612−9.
(16) Wösten, H. A.; Schuren, F. H.; Wessels, J. G. Interfacial self-assembly of a hydrophobin into an amphipathic protein membrane mediates fungal attachment to hydrophobic surfaces. *EMBO J.* **1994**, *13* (24), 5848−54.
(17) Takahashi, T.; Maeda, H.; Yoneda, S.; Ohtaki, S.; Yamagata, Y.; Hasegawa, F.; Gomi, K.; Nakajima, T.; Abe, K. The fungal hydrophobin RolA recruits polyesterase and laterally moves on hydrophobic surfaces. *Mol. Microbiol.* **2005**, *57* (6), 1780−1796.
(18) Nakari-Setala, T.; Aro, N.; Ilmen, M.; Munoz, G.; Kalkkinen, N.; Penttila, M. Differential expression of the vegetative and spore-bound hydrophobins of Trichoderma reesei--cloning and characterization of the hfb2 gene. *Eur. J. Biochem.* **1997**, *248* (2), 415−23.
(19) Bell-Pedersen, D.; Dunlap, J. C.; Loros, J. J. The Neurospora circadian clock-controlled gene, ccg-2, is allelic to eas and encodes a fungal hydrophobin required for formation of the conidial rodlet layer. *Genes Dev.* **1992**, *6* (12A), 2382−94.
(20) De Vries, O. M.; Moore, S.; Arntz, C.; Wessels, J. G.; Tudzynski, P. Identification and characterization of a tri-partite hydrophobin from Claviceps fusiformis. A novel type of class II hydrophobin. *Eur. J. Biochem.* **1999**, *262* (2), 377−85.
(21) Askolin, S.; Linder, M.; Scholtmeijer, K.; Tenkanen, M.; Penttila, M.; de Vocht, M. L.; Wosten, H. A. Interaction and comparison of a class I hydrophobin from Schizophyllum commune and class II hydrophobins from Trichoderma reesei. *Biomacromolecules* **2006**, *7* (4), 1295−301.
(22) De Stefano, L.; Rea, I.; Giardina, P.; Armenante, A.; Rendina, I. Protein-modified porous silicon nanostructures. *Adv. Mater.* **2008**, *20* (8), 1529−+.
(23) Wang, X.; Shi, F.; Wosten, H. A.; Hektor, H.; Poolman, B.; Robillard, G. T. The SC3 hydrophobin self-assembles into a membrane with distinct mass transfer properties. *Biophys. J.* **2005**, *88* (5), 3434−43.
(24) Houmadi, S.; Ciuchi, F.; De Santo, M. P.; De Stefano, L.; Rea, I.; Giardina, P.; Armenante, A.; Lacaze, E.; Giocondo, M. Langmuir-Blodgett Film of Hydrophobin Protein from Pleurotus ostreatus at the Air-Water Interface. *Langmuir* **2008**, *24* (22), 12953−12957.
(25) Wosten, H.; De Vries, O.; Wessels, J. Interfacial Self-Assembly of a Fungal Hydrophobin into a Hydrophobic Rodlet Layer. *Plant Cell* **1993**, *5* (11), 1567−1574.
(26) Aimanianda, V.; Bayry, J.; Bozza, S.; Kniemeyer, O.; Perruccio, K.; Elluru, S. R.; Clavaud, C.; Paris, S.; Brakhage, A. A.; Kaveri, S. V.; Romani, L.; Latge, J. P. Surface hydrophobin prevents immune recognition of airborne fungal spores. *Nature* **2009**, *460* (7259), 1117−21.
(27) Linder, M.; Szilvay, G. R.; Nakari-Setala, T.; Soderlund, H.; Penttila, M. Surface adhesion of fusion proteins containing the hydrophobins HFBI and HFBII from Trichoderma reesei. *Protein Sci.* **2002**, *11* (9), 2257−66.
(28) Martin, G. G.; Cannon, G. C.; McCormick, C. L. Adsorption of a fungal hydrophobin onto surfaces as mediated by the associated polysaccharide schizophyllan. *Biopolymers* **1999**, *49* (7), 621−633.
(29) Linder, M.; Selber, K.; Nakari-Setala, T.; Qiao, M.; Kula, M. R.; Penttila, M. The hydrophobins HFBI and HFBII from Trichoderma reesei showing efficient interactions with nonionic surfactants in aqueous two-phase systems. *Biomacromolecules* **2001**, *2* (2), 511−7.
(30) Ulman, A. Formation and Structure of Self-Assembled Monolayers. *Chem. Rev.* **1996**, *96* (4), 1533−1554.
(31) Hall, H. K. Correlation of the Base Strengths of Amines. *J. Am. Chem. Soc.* **1957**, *79* (20), 5441−5444.
(32) Sugihara, K.; Teranishi, T.; Shimazu, K.; Uosaki, K. Structure dependence of the surface pKa of mercaptoundecanoic acid SAM on gold. *Electrochemistry* **1999**, *67* (12), 1172−1174.
(33) Rodahl, M.; Hook, F.; Fredriksson, C.; Keller, C. A.; Krozer, A.; Brzezinski, P.; Voinova, M.; Kasemo, B. Simultaneous frequency and dissipation factor QCM measurements of biomolecular adsorption and cell adhesion. *Faraday Discuss* **1997**, *107*, 229−46.
(34) Hedlund, J.; Lundgren, A.; Lundgren, B.; Elwing, H. A new compact electrochemical method for analyzing complex protein films adsorbed on the surface of modified interdigitated gold electrodes. *Sens. Actuators B−Chem.* **2009**, *142* (2), 494−501.
(35) Lugones, L. G.; Wosten, H. A.; Wessels, J. G. A hydrophobin (ABH3) specifically secreted by vegetatively growing hyphae of Agaricus bisporus (common white button mushroom). *Microbiology* **1998**, *144* (Pt 8), 2345−53.
(36) Lugones, L. G.; Scholtmeijer, K.; Klootwijk, R.; Wessels, J. G. Introns are necessary for mRNA accumulation in Schizophyllum commune. *Mol. Microbiol.* **1999**, *32* (4), 681−9.
(37) Scholtmeijer, K.; Janssen, M. I.; Gerssen, B.; de Vocht, M. L.; van Leeuwen, B. M.; van Kooten, T. G.; Wosten, H. A.; Wessels, J. G. Surface modifications created by using engineered hydrophobins. *Appl. Environ. Microbiol.* **2002**, *68* (3), 1367−73.
(38) Martin, G. G.; Cannon, G. C.; McCormick, C. L. Sc3p hydrophobin organization in aqueous media and assembly onto surfaces as mediated by the associated polysaccharide schizophyllan. *Biomacromolecules* **2000**, *1* (1), 49−60.
(39) Armenante, A.; Longobardi, S.; Rea, I.; De Stefano, L.; Giocondo, M.; Silipo, A.; Molinaro, A.; Giardina, P. The Pleurotus ostreatus hydrophobin Vmh2 and its interaction with glucans. *Glycobiology* **2010**, *20* (5), 594−602.
(40) Scholtmeijer, K.; de Vocht, M. L.; Rink, R.; Robillard, G. T.; Wosten, H. A. Assembly of the fungal SC3 hydrophobin into functional amyloid fibrils depends on its concentration and is promoted by cell wall polysaccharides. *J. Biol. Chem.* **2009**, *284* (39), 26309−14.

Publication IV

Grunér, Mathias S; Paananen, Arja; Szilvay, Géza R; Linder, Markus B. *Dynamics and interactions of hydrophobin HFBII assembly in solution by stopped-flow spectroscopy*. Submitted manuscript in the year 2015.

ARTICLE

Dynamics and interactions of hydrophobin HFBII assembly in solution by stopped-flow spectroscopy

Received 00th January 20xx,
Accepted 00th January 20xx

DOI: 10.1039/x0xx00000x

M. S. Grunér[a,b], A. Paananen[b], G.R. Szilvay[b] and M. B. Linder[a]

Hydrophobins are surface active proteins produced by filamentous fungi. In solution the proteins form multimers that dissociate at interfaces and rearrange to self-assemble into films that can have a very ordered structure and can be very tighly bound. Little is known on dynamics of multimer interactions in solution and how this is affected by other components. In this work we examine the multimer dynamics by stopped-flow fluorescence measurements and Förster Resonance Energy Transfer (FRET) using the class II hydrophobin HFBII. The half-time of exchange in the multimer state was about 0.9 sec at 22° C with an activation energy of 92 kJ/mol. The multimer exchange process was also shown to be concentration dependent. The effect of solution conditions, surfactants and other proteins on the dynamics of HFBII multimerization in solution was also examined. Proteins did not affect the multimer but the closely related HFBI hydrophobin destabilized it significantly.

1. Introduction

Hydrophobins are amphiphilic proteins produced by filamentous fungi. In solution the proteins form different multimers which at the air water interface disassociate and the hydrophobins rearrange to self-assemble into films that can have a very ordered structure[1]. Hydrophobin films have the highest value of interfacial elasticity, G', of protein films reported in literature[2,3], suggesting an important role of intermolecular interactions. The protein multimers can also rearrange to bind to solid surfaces, forming films that can be very tightly bound[1]. Hydrophobin assemblies, films and coatings could be used to e.g. promote biocompatibility of materials, improve stability of dispersions and foams or to act as adsorption mediating modules on surfaces for e.g. proteins, cells and nanoparticles[4–6]. Hydrophobins can be divided into two classes, class I and class II, based on the occurrence of hydrophilic and hydrophobic amino acid residues in the protein sequence[7]. The first crystallographic structure of a hydrophobin was made of the class II hydrophobin HFBII from *Trichoderma reesei*[8]. About 12 % of the surface area consisted nearly entirely of hydrophobic aliphatic side chains, forming a "hydrophobic patch". The rest of the surface is largely hydrophilic making the protein amphiphilic. Charged residues are also present on the hydrophilic surface area. As a large part of the hydrophobic residues of the protein were situated in the hydrophobic patch, the core of the protein was stabilized by eight Cys-residues forming four disulfide bridges. This pattern of Cys-residues is conserved in all hydrophobins, of both classes[9].

The class II hydrophobins HFBI and HFBII have been shown to form dimers and tetramers in solution[10,11], clustered together through their hydrophobic patches[8,12]. The behavior of HFBI in solution has been shown to be dependent on hydrophobin concentration[13]. By increasing hydrophobin concentration, a change from monomers to tetramers was reported. Hydrophobin multimers were shown to continuously disassemble and reassemble as a stable FRET signal was formed.

HFBII has previously been shown to have an excellent stabilizing ability for aqueous foams used for foods[14]. The high surface elasticity of HFBII (500-700 mNm-1) has been described as a cause of this property. HFBII could stabilize single bubbles to disproportionalization with air at significantly longer periods of times compared to the milk proteins β-lactoglobulin and β-casein[3]. HFBII has also been shown to stabilize oil in water emulsions[15].

[a] Department of Biotechnology and Chemical Technology, School of Chemical Technology, Aalto University, P.O. Box 16100, Fi-00076 AALTO, Finland
[b] VTT Technical Research Centre of Finland, Tietotie 2, Fi-02150 Espoo, Finland
DOI: 10.1039/x0xx00000x

In this work we examine the dynamic properties of multimers formed by the class II hydrophobin HFBII, using stopped-flow fluorescence measurements and Förster Resonance Energy Transfer (FRET). The rate of exchange is described by $t_{1/2}$ where half of all multimers in solution have associated and disassociated. Activation energies were determined by measuring the temperature dependency of the multimer exchange. The results give an understanding the kinetics and thermodynamics of hydrophobin solution multimers and how this is affected by other proteins and surfactants.

2. Experimental

2.1 Materials:

Hydrophobin proteins. The class II hydrophobin proteins HFBI and HFBII were purified from *T. reesei* mycelium (HFBI) or culture supernatant (HFBII) using two-phase extraction and reversed phase chromatography as described earlier[1612]. In order to conjugate HFBII at specific sites we engineered a variant termed HFBII-CysC that has an additional Cys residue at the C-terminus. The *T. reesei* hfb2 gene in plasmid pTNS31[17] was mutated using a site-directed mutagenesis kit (QuikChange, Stratagene, USA) and oligonucleotides 5'-GCCATCGGCACCTTCTGCACCTAAGGATCCCCCGGG-3' (sense) and 5'-CCCGGGGGATCCTTAGGTGCAGAAGGTGCCGATGGC-3' (antisense) (Sigma-Genosys Ltd) in order to insert residues Cys-Thr before the stop codon. The resulting plasmid, termed pGZ14, contained the HFBII-CysC encoding sequence and was controlled by cbh1 promoter and terminator. Transformation into *T. reesei* (resulting in strain VTT-D-061177), expression and purification were done as described earlier[13]. HFBII-CysC was conjugated with either cyanine dye 3 donor (Cy3-monomaleimide), or cyanine dye 5 acceptor (Cy5-monomaleimide, both from GE-Healthcare) in order or create a FRET pair[13].

2.2 Fluorescence spectroscopy and FRET

The fluorescence spectra of the samples were measured with a fluorescence spectrophotometer, Cary Eclipse (Varian inc., USA) at 22° C. The efficiency of energy transfer, E, was calculated as described previously[18,13]. The samples were excited at 516 nm (donor excitation), and the emission spectra from both the donor and acceptor was recorded.

2.3 Stopped-flow FRET measurements:

Sample concentration and volumes: Stopped-flow FRET was measured between fluorescently labelled hydrophobin proteins using a Chirascan SF.3 spectrometer (Applied photophysics, UK) with a fluorescence detector and a CS/SF stopped-flow unit. Cy3- and Cy5- labelled HFBII-CysC at equal concentrations were mixed in the stopped-flow cell and excited with donor wavelength (516 nm). The FRET signal arises when labeled proteins are brought into close proximity, and a transfer of energy will occur from donor molecules to acceptor molecules[18]. Growth of the acceptor emission (or decay of the donor emission) can be measured on a time scale suitable for following molecular processes. The samples were prepared with 1:10 ratio of labelled HFBII-CysC to unlabelled HFBII where each syringe was loaded with 10 µg/ml labelled HFBII and 90 µg/ml wild-type HFBII, with the cy3 in syringe 1 and cy5 label in syringe 2 resulting in a total HFBII concentration in each syringe of 100 µg/ml. The 100 µg/ml total HFBII was set as reference. The addition of wild-type mas made in order to reduce the very high fluorescence signal as performed before[13]. Measurements of the FRET signal as a function of time were performed at acceptor emission at 665 nm, the drive volume was set to 140 µl. As the protein concentration did not change during the course of each measurement the observed change in FRET signal corresponds to the rate of monomer exchange in the multimers. Activation energies were determined by measuring the exchange rate at three different temperatures (21.5°, 17.5° and 12.5° C). Furthermore, the effect of additional proteins (Milk proteins β-lactoglobulin (βLG) (1mg/ml), and β-casein (βCas) (1mg/ml), (Sigma-Aldrich, USA)), surfactants (Tween-20 (0,1 %), Sodium dodecyl sulfate (SDS) (0.01 % in 1:20 labelled:unlabelled HFBII)) (Sigma-Aldrich, USA) as well as ethanol (5 %) and salt (NaCl 10, 50, 100 and 200 mM) on HFBII dynamics were examined compared to the reference of 100 µg/ml total HFBII. In all cases the concentrations and ratios of all components were equal in both syringes.

2.4 Data collection and analysis

Pro-data viewer (Applied Photophysics, UK) was used for fitting, conducted by a Marquardt-Levenberg algorithm. The algorithm iterate until convergence to a chosen suitable equation, in this case a single exponential, a*e(-kx) +c where k is the reaction rate constant, as seen in Fig. 1. $t_{1/2}$ was calculated as ln(2)/k. The estimated standard error of fitting were in all cases < 0.002.

2.5 Arrhenius equation and activation energy.

Three temperature sets were chosen, 21.5°, 17.5° and 12.5° C in order to examine the temperature dependency of the multimer exchange of HFBII by stopped-flow FRET. The Arrhenius equation, $k = Ae^{-E_a/RT}$ gives activation energy Ea and frequency factor A by plotting ln(k) vs. 1/T (K), where k is the reaction rate constant from fitting and T temperature. Example seen in Fig. 2

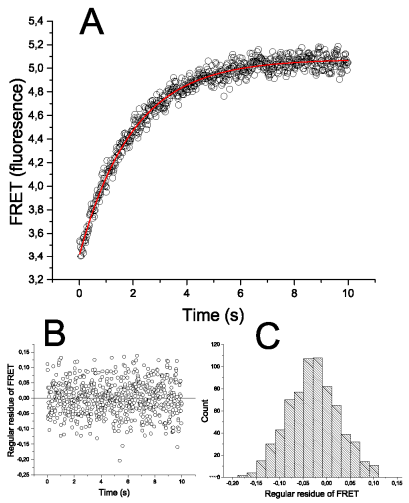

Fig. 1 A) Fitting of a single exponential curve of the general form y = A*exp(-x/t1) + y0 to the FRET data. B) Residuals show an even distribution throughout the time range of collecting data. C) Residuals have a normal distribution around the fitted curve.

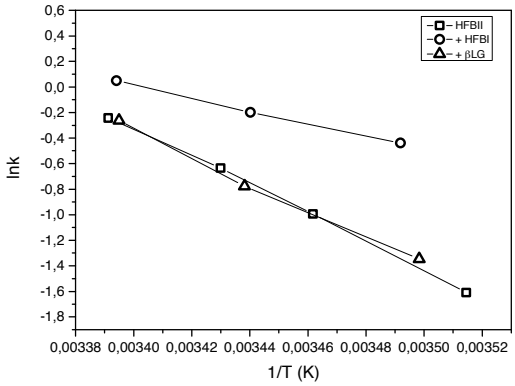

Fig. 2 Example of plotting for Arrhenius calculation

3. Results and discussion

3.1 Kinetics of hydrophobin multimer exchange, $t_{1/2}$

The formation of FRET signal followed a single exponential curve showing the time dependence of multimer exchange. From the fitted curve a half time for the multimer exchange ($t_{1/2}$) was calculated. The $t_{1/2}$ values for all cases compared to HFBII reference case using extrapolated data at 20.0° C are listed in Table 1.

$t_{1/2}$, effect of hydrophobins. The $t_{1/2}$ was measured at different hydrophobin concentration and ratios of labelled to unlabelled HFBII. HFBII 100 µg/ml displayed a $t_{1/2}$ of 1-4 sec in the temperature range and was set as reference (Fig. 3). The addition of HFBI 100 µg/ml, giving final hydrophobin concentration of 200 µg/ml resulted in a decrease in $t_{1/2}$ in the whole temperature range, increasing at lower temperatures compared to the reference. At 20° C, a decrease of 32 % was calculated (Table 1). An Increase of the total HFBII concentration to 200 µg/ml (10 µg/ml labelled HFBII and 190 µg/ml wt HFBII) resulted in a 10 % decrease in $t_{1/2}$ compared to the reference case (Fig. 3, Table 1).

β -casein and β –lactoglobulin. The addition of β- casein and β – lactoglobulin showed very little effect on $t_{1/2}$ values compared to the HFBII reference, except from lower temperatures where the $t_{1/2}$ were slightly lower (Fig. 3). At 20° C, calculated differences are minor compared to the reference (Table 1).

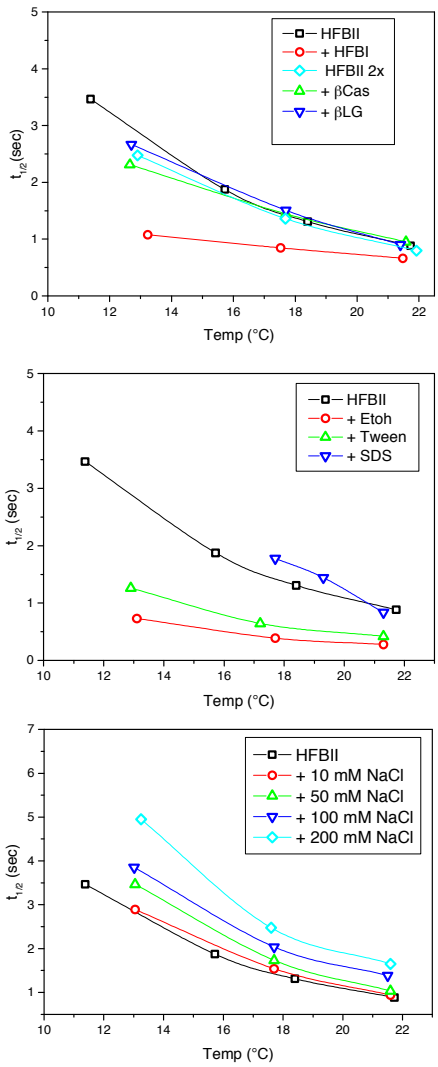

Fig. 3 **Top**:, Effect of HFBI, β-casein, β-lactoglobullin and HFBII 2x on $t_{1/2}$ **middle**: effect of Tween (0,1 %), ethanol (5 %) and SDS (0.01 % in 1:20 labelled:unlabelled HFBII) on $t_{1/2}$ **bottom**: Effect on $t_{1/2}$ by increasing NaCl concentration.

Table 1 $t_{1/2}$ compared to HFBII reference case using extrapolated data at 20.0° C. Concentrations: Tween (0.1 %), ethanol (5 %) and SDS (0.01 % in 1:20 labelled:unlabelled HFBII) HFBII 100 µg/ml reference is also compared to HFBII 2x (200 µg/ml HFBII, 10 µg/ml labelled HFBII and 190 µg/ml wt HFBII)

	20,0°
HFBII	
+ HFBI	-32 %
HFBII 2x	-10 %
+ βCas	2 %
+ βLG	2 %
+ ethanol	-71 %
+ Tween	-55 %
+ SDS	5 %
+ Nacl (mM)	
10	5 %
50	16 %
100	49 %
200	78 %

Extrapolated values.

$t_{1/2}$, effect of surfactants, ethanol, polymers and NaCl. The addition of Tween-20 and ethanol to HFBII 100 µg/ml resulted in a decrease of $t_{1/2}$ in the whole temperature range (Fig. 3, Table 1). For ethanol the calculated decrease at was as high as 71 % at 20° C. The decrease on $t_{1/2}$ for Tween-20 was large over the whole temperature range, calculated as 55 % at 20° C. SDS was added as 0.01 % SDS to 15 µg/ml labelled HFBII and 95 µg/ml wt HFBII in order to attain measurable signal and avoid aggregation and showed only a small difference compared to the reference. The effect on $t_{1/2}$ on increasing salt temperature can be seen in Fig. 3 and Table 1. Addition of NaCl led to an increase of $t_{1/2}$. At 10 mM, $t_{1/2}$ was only marginally increased, but already at 50 mM NaCl, the calculated difference was 16 % at 20° C. The same pattern can be seen at 100 and 200 mM where the difference compared to the reference HFBII 100 µg/ml was 49 % and 78 % respectively.

3.2 Thermodynamics of hydrophobin multimer exchange

Activation energies (Ea) and Frequency factors (A) are shown in Table 2. Comparing HFBII (92.51 kJ/mol) with other proteins, the largest difference in activation energy can be seen after the addition of HFBI. Ethanol and Tween only have a marginal effect on Ea, whereas values for SDS were not possible to obtain due to the precipitation of SDS, data points at lower temperatures were not possible to obtain.

Table 2 Activation energies, frequency factors. Concentrations: Tween (0.1 %), and ethanol (5 %).

	Ea, kJ/mol	A (Freq. Factor), s^{-1}
HFBII	92.51	1.95E+16
+HFBI	41.38	2.26E+07
HFBII 2x	88.17	3.51E+15
+ βCAS	69.44	1.46E+12
+ βLG	86.83	1.88E+15
+ Etoh	83.38	1.60E+15
+ Tween-20	91.81	3.31E+16
+ Nacl (mM)		
10	92.42	1.77E+16
50	99.33	2.70E+17
100	84.88	5.72E+14
200	92.70	1.17E+16

Note: values for addition of SDS were not possible to obtain due to precipitation in the sample

3.3 Concentration dependency of hydrophobin multimerization.

FRET was determined at different hydrophobin concentrations by thermodynamic equilibrium studies as described previously[13]. FRET was first measured with labelled hydrophobin only (one part donor-labelled and one part acceptor labelled) up to a concentration of 3 µM. The labelled sample was also mixed with non-labelled HFBII in order to study the behaviour of HFBII at higher protein concentrations in ratios: 1:4.5 and 1:9. As was seen with HFBI previously[13], it was shown that the addition of wild-type HFBII resulted in two effects on the FRET efficiency. At lower concentrations, the effect of increased FRET due to increased overall concentration is outbalancing the effect of competition between labelled and non-labelled HFBII. At higher concentrations the effect of competition is taking over, seen comparing 1:4.5 and 1:9 dilutions (Fig. 4). The labelling degree reduction effect of added HFBII taken into account as described in materials and methods

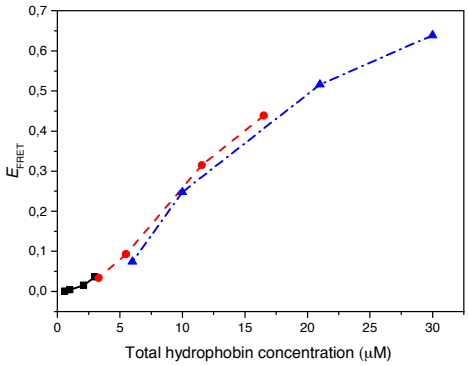

Fig. 4. Concentration dependence of energy transfer between fluorescent labelled hydrophobins. Ratio of labelled hydrophobin/nonlabelled HFBI was 1:1 (■), 1:4.5(●) and 1:9 (▲)

4. Conclusions

The solution multimer formation of the class II hydrophobin HFBII is here shown to be a dynamic exchange process where multimers continuously disassemble and reassemble. The kinetics of the multimer exchange reaction was monitored by stopped-flow measurements, giving a $t_{½}$ for the exchange of 0.88 sec at 22° C, fitted as single exponential.

Table 3. Ea, $t_{1/2}$ diss for selected proteins including HFBII

Protein	Ea (kJ/mol)	$t_{1/2}$ diss.	Temp °C
HFBII multimer	92.51	0.88 sec	22
Insulin monomer-dimer[19]	10.5 ass. 30.9 diss.	6.08E-09 sec [a]	23
Phosphorylase b, two dimers to tetramer[20]	12.3 ass.[b] 32.3 diss. [b]	1.5 min [a]	25
recombinant humanized antibody (rhuMAb) VEGF self-association[21]	45.2.	1 h [a]	30
Spectrin dimer – tetramer[22]	250.0 ass. 460.0 diss.	10 h [a]	29,5
Intermediate state of folding of Cytochrom C [23]	50.0	0.04 sec [a]	20
Bence-Jones protein Au variable fragment dimerization[24]	N/A	0.005 sec[a]	20
TATA binding protein (TBP) dimer dissacociate[25]	N/A	7.4 min	25

Data has been converted to the appropriate units when necessary.[a] Calculated from $k_{diss.}$ assuming first order kinetics ($t_{1/2} = \ln(2)/k_{diss.}$) [b]Approximated using two-point Arrhenius.

The small surfactant molecules SDS and Tween-20 as well as ethanol affected the multimer exchange rate. Ethanol and Tween considerably increased the rate of exchange as seen with lower $t_{1/2}$ values. Tween is likely to interact with the hydrophobic patch of the proteins and ethanol has been shown to dissolve some of the aggregates formed by class II hydrophobins. As a result we suggest that these molecules are altering hydrophobic interactions in the multimers. The exchange is also shown to be affected by increased ionic strength, with larger $t_{1/2}$ observed at higher concentration of NaCl, supporting this conclusion. Furthermore, if electrostatic interactions were involved one would expect a destabilization of the complex and a lower $t_{1/2}$ as a result of salt increase.

β-lactoglobullin and β-casein did not affect the exchange showing that there is no interaction between these relative large molecules and the HFBII. Doubling the concentration of HFBII led to a small decrease in $t_{1/2}$, indicating that a higher protein concentration to some extent affects how multimers are formed and disassembled. This may be due to a shift in the relative distribution of sizes of multimers, e.g. from dimers to more tetramers. These may have different rates of formation, but with the current approach it is not possible to distinguish between these. On the other hand, HFBI considerably lowered the $t_{1/2}$. This suggests that there is an interaction between HFBI and HFBII. In this interaction HFBI shows clearly different characteristics compared to HFBII. The interaction apparently leads to a destabilization of the HFBII complex making the multimers reassemble at a faster rate. This is also indicated by the much lower Ea (Table 2) when adding HFBI. The Ea did not significantly change for the other mixtures. The biological significance of this interaction remains unclear but suggests that hydrophobins do interact with each other and clearly affect the behaviour of each other.

The half-life life of several protein complexes have been studied previously (Table 3). These can be divided broadly into two groups, the ones with values in the millisecond regime and those with much higher stability with values in minutes or even hours. The disassociation of insulin dimers into monomers is several times faster, whereas self-association of an antibody or the dimerization of a DNA-binding protein is slower, with $t_{1/2}$ from minutes to hours. Clearly these differences reflect biological functionality. HFBII is curiously placed somewhere in between these groups. It shows a much faster exchange rate than structural interactions, but is still significantly slower than the cases in which exchange has a biological role such as in signalling. Our interpretation of the relatively slow half-life of the HFBII multimer exchange reflects its biological function. The multimers driving forces are strong, leading to slow exchange, but still allowing dynamic interactions at the timescale of functions that are relevant such as growth or surface interactions.

The activation energy for the HFBII multimer exchange in solution was 92.5 kJ/mol, which is in the lower range compared to multimerization of a variety of proteins (Table 3), although several times larger than e.g. an antibody self-association process. Interestingly, the Ea of the self-healing process of supramolecular polymers known as ionomers has been described as 96.5 kJ/mol[26], which is in close proximity of HFBII described here.

In summary the multimerization in solution of HFBII is shown to be a relatively slow exchange process between different multimers. Small surfactant molecules as well as increased ionic strength affect the exchange rate showing that hydrophobic interactions are important in multimer formation. The exchange process is destabilized by hydrophobin HFBI, showing that the two highly specialised class II proteins of *T. reesei* behave differently despite their many structural similarities.

Acknowledgements
Financial support from ISB – National Doctoral Program in Informational and structural biology is acknowledged.

Notes and references

1 M. B. Linder, *Curr. Opin. Colloid Interface Sci.*, 2009, **14**, 356–363.

2 M. Lienemann, M. S. Grunér, A. Paananen, M. Siika-Aho and M. B. Linder, *Biomacromolecules*, 2015, **16**, 1283–92.

3 A. R. Cox, F. Cagnol, A. B. Russell and M. J. Izzard, *Langmuir*, 2007, **23**, 7995–8002.

4 H. A. Wösten and M. L. de Vocht, *Biochim. Biophys. Acta*, 2000, **1469**, 79–86.

5 K. Kisko, M. Torkkeli, E. Vuorimaa, H. Lemmetyinen, O. H. Seeck, M. Linder and R. Serimaa, *Surf. Sci.*, 2005, **584**, 35–40.

6 K. Scholtmeijer, M. I. Janssen, B. Gerssen, M. L. de Vocht, B. M. van Leeuwen, T. G. van Kooten, H. A. B. Wösten and J. G. H. Wessels, *Appl. Environ. Microbiol.*, 2002, **68**, 1367–73.

7 J. G. H. Wessels, *Annu. Rev. Phytopathol.*, 1994, **32**, 413–437.

8 J. Hakanpää, A. Paananen, S. Askolin, T. Nakari-Setälä, T. Parkkinen, M. Penttilä, M. B. Linder and J. Rouvinen, *J. Biol. Chem.*, 2004, **279**, 534–9.

9 M. B. Linder, G. R. Szilvay, T. Nakari-Setälä and M. E. Penttilä, *FEMS Microbiol. Rev.*, 2005, **29**, 877–96.

10 M. Torkkeli, R. Serimaa, O. Ikkala and M. Linder, *Biophys. J.*, 2002, **83**, 2240–7.

11 K. Kisko, G. R. Szilvay, U. Vainio, M. B. Linder and R. Serimaa, *Biophys. J.*, 2008, **94**, 198–206.

12 J. Hakanpaa, *Protein Sci.*, 2006, **15**, 2129–2140.

13 G. R. Szilvay, T. Nakari-Setälä and M. B. Linder, *Biochemistry*, 2006, **45**, 8590–8598.

14 A. R. Cox, D. L. Aldred and A. B. Russell, *Food Hydrocoll.*, 2009, **23**, 366–376.

15 S. O. Lumsdon, J. Green and B. Stieglitz, *Colloids Surf. B. Biointerfaces*, 2005, **44**, 172–8.

16 M. Linder, K. Selber, T. Nakari-Setälä, M. Qiao, M. R. Kula and M. Penttilä, *Biomacromolecules*, 2001, **2**, 511–7.

17 M. J. Bailey, S. Askolin, N. Hörhammer, M. Tenkanen, M. Linder, M. Penttilä and T. Nakari-Setälä, *Appl. Microbiol. Biotechnol.*, 2002, **58**, 721–7.

18 R. M. Clegg, *Methods Enzymol.*, 1992, **211**, 353–88.

19 R. Koren and G. G. Hammes, *Biochemistry*, 1976, **15**, 1165–1171.

20 F. Muñoz, M. A. Valles, J. Donoso, G. Echevarria and F. García Blanco, *J. Biochem.*, 1983, **94**, 1649–59.

21 J. M. Moore, T. W. Patapoff and M. E. Cromwell, *Biochemistry*, 1999, **38**, 13960–13967.

22 E. Ungewickell and W. Gratzer, *Eur. J. Biochem.*, 1978, **88**, 379–385.

23 S. R. Yeh, S. Takahashi, B. Fan and D. L. Rousseau, *Nat. Struct. Biol.*, 1997, **4**, 51–6.

24 H. Maeda, E. Steffen and J. Engel, *Biophys. Chem.*, 1978, **9**, 57–64.

25 R. A. Coleman and B. F. Pugh, *Proc. Natl. Acad. Sci. U. S. A.*, 1997, **94**, 7221–6.

26 R. K. Bose, N. Hohlbein, S. J. Garcia, A. M. Schmidt and S. van der Zwaag, *Polymer (Guildf).*, 2015.

Molecular interactions of hydrophobin proteins with their surroundings

Aalto-DD 206/2015
VTT SCIENCE 114

ISBN 978-952-60-6556-4 (printed)
ISBN 978-952-60-6557-1 (pdf)
ISSN-L 1799-4934
ISSN 1799-4934 (printed)
ISSN 1799-4942 (pdf)

978-951-38-8367-6 (printed)
978-951-38-8366-9 (pdf)
2242-119X
2242-119X (printed)
2242-1203 (pdf)

Aalto University
School of Chemical Technology
Department of Biotechnology and Chemical Technology
www.aalto.fi

BUSINESS + ECONOMY

ART + DESIGN + ARCHITECTURE

SCIENCE + TECHNOLOGY

CROSSOVER

DOCTORAL DISSERTATIONS